POLISH ACADEMY OF SCIENCES, GDAŃSK BRANCH
COMMITTEE OF ACOUSTICS

SOUND
IN THE NATURE

GDAŃSK 2023

Sound in the Nature

This publication is devoted to the memory of Professor Grażyna Grelowska, initiator of this publication

Polish Academy of Sciences, Gdańsk Branch
Committee of Acoustics

Sound in the Nature

Eugeniusz Kozaczka,
Grażyna Grelowska
(editors)

Gdańsk 2023

Editors
Eugeniusz Kozaczka
Grażyna Grelowska

ISBN 978-83-66847-55-2

DTP
LogoScript Sp. z o.o.

CONTENTS

IN MEMORIAM
PROFESSOR GRAŻYNA GRELOWSKA

1955—2022

We write these words with great sadness and regret, feelings caused by the loss of such a special person as Professor Grażyna Grelowska was. Our memories and thanks for the gift of acquaintance, friendship and the possibility of working together provide evidence of that what united us and made us focus on the issues of science and the effort to explore the surrounding world, and more specifically – the sea depths and the sound propagating in water, acoustics and hydroacoustics.

Professor Grażyna Grelowska was professionally associated with the Polish Naval Academy in Gdynia (PNA) "Heroes of Westerplatte" and the Gdańsk University of Technology. At the Naval Academy, she served as vice-rector for science and director of the

Hydroacoustics Institute at the Faculty of Navigation and Naval Weapons. She headed the Department of Hydromechanics and Hydroacoustics at the Faculty of Ocean Engineering and Ship Technology of the Gdańsk University of Technology. She was a member of the Senate of the Naval Academy, and also participated in the scientific councils of other universities and institutes. Both the interests and scientific achievements of Professor Grelowska concerned the application of acoustic methods in the research of the marine environment; the area of Her activity also included research for the navy and merchant navy needs, Border Guard, and environmental protection.

The education and the path of scientific development of Professor Grelowska were related to technical sciences. She started at the Gdańsk University of Technology, where in 1978 she obtained a master's degree in engineering at the Faculty of Electronics, specializing in electronic equipment. In 1990 at the Military University of Technology, Faculty of Chemistry and Technical Physics, she received PhD in technical sciences (the specialization of materials engineering) with honors, and in 2002 at the Institute of Oceanology of the Polish Academy of Sciences in Sopot, she received the degree of habilitated doctor in the specialization of oceanology. The culmination of the research work was the title of professor of technical sciences, awarded by the President of the Republic of Poland in 2017. It is a beautiful, impressive card of strenuous and fruitful scientific work, daily effort, and sacrifice.

From the beginning of her rich scientific career, Professor Grelowska was passionate about marine research. At the turn of 1978 and 1979, she took part in a research cruise to Antarctica on the RV “Profesor Siedlecki”. In addition, while working at the Naval Academy and the Gdańsk University of Technology, she organized numerous research cruises in the waters of the Baltic and the North Seas, measuring the parameters of sea water and the structure of the seabed using non-linear acoustics.

An important area of Professor Grażyna Grelowska's scientific and social activity was a membership in scientific societies, organizations, institutions, and scientific consortia. She was a member of the Polish Acoustical Society since 1986, a member of the European Acoustics Association since 1998, and a member of the Marine Research Committee of the Polish Academy of

Sciences from 2007 to 2014. From 2011 to 2014, she served as the vice-chairwoman of the Acoustics Committee of the Polish Academy of Sciences and the chairwoman of the Board of Directors of the Polish Acoustics Society. From 2012 to 2013, she was a member of the Awards Team of the Ministry of Science and Higher Education, and from 2013 to 2016, she represented Poland in the International Commission for Acoustics as a member of the Board. Since 2019, she was the chairwoman of the Committee on Acoustics of the Polish Academy of Sciences and an honorary member of the Polish Acoustical Society. Professor Grelowska actively participated in the editorial board of scientific journals. She served as the chairwoman of the Editorial Committee of Hydroacoustics, the vice-chairwoman of the Editorial Committee of the Naval Academy's Scientific Journals, and the editor of the hydroacoustics section of Archives of Acoustics.

Among the scientific achievements of Prof. Grażyna Grelowska were her contribution to the development of nonlinear hydroacoustics. In particular, there should be mentioned:

- development of the theory of wave propagation of finite amplitude in sea with low salinity,
- determination of the non-linear B/A parameter for the southern Baltic using thermodynamic and acoustic methods,
- broadening the knowledge about the phenomenon of nonlinear interactions in the near field of multi-element sources radiating high intensity waves, and
- carrying out original studies of the structure of bottom sediments in the Gulf of Gdańsk.

We are honored and privileged to have spent part of our lives with Professor Grelowska, a wonderful person and friend. In the last words of this farewell, we would like to thank Her for all the moments spent working together at the Naval Academy and the Gdańsk University of Technology. She contributed so much good to the life of our academic communities. We would like to thank Her cordially for this.

We wish You a peaceful watch Dear Grażyna, Madam Professor! The memory of You and respect for You will remain with us forever.

Professor Eugeniusz Kozaczka, PhD, DSc, Eng.

Rear Admiral ret. Czesław Dyrcz, PhD Eng.

MICHAEL VORLÄNDER
Institute for Hearing Technology and Acoustics, R WTH Aachen University,
Kopernikusstraße 5, 52074 Aachen
mvo@akustik.rwth-aachen.de

AURALIZATION OF ENVIRONMENTAL NOISE

KEYWORDS: Auralization, computer simulation, real-time audio signal processing

INTRODUCTION

Imagine if time travel were possible and one could experience the future, i.e. to see and hear an urban or rural environment, which does not exist yet. In fact, this is possible with the technology of Virtual Reality. In virtual reality, almost any environment can be experienced auditory-visually, even if it is in the future. It goes without saying that a halfway correct description of the environment is a very big challenge. But once all characteristics of the environment and the sound sources have been specific and implemented, the task of technical realization still remains. This requires a complex Virtual Reality (VR) technology, namely a display device for visual presentation ("3D glasses") and a 3D audio playback technology ("surround sound technology"). The point is that with technology, both 3D viewing and 3D listening are available in virtually every home. Smartphones already

provide rudimentary approaches. Head-Mounted Displays (HMD) have arrived on the computer games market and at correspondingly affordable prices. Binaural playback via headphones is both old-fashioned and once again the focus of current research when it comes to perfected individualized solutions.

The technology is basically available, what do we do with it now? First of all, acoustics in research and practice and also interdisciplinary research with other sciences!

Before the introduction to the acoustic-technical basics of virtual acoustics, here is a look at examples: VR technology can be used to plan runways or flight routes near airports. The major challenge here is to characterize the generation of aircraft noise with sufficient accuracy and to generate sound source signals from this, which then reach the receiver via models of atmospheric sound propagation. This application will be discussed in more depth below.

FROM SIMULATION TO AURALIZATION TO ACOUSTIC VIRTUAL REALITY

The progress of virtual acoustics over the last decades can be divided into the phases of the development of simulation techniques, audio signal processing, 3D audio technology and integration into VR system technology. In the fields of acoustics, the first steps were taken in room acoustics, then in building acoustics and vehicle acoustics, from which modular approaches were created through the generalization of components and work steps, which can now be used in practically all applications of audible sound.

Early as 1962, Manfred Schroeder formulated a vision of computer simulations in room acoustics, which were later developed by Krokstad et al. (1968) were actually presented. In the 1990s, these methods were finally developed to such an extent that results in great detail could be achieved after just a few minutes or hours on standard PCs (which only then became widespread), if necessary “over a weekend”. These programs represent a very useful addition to the model measurement technology, which

also has its advantages, but is not exactly easy to use for the rapid prediction of room-acoustic impulse responses. From around 1990, first auralizations were presented, which enable to create audio files from the computed impulse responses (Kleiner et al. 1993).

Reproducing a previously made recording of a sound source in that exact environment should ideally provide exactly the same listening experience. While this is not an auralization in particular, it is a good reference for auralization validations. The key feature of auralization is that it considers the source and transmission environment separately, see Fig. 1 (Vorländer 2020). As a result, different sound sources can be listened to, for example, with existing audio filters, without all of these having been previously recorded in the relevant transmission environment. Or a source can be listened to in different environments.

Accordingly, auralization consists of a modular approach in the separation of sound source, sound propagation components and receiver. In principle, all parts are interchangeable, so that when the components are varied, the resulting effect on the auditory event can be perceived immediately. It is now only a small step to integrate it into the system technology of virtual reality. However, it took 30 years to go there, rather there were many small steps from the first multimodal interactive VR implementations such as “SCATIS” 1992–1995 (Blauert et al. 2000) and “DIVA” (Savioja et al. 1999) up to today's established VR systems

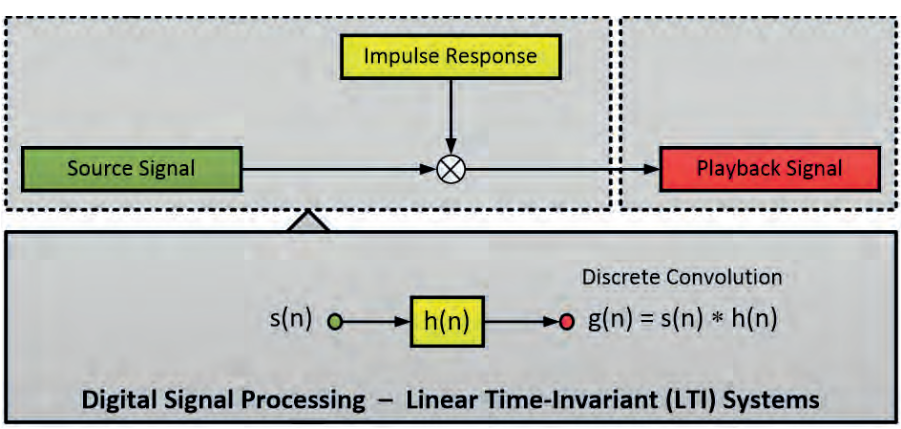

Figure 1. Key features of auralization: sound signal, sound propagation filter (impulse response), and sound playback.

such as “TASCAR” (Grimm 2015 [1]) or “VA” (Wefers and Vorländer 2018 [2]). Interestingly, in both of the early VR systems, multimodal investigations of haptics and acoustics were in the foreground, while the visual component was of only rudimentary importance. This can be explained by the fact that 3D computer graphics were still in the early stages of development.

Today, next to haptics, computer graphics is the most important component of VR technology and is evident in the majority of VR applications and publications in the field. However, the acoustics are playing an increasingly important role, especially since the feeling of presence in the virtual world (“immersion”) is increased enormously with a plausible 3D acoustic simulation.

VR tools are now an integral part of research and development. An overview of the system components is shown in Fig. 2. The environment model contains all the input data needed for the simulation, and just like with auralization, these are sound source position, sound power, orientation, directivity, etc. as well as all the input data for the environments, be it indoors or outdoors. The receiver must also be placed, also with regard to the

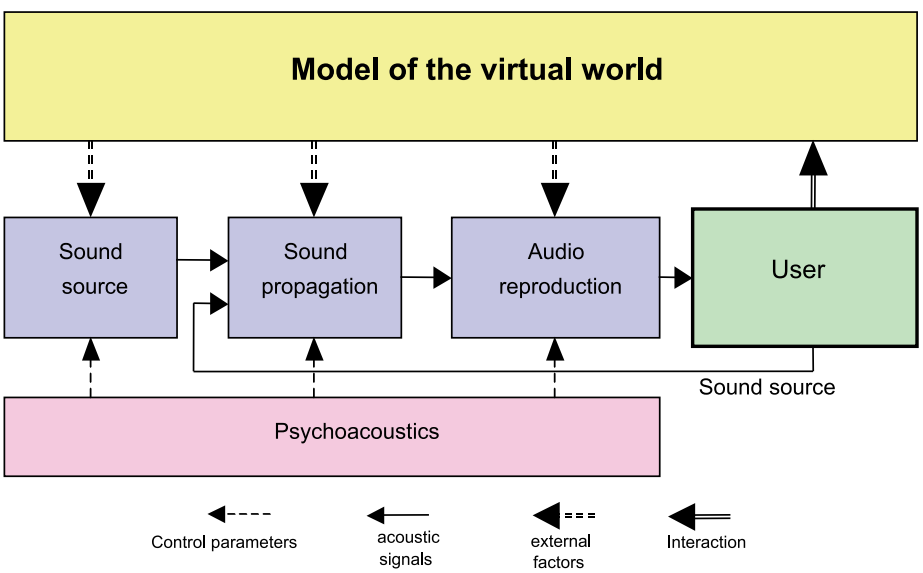

Figure 2. Implementation of an acoustic VR system

[1] https://github.com/gisogrimm/tascar
[2] http://virtualacoustics.org/

viewing/listening direction. The acoustic virtual reality must then be produced and presented in “real time” in such a way that it is perceived as quasi-real. And this in synchronization with the simulations for the other sensory perceptions in virtual reality (visual, tactile, tactile, olfactory), of which not all, but as many as possible should interact in order to achieve complete immersion. At this point, psychoacoustics provides valuable information on the perception thresholds of details in spectral, temporal and spatial sound, loosely based on the motto “simulate only as complex and precise as humans can resolve differences”.

STEPS TO CREATE VIRTUAL ACOUSTIC SCENES

It should be pointed out once again that not only “sound effects” but physically-based virtual acoustic scenes are to be created. Depending on the application, it must be decided which psychoacoustic criteria are particularly important and in which components the auralization must be applied particularly precisely. It is indeed the case that every auralization only creates an illusion, but never a real image of reality, even if an existing environment is supposed to be reproduced exactly. This consideration brings us to the question of validation against comparisons between reality and virtual reality, but more on that later.

SOUND SOURCE CHARACTERIZATION

The work steps in virtual acoustics begin with the recording or synthesis of sound signals. However, one important condition must be taken into account here: Examples of pieces of music recorded in 3D are multi-channel recordings and simulations (e.g. Rindel et al. 2004), which can also be used with sound-dependent radiation characteristics. The source characterization of musical instruments and the human voice is therefore much more than a simple "recording" like in a music studio. Many other factors have to be considered, e.g. suitable data formats with sufficient resolutions in spatial and spectral dimensions.

Now it would be nice if the same concept could be more generally applicable with an enveloping microphone array. Unfortunately, this is not possible with moving sources whose sound emissions are to be recorded during normal operation. We think of sources of traffic noise such as vehicles, trains or airplanes, which are the relevant sources in environmental noise. Theoretical source models, computer simulations or experimental methods must be used here, also in combination, in order to at least approximately estimate the spectral envelopes of the partial sound power of stochastic noise components (jet noise, tire noise, wind noise, etc.). In a synthesis step, previously neutral noise signals (white, pink) can be parametrically filtered from this data in such a way that the spectral and directional sound intensities correspond to those of the traffic sources. The signal components from periodic or rotational processes in machines or engines, in the case of rolling noise, a synthesis can be added, which is controlled using revolutions per minute data. This was, for example, by Pieren et al. (2017) for a rail noise simulation and, as described in the overview by Rizzi (2016) for the aircraft noise simulation, most recently also by Dreier and Vorländer (2020) for the auralization of commercial aircraft.

Now that the source signals are at least available in an approximate form, one can now ask how the sound propagates into the environment. Here, too, there are simply cases and situations with extreme challenges. In many cases, the radiated power is independent of the environment. This is not generally the case with primary sources of structure-borne noise, but it is definitely the case with the vast majority of airborne noise sources.

SOUND PROPAGATION MODELS

In general, the simulation of the impulse responses must include all relevant effects on the sound wave propagation, such as reflection, scattering, transmission, diffraction, refraction, attenuation, wind speeds and temperature profiles in the atmosphere, etc.

A more elegant solution is the direct solution with simulation methods that deliver results in real time, i.e. within around 50 milliseconds. In an indoor scene, for example, the VR user could look around or “walk around in the room”, sound sources

can also move, which creates the need to constantly calculate new impulse responses. This is especially true for a virtual scene with aircraft noise, where the source is moving very quickly while looking around the virtual environment. However, real-time impulse response calculations are only possible with the help of approximations, which entail substantial acceleration of the calculation time. This applies in particular to "geometric acoustics" (Savioja and Svensson 2015). This is known, among other things, in the form of image source methods and ray tracing. In geometrical acoustics, sound paths are constructed by connecting the source point and receiving point with a straight line, which "rays" are considered to be the counterpart to waves (ray/particle-wave dualism), just as in ray optics. It is not so well known that curved paths can also be calculated, namely in the case of refraction in stratified media such as the atmosphere (Wilson 2015). For the propagation of sound in addition to the direct line of sight between the source and receiver, i.e. via reflection, scattering and diffraction, the computer has to find the relevant beam paths in no time at all. Special algorithms will not be discussed here, but it should be said that parallel to the historical development of virtual acoustics there has been a rapid development of numerical methods, some of which are ideally suited for real-time applications (Savioja and Svensson 2015).

Source data and sound propagation models are now available, which can be used to simulate the sound field at the reception point. But the receiver is no longer a mathematical point. There is someone standing there, and this person hears the virtual sound event in a three-dimensional space.

3D HEARING AND SEEING IN VIRTUAL WORLDS

Playback technology for "3D audio" is an essential part of VR systems, which must be able to meet high quality standards with regard to the psycho-acoustically relevant aspects of perception. Details may vary from one VR application to the next. Some applications require accurate localization, while for others monaural spectral features such as reproduction with exact loudness and timbre are more important.

In a visual analogy, modern “shutter glasses” based on polarization filters or green-red filters in conjunction with high-resolution video displays deliver very good stereoscopic images, as do the head- mounted displays (HMD) or “VR goggles”. HMDs have two small video displays built into goggles or a helmet. Two slightly shifted images for the left and right eyes are created for the illusion of depth in the video, similar to old stereoscopic devices. Binocular vision allows distances to be estimated when looking at nearby objects. With the right eye, we see a nearby object projected onto a different part of the retina than the left, and this difference becomes more significant when the object is close. In this respect, technologies for three-dimensional vision are already available in good quality solutions. This is now also the case with loudspeaker-based 3D audio technology such as Ambisoncs (Gerzon 1985).

A 3D audio playback system for VR applications in research should not be confused with surround sound systems in consumer electronics. The main difference is that VR applications are based on physical models and the highest possible degree of realism in the components of sound and vibration generation, transmission and reproduction. This is a different goal than that pursued by an audio engineer for a music production. Even when recording live, he or she uses recording techniques and strategies for aesthetic optimization and instrument placement to achieve the best result for a home speaker setup, which then reproduces stereo or 5.1 signals.

APPLICATION IN ENVIRONMENTAL NOISE

The acoustics of outdoor environments are subject of research in environmental noise and in soundscape studies. This may apply to nature and in particular to the built environment in the context of human well-being and health. The sound sources are natural sources such as animals and waterfalls, and man-made objects such as vehicles, etc. Traffic noise play a very large role in these studies, and the sound propagation from the road, rail or air vehicles in the outdoor environment must be computed.

LINKING ATMOSPHERIC AND URBAN SOUND PROPAGATION

Real-time computation of atmospheric sound propagation can be implemented by using approximations of geometrical acoustics. A common method is ray tracing, which provides estimates of the acoustic paths. However, the atmosphere is a dynamic inhomogeneous medium. More specifically, speed of sound variances as well as wind have to be taken into account. Therefore, refraction and translation effects, which arise from interaction of the sound wave with the medium are included in the ray tracing algorithm. The method delivers so-called eigenrays, which connect the (moving) source with the receiver. Since the propagation through inhomogeneous media causes curved rays, the identification of eigenrays is not trivial. In an efficient implementation (ray zooming), the simulation is carried out with a low angular resolution. Based on the results, the resolution is stepwise increased around certain emission angles. This procedure is repeated multiple times until the receiver is reached within a certain accuracy. With this method, eigenrays between an aircraft and a receiver on the ground (reflecting plane) can be efficiently determined (Schäfer and Vorländer 2021). This does not include, however, any realistic urban environment with buildings, etc.

In order to extend the applicability to full scenarios of the built environment, Schäfer and Vorländer (2022) introduced the so-called virtual source method (VSM). It combines the properties of a curved free-field path calculated with the atmospheric model to sound paths of the urban model. For this purpose, a virtual source position is determined from the atmospheric path, which is then used for the urban simulation as shown in Fig. 3. This position is further serving as apparent source position, so that the incident direction at the receiver as well as the atmospheric propagation delay are maintained for the direct urban sound path. Thus, the distance between apparent source and the receiver is calculated using speed of sound of the urban domain. With this, the atmospheric propagation path can be smoothly integrated into the urban propagation simulation algorithm.

Real-time sound path computation in urban areas is based on geometrical acoustics as well. The main propagation effects are

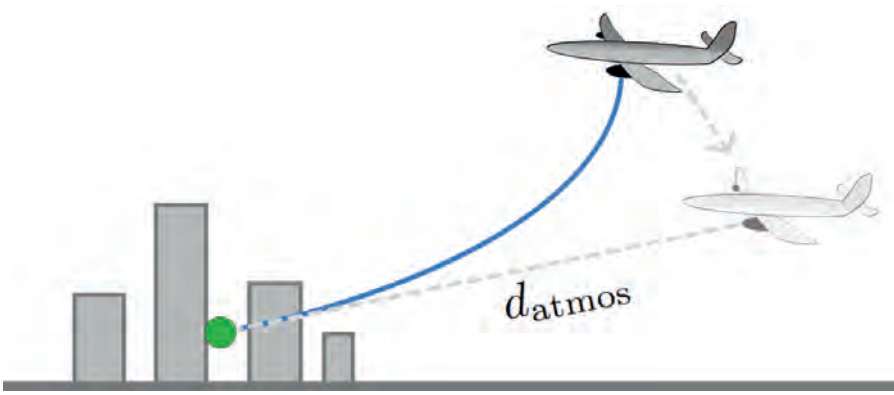

Figure 3. Definition of virtual source based on an atmospheric free field path (after Schäfer and Vorländer 2021).

reflection, scattering, and diffraction. While reflection and scattering components can be determined with classical ray tracing similar as applies to room acoustics, higher-order diffraction is crucial due to rather sparse impulse responses. Pathfinder algorithms and strategies for culling, i.e. extraction of irrelevant (inaudible) paths, is essential in order to achieve real-time performance. First steps are published by Erradj et al. (2021) and will be continued in the context of traffic noise auralization (Dreier et al. 2022) and, as mentioned above, in the combination of atmospheric and urban sound propagation. With this overarching approach, complex scenarios consisting of aircrafts and road or rail vehicles can be auralized.

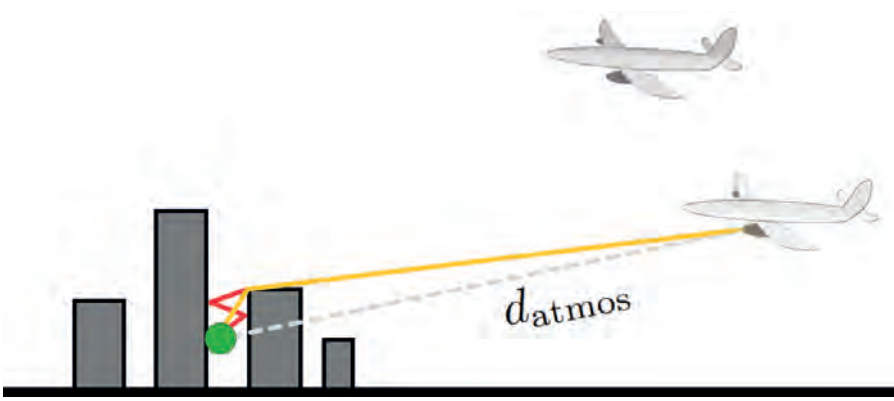

Figure 4. Atmospheric free field path (dashed, grey) and determination of urban paths (yellow and red) based on this virtual source position and an urban propagation model.

As shown in Fig. 4, after the relevant sound paths are known each path with its features (spectrum and delay) can be further processed by means of digital filters.

REAL-TIME SIGNAL PROCESSING

A real-time audio processing framework must be able to acoustically render virtual outdoor environments with dynamic, moving sources, partly fast-moving sources and interactive receivers in a built environment. To comply with aspects of real-time auralization constraints, it is required to implement dynamic scene handling, acoustic simulation and audio processing. The approach introduces an auralization timeline to record and up-sample scene updates and sort simulation results from a scalable scheduler instance in a chronological, layered history (Stienen 2022). Based on the history data, a smooth treatment of propagation delays is achieved by interpolation and extrapolation methods and chronologically correct event scheduling. A Digital Signal Processing (DSP) network processes propagation effects such as spectral effects from reflection and diffraction. Time-variant Doppler shift for many individual geometrical sound paths in real time using low-order Infinite Impulse Response (IIR) filter units. Key feature of the design is the implicit capacity to adapt to fast motion by introducing Single-Input Multiple-Output Variable Delay Lines (SIMO-VDLs). For spatial audio reproduction, binaural technology with a directional clustering routine at the receiver operates at a quasi-constant computational load.

The method uses Head-Related Impulse Response (FIR_1, FIR_2, ...) convolutions and adjusts the Inter-aural Time Difference (ITD) mismatch using Fractional Delays or each individual propagation path, while maintaining efficiency by merging Doppler interpolation and ITD correction into a single routine. The complete layout of the DSP network that represents the core of the audio rendering module is visualised schematically in Fig. 5.

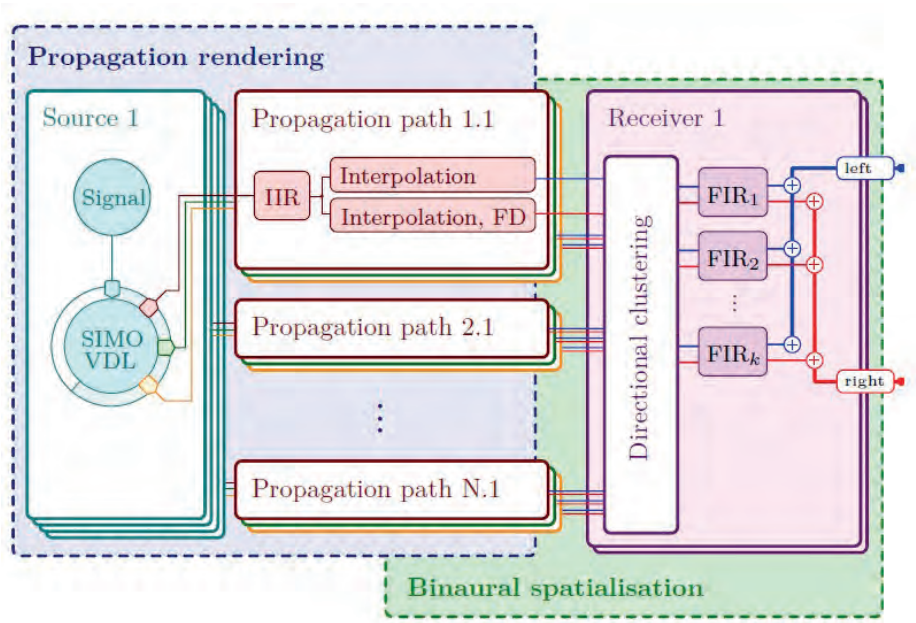

Figure 5. DSP network for real-time auralization of dynamic, outdoor environments. Each of *N* sources provides a signal that feeds a SIMO-VDL. Read cursors per source receiver pair transfer a delayed propagation path signal including spectral propagation effects.

CONCLUSION

Using a combined scenario, an aircraft flyover over an urban area was auralized[3]. The resulting audio demonstration underlines how considering reflections and diffraction at urban structures, increases the stereophonic realism significantly. This holds particularly regarding the localization of the source when the direct path is occluded, so that secondary sound paths become dominant.

Next steps towards improvements and extensions are in progress. This concerns listening tests with variants of diffraction filters in order to optimize computational effort with reference to perception. Also, inclusion of surface scattering is relevant when it comes to complex building facades with roughness tex-

[3] Audio-visual demonstration of an aircraft flyover. ### Youtube or IHTA-website, link will be added in the author proofs ###

ture on various scales. Regarding atmospheric propagation, turbulence is an important aspect, which can be included in the auralization process using time-variant filters. While this was successfully done for auralizations based on the Atmospheric Ray Tracing framework alone where only two sound paths are considered, this is ongoing work for the presented approach. Finally, the combination of the aircraft sound component with that of other sound sources in urban environments will lead to the ultimate goal of establishing an open-source Virtual Reality toolbox for soundscape research.

It can be seen that each application requires careful consideration of the entire simulation chain from source to receiver and beyond to experimental design. This is exactly what distinguishes virtual acoustics in acoustic research and practice from 3D sound in computer games, in which impressive 3D scenarios are presented, also highly interactive, but without any reference to the physically real conditions in the respective scene.

ACKNOWLEDGEMENTS

The author would like to thank the former and current members of the VR working group at the Institute for Hearing Technology and Acoustics at RWTH Aachen University: Lukas Aspöck, Christian Dreier, Anne Heimes, Simon Kersten, Michael Kohnen, Tobias Lentz, Josep Llorca-Bofí, Imran Muhammad, Sönke Pelzer , Philipp Schäfer, Oliver Schmitz, Dirk Schröder, Jonas Stienen and Frank Wefers as well as the VR group in the IT department headed by Prof. Torsten Kuhlen. The work of Michael Vorländer and his group was mainly supported by the Deutsche Forschungsgemeinschaft.

FURTHER MULTIMEDIA EXAMPLES

Virtual acoustics at the IHTA of the RWTH Aachen University: https://bit.ly/36ZIqUw

Park and Convention Center: https://bit.ly/33L4foW

Aircraft noise: https://bit.ly/33KzgcB
Interactive scene in a park: https://bit.ly/2peKdnE
A look into a sports arena: https://bit.ly/2X8CxQs
Interacting with Virtual Humans: https://bit.ly/373l0hd

REFERENCES

Blauert J, Lehnert H, Sahrhage J and Strauss H (2000). An Interactive Virtual-Environment Generator for Psychoacoustic Research. I: Architecture and Implementation. Acustica united with Acta Acustica 86, 94

Dreier C and Vorländer M, Psychoacoustic optimization of aircraft noise - challenges and limits. Proc. Internoise 2020, Seoul, Korea

Dreier C, Hahn J, Heck J, Llorca-Bofi J and Vorländer M (2022) Real-time vehicle pass-by noise synthesis for urban sound auralization. Proc. ICA 2022 Gyeongju, Korea.

Erradj A, Stienen J and Vorländer M (2021) The Image Edge Model. Acta Acustica 5, 17.

Gerzon MA (1985) Ambisonics in multichannel broadcasting and video. J. AES 33, 859

Grimm G, Luberadzka J, Herzke T and Hohmann V (2015) Toolbox for acoustic scene creation and rendering (TASCAR): Render methods and research applications. Proc. Linux Audio Conference, 9

Kleiner M, Dalenbäck BI and Svensson P (1993) Auralization – an overview. J. AES 41, 861

Krokstad A, Strøm S and Sørsdal S (1968) Calculating the acoustical room response by the use of a ray-tracing technique. J. Sound Vib. 8, 118

Pieren R, Heutschi K, Wunderli JM, Snellen M and Simons DG (2017) Auralization of railway noise: Emission synthesis of rolling and impact noise. Applied Acoustics 127, 34

Rindel, JH, Otondo, F and Christensen CL (2004). Sound source representation for auralization. Proc. International Symposium on Room Acoustics: Design and Science, Awaji, Japan, April 11-13, 2004.

Rizzi SA (2016) Toward reduced aircraft community noise impact via a perception-influenced design approach. Proc. Internoise, Hamburg, Germany, 220

Savioja L, Huopaniemi J, Lokki T and Väänänen R (1999) Creating Interactive Virtual Acoustic Environments. J. AES 47, 675

Savioja L and Svensson UP (2015) Overview of geometrical room acoustic modeling techniques. J. Acoust. Soc. Am 138(2), 708

Schäfer P and Vorländer M (2021) Atmospheric Ray Tracing: An efficient, open-source framework finding eigenrays in a stratified, moving medium. Acta Acustica 5, 26.

Vorländer M (2020) Auralization - Fundamentals of acoustics, modelling, simulation, algorithms and acoustic virtual reality. 2nd edition. Springer Nature Switzerland AG 2020. (383 pages)

Wefers F and Vorländer M (2018). Flexible data structures for dynamic virtual auditory scenes. Virtual Reality 22(4), 281

Wilson DK (2015) Outdoor Sound Propagation Calculator. In VE Ostashev and DK Wilson, Acoustics in Moving Inhomogeneous Media (Second Edition). Taylor & Francis, 2015. https://www.routledge.com/downloads/Y105698/Y105698_Web_Download.zip

LUIGI MAFFEI
MASSIMILIANO MASULLO
ROXANA ADINA TOMA
Department of Architecture and Industrial Design,
Università degli Studi della Campania "Luigi Vanvitelli"

THE ROLE OF WATER SOUNDS IN MULTI-SENSORY ENVIRONMENTS

ABSTRACT

Water sounds have always been, and are still nowadays, absolutely among the most appreciated natural sounds. Besides its multiple types of emission in terms of loudness, temporal variation and spectral sound distribution, water sounds are rarely interpreted as a negative element.

Furthermore, water sounds evoke positive sensations and expectations, and the informational masking of water sounds is effective in mitigating the adverse effects of noise. From a psychophysiological perspective, listening to water sounds can improve the perceived Restorativeness of a place, induce neural relaxation, or activate the parasympathetic nervous system responsible for stress relief.

This review analyses the role of water sound in multi-sensory environments through the investigation performed in several disciplines. In the first part, we briefly describe the typologies of sounds generated by water, then the effects that water sounds can have on humans, and in the end, are presented the preliminary results of a study on the emotions elicited by water noise conducted at Isola del Liri, a unique historical village in central Italy where inhabitants cohabit daily with a waterfall noise.

1. THE CHARACTER OF WATER SOUND

The water sound is produced by water movement, the flowing along a path, or the falling on a surface. It is mainly a white sound, characterized by equal energy across all frequencies and with no dominant tones. Water sound is associated with the movement of water along natural elements, such as rivers or waterfalls. Moreover, water sounds can also be produced by artificial elements which mimic natural ones, like water structures. Dewar [1] grouped water structures into three types: still water structures, moving water structures, and fountains. A classification of sounds produced by moving water structures and fountains was proposed by Rutherford [2] into: 1) jet and basin fountains made up of single or multiple nozzles, distinguished by the sounds produced by the hissing of the geysers and the splashing and bubbling of the water falling into the basin; 2) naturalized waterfalls, whose sound is characterized by the turbulence of the water splashing into a pool of waterfall or impacting on surfaces as it falls; and 3) Linear step or cascade structures generate a line source of sound by involving a series of formal or naturalized steps with vertical drops ranging from centimetres to metres.

The aforementioned water structures produce varying levels of sound. According to Brown and Rutherford [2], a fountain with three large geysers and four smaller geysers distributed over a basin of 18 x 7 meters with an overall flow rate of 20 l/s can generate sound levels ranging from 73 to 79 dB(A), a naturalized waterfall of 6 meters high and 11 meters wide with a flow rate of 125 l/s produces sound levels of 79 dB(A) at its base, and a continuous flow of water with low volume dropping down a series of 20 steps generate sound levels of 67 dB(A).

You et al. in [3] investigated the characteristics of some previously mentioned water structures finding that sounds from streams, falling water, and waterfalls are distinguished by continuous sound pressure levels, whereas water sounds from fountains have different temporal variability of the sound pressure levels. The fountains have been found to have the highest sound pressure level, while the stream has the lowest.

2. THE EFFECTS OF WATER ON HUMANS

Exposure to water sounds protects people against the impact of environmental stressors, improving the human perception of a place and mediating the adverse effects of stress by enhancing positive emotions and changes in physiological activity [4–10].

2.1. HUMAN PERCEPTION

Paton et al. in [11], aiming to determine the factors that affect human acoustic comfort, investigated 16 different water sounds:

1) natural: streams, small waterfalls (< 2 m), surf or soft waves (< 1 m), heavy rain during a winter storm and a weak rain in spring;
2) water jets: jets of medium size (~ 2 m), jets of long size (> 4 m), intermittent jets, multiple jets that do not collide and jets that collide;
3) waterfall of small (50 cm), medium (1.5 m) and high (> 4 m) height;
4) faucet/dripping, with regular, irregular, temporary, or multiple simultaneous drips.

According to the responses of a sample of 135 subjects, natural sounds are preferred over artificial sounds, and more specifically, water jets and waterfalls produce a marked acoustic aversion to humans.

On the other hand, Pérez-Martínez et al. [12] investigated the perception of dominant sounds in 19 sites in the Alhambra (Granada), which are primarily distinguished by the presence of water sounds in large part of its extension and in various forms (e.g., fountain, water flowing, and waterfalls). According to a survey conducted on a sample of 385 people, 58.7% of participants identified the water sound, while 38.2% of participants identified the water sound as dominant, mainly in 8 locations. Moreover, 83.6% of participants evaluated the water sound as pleasant, only 3.1% as unpleasant, and the remaining part (13.3%) as neutral.

As the water sound spectrum may be similar to the city noise spectrum, some components of urban noise can be masked by water sounds. In effect, when the city background noise is at

least 8 to 10 dB(A) below the water sounds, it can be completely masked. Partial masking occurs when the differences become smaller [2]. De Coensel et al. [13] explored the potential of fountains as a partial masking means. They showed that introducing sound from water structures into the urban setting reduces the perceived loudness of the freeway and major road traffic noise.

Moreover, water structures characterized by sounds with low sharpness and large temporal variation, such as sea and water streams, are highly effective in terms of information masking of road traffic noise, improving the sound environment's overall pleasantness preferable to fountains and waterfalls [14,15].

2.2. PSYCHOPHYSICAL EFFECTS

The effects induced by evocative audio-visual water structure on the perceived restorativeness in an urban park were investigated by Masullo et al. [16]. An immersive audio-visual virtual reality experiment with different water structures was used.

More specifically, water structures with regular or wrapping shapes combined with four different water sounds (big and small sea waves; big and small river) and a basic scenario simulating the urban park as it was, were used. The degree of Restorativeness of each scenario was measured using the Perceived Restorativeness Scale. The results showed that all the scenarios were perceived as restorative compared to those without water structures. The river sound seemed to induce a greater perceived Restorativeness with respect to the sound of sea waves (Figure 1).

The overall mental state assessment and brain network changes of brain processes related to informational masking of road traffic noise were investigated using EEG measurements by Li et al. [17]. During the listening test, the road traffic noise was combined with fixed, switching and moving water sound sources. The EEG spectrum results showed that the introduction of water sound in a traffic noise environment increases the power of the alpha band with a consequent enhancement of neural relaxation confirmed by the alpha-beta ratios (Figure 2), an index representative of mental relaxation opposite to mental fatigue and mental stress.

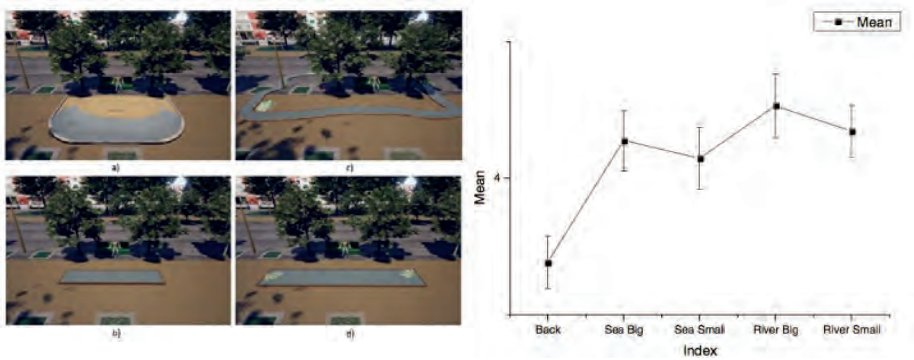

Figure 1. Left: The virtual reality scenarios: (a) big sea waves; (b) small sea waves; (c) big river; (d) small river. Right: Result of perceived Restorativeness extracted from Masullo, M., Maffei, L., Pascale, A. Effects of combination of water sounds and visual elements on the traffic noise mitigation in urban green parks. Proceedings of Internoise 2016, Hamburg, Germany, 21-24 August.

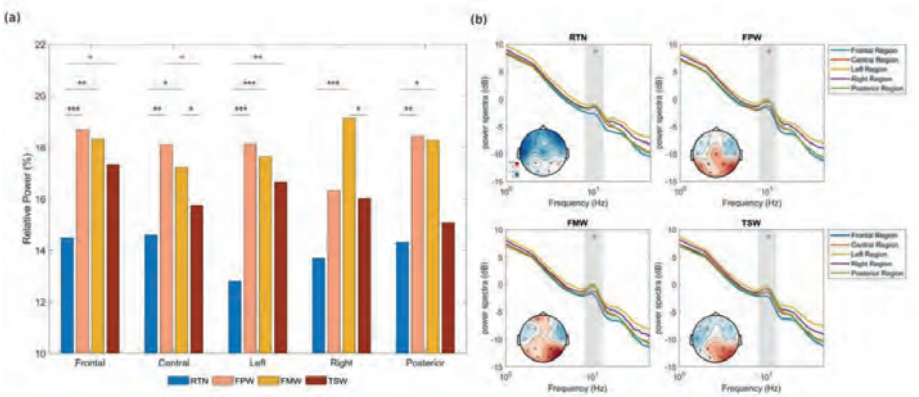

Figure 2. Left: The average relative power of alpha band across five regions between four conditions: RTN – road traffic noise; FPW — frontal position-fixed water sound; TSW - two-position switching water sound; FMW- four positioned — randomized moving water sound. Right: power spectrum of EEG across five regions between four conditions with topography of the alpha band is depicted. The asterisks indicate the significance level of the post hoc ANOVAs results: *p < 0.05, **p < 0.01, and ***p < 0.001 extracted from Li, J., Maffei, L., Pascale, A., Masullo, M. (2022). Neural Effects of the Spatialisation of Water-Sounds Sequences on Masking Traffic Noise: a Psychophysical Study. J. Acoust. Soc. Am. 152(1), 172-183.

Furthermore, Shu and Ma have investigated the physiological responses (Electrodermal Activity, EDA; Hearth Rate Variability, HRV) [18]. Their study tested the restorative effects of different soundscapes on children's stress in a simulated urban park setting. The study used a stream and a fountain sound as potential restorative water structure. The physiological responses were measured during and after a stressor task. When comparing the stressor and recovery periods, the findings revealed that children's levels of EDA and HRV (Beats Per Minutes) decreased significantly during both water sounds structures exposure. More specifically, the EDA decreased more during fountain sound exposure.

3. EMOTIONS AND WATERFALLS SOUND POWER

Isola del Liri is a small town in central Italy whose historic centre is characterized by the presence of waterfalls. The territory is rich in watercourses such as those of the river Liri, Melfa, Rapido and Fibreno, which led to the installation of numerous paper mills [19]. The town is characterized by two waterfalls named "Cascata Grande" and "Cascata del Valcatoio". The waterfall named "Cascata Grande" is the big one (Figure 3), and it is formed by the right arm of the Liri river, and it is about 27 meters high.

The waterfall area is surrounded by the Boncompagni - Viscogliosi Castle, Via Cascata, which is lined with restaurants, bars,

Figure 3. Isola del Liri. Cascata Grande Waterfall.

and pizzerias, the town hall, and the ex-felt factory Ippolito & Pisani, which houses a gallery and the panoramic terrace overlooking the waterfall. The sonic environment is defined by typical café and restaurant sounds, music, people's conversations, road traffic noise, and, most notably, the sound of the waterfall.

Spot binaural recordings were carried out on September 2022 while the waterfall flow rate was medium-low. A 4-channel recording/playback system SQobold and a binaural headset BHS II were used. For the acoustic measurements were selected three sites: the panoramic terrace overlooking the waterfall (ex-felt factory Ippolito & Pisani); via Cascata (closer to Boncompagni – Viscogliosi castle) and an area hidden from the view of the waterfall (Piazza San Lorenzo) (Figure 4).

The acoustic measurement results showed that the A-weighted sound equivalent level is 77.2 dB(A) in the proximity of the waterfall, and it decreases in the shadow area where the A-weighted sound equivalent level becomes 55 dB(A). In the intermediate area overlooking the waterfall, the noise level was measured at 67 dB(A).

Simultaneously, to investigate the effects of the waterfall sounds on the surrounding environment, a questionnaire was

Figure 4. a) Maps of site selected for acoustic measurements. b) Spot binaural recordings. c) area overlooking the waterfall. d) shadow area from view of the waterfall.

administered to local people who were present in the waterfall area. The questionnaire was divided into three sections: 1) General information on socio-demographic data; 2) Weinstein Noise Sensitivity Scale [20, 21]; and; 3) Emotional Salience [22]. More specifically, the last section of the questionnaire aimed to assess the sonic environment perception and the feelings provoked by the auditory stimuli. To this aim, two 6-items questionnaires on a 9-point Likert scale were used.

Ten people were involved in the survey (7 male and 3 female) ranging from 18 to 39 years. Half of them visit the waterfall area daily, while the rest stay in the area several times per year (3) or per week (2). The participants' noise sensitivity was measured using the italian version of the Weinstein Noise Sensitivity Scale.

The subjective questionnaire results revealed that the waterfall sound is perceived as Pleasant, Attractive, and Stimulating (Fig 5 left), while, on the other hand, it induces a state of Calm, causing people to feel Happy and to be Energetic (Fig 5 right).

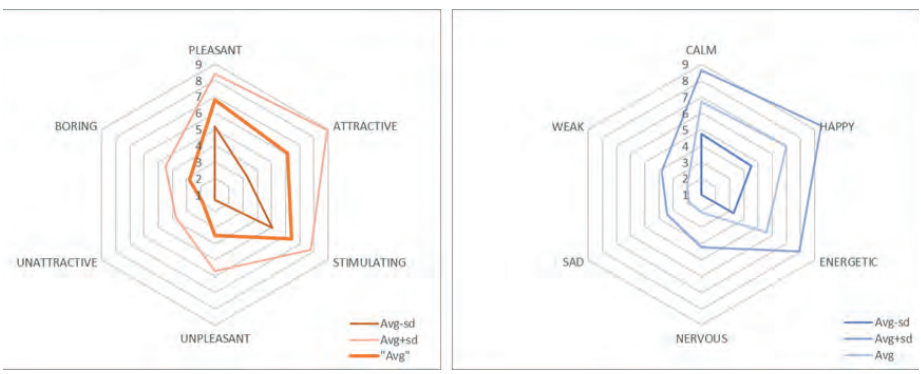

Figure 5. Results of the 6-items questionnaires. Left: sonic environment perception; Right: feelings provoked by the auditory stimuli.

4. CONCLUSIONS

In this paper, the role of water sound in multisensory environments has been described. The results that emerged from the studies of different disciplines showed that the use of water sounds has a positive effect on human well-being and environ-

mental perception. Among the various water sounds investigated, the waterfall is less preferred when compared to other water sounds.

However, the investigation carried out in the small town of Isola del Liri where the presence of a huge and continuous waterfall is responsible, all day and night long, for sound levels in the range 55–77 dB(A), showed that the sound environment is evaluated positively by the people interviewed and induces positive emotions.

REFERENCES

[1] Dewar, S., Water features in public places-human responses, Grad. Dip. Landscape and Architecture thesis, Queensland University of Technology, 1990.
[2] Brown, A. L., Rutherford, S., Using the sound of water in the city, Landscape Australia, 1994, 2, 103–107.
[3] You, J., Lee, P.J., and Jeon, J.Y., Evaluating water sounds to improve the soundscape of urban areas affected by traffic noise. Noise Control Eng. J. 2010, 58 (5).
[4] Berto, R., The Role of Nature in Coping with Psycho-Physiological Stress: A Literature Review on Restorativeness. Behav. Sci. 2014, 4, 394–409.
[5] Kaplan, R.; Kaplan, S. The Experience of Nature: A Psychological Perspective; Cambridge University Press: Cambridge, NY, USA, 1989.
[6] Ulrich, R.S.; Simons, R.F.; Losito, B.D.; Fiorito, E.; Miles, M.A.; Zelson, M. Stress Recovery during Exposure to Natural and Urban Environments. J. Environ. Psychol. 1991, 11, 201–230.
[7] Hartig, T.; Evans, G.W.; Jamner, L.D.; Davis, D.S.; Garling, T. Tracking restoration in natural and urban field settings. J. Environ.Psychol. 2003, 23, 109–123.
[8] Scopelliti, M.; Carrus, G.; Bonaiuto, M. Is it Really Nature That Restores People? A Comparison with Historical Sites with High Restorative Potential. Front. Psychol. 2019, 28, 2742.
[9] Zhang, T.; Liu, J.; Li, H. Restorative Effects of Multi-Sensory Perception in Urban Green Space: A Case Study of Urban Park in Guangzhou, China. IJERPH 2019, 16, 4943.
[10] Lugten, M.; Karacaoglu, M.; White, K.; Kang, J.; Steemers, K. Improving the soundscape quality of urban areas exposed to aircraft

noise by adding moving water and vegetation. J. Acoust. Soc. Am. 2018, 144, 2906–2917.
[11] Paton, D., Delgado, P., Galet, C., Muriel, J., Mendez-Suarez, M., Hidalgo-Sanchez, M., Using acoustic perception to water sounds in the planning of urban gardens. Building and Environment 2020, 168, 106510.
[12] Pérez-Martínez, G., Torija, A.J., Ruiz, D.P., A methodology for soundscape management of monumental spaces. Proceedings of EuroRegio 2016, Porto, Portugal, 13–15 June.
[13] De Coensel, B.; Vanwetswinkel, S.; Botteldooren, D. Effects of natural sounds on the perception of road traffic noise. J. Acoust. Soc. Am. 2011, 129, 148–153.
[14] Rådsten-Ekman, M.; Axelsson, Ö.; Nilsson, M.E. Effects of sounds from water on perception of acoustic environments dominated by road-traffic noise. Acta Acust. United Acust. 2013, 99, 218–225.
[15] Jeon, J.Y.; Lee, P.J.; You, J.; Kang, J. Acoustical characteristics of water sounds for soundscape enhancement in urban open spaces. J. Acoust. Soc. Am. 2012, 131, 2101–2109.
[16] Masullo, M., Maffei, L., Pascale, A. Effects of combination of water sounds and visual elements on the traffic noise mitigation in urban green parks. Proceedings of Internoise 2016, Hamburg, Germany, 21–24 August.
[17] Li, J., Maffei, L., Pascale, A., Masullo, M. (2022). Neural Effects of the Spatialisation of Water-Sounds Sequences on Masking Traffic Noise: a Psychophysical Study. J. Acoust. Soc. Am. 152(1), 172–183.
[18] Shu, S.; Ma, H. Restorative effects of urban park soundscapes on children's psycho-physiological stress. Appl. Acoust. 2020, 164, 107293.
[19] Leonardi, S. La Valle del Liri: da Terra di Lavoro a distretto industriale. Atti 14° conferenza nazionale ASITA- Brescia 9–12 Novembre 2010.
[20] Weinstein, N.D. Individual differences in critical tendencies and noise annoyance. J. Sound Vib. 1980, 68, 241–248. 26.
[21] Senese, V.P.; Ruotolo, F.; Ruggiero, G.; Iachini, T. The italian version of the weinstein noise sensitivity scale. Measurement invariance across age, sex, and context. Eur. J. Psychol. Assess. 2012, 28, 118–124.
[22] Masullo, M., Iachini, T., Maffei, L., Rapuano M., Cioffi, F., Ruotolo, F. A questionnaire investigating the emotional salience of sounds. Applied Acoustics, 2021, 182, 108281.

T.G. LEIGHTON,[1,2] C.N. DOLDER,[2]
T. SECKER,[2,3] M.ZHU,[2]
AND A. WESTLEY[1]

[1] Institute of Sound and Vibration Research, University of Southampton, Highfield, Southampton SO17 1BJ, UK

[2] Sloan Water Technology Limited, 1 Venture Road Chilworth, Southampton SO16 7NP, UK

[3] School of Biological Sciences, University of Southampton, Highfield, Southampton SO17 1BJ, UK

BIOFILMS: REMOVING MARINE BIOFOULING FROM HULLS, AND CLEANING WOUNDS (AND GROWING SKIN BACK OVER THEM) IN HUMANS, USING JUST AIR SOUND AND WATER

ABSTRACT

The growth of marine biofouling on ship hulls, and chronic infections in wounds, have a common foundation in the initial growth of bacterial biofilms over the surface. Biofilms are communities of bacteria that form living 'aggregates' that are far more resistant to removal (by chemicals, antibiotics, or mechanical scrubbing) than single (planktonic) bacteria. As it matures, the biofilm forms the foundation in which other species can grow, leading to marine biofouling on ship hulls, and chronic infections in human and animal wounds. The existence of chronic wounds in humans shows that current treatments are not wholly effective (the estimated cost of healthcare services in the UK for chronic wounds alone was £5.6 bil-

lion in 2017/18). The toxicity of antifoul for hulls, and the effort required to mechanically remove marine biofoulant, has led to the development of through-hull ultrasonic deterrents to reduce biofouling growth, but variable performance has stopped widespread adoption.

This report introduces new technology that has combined air, sound, and saltwater, to reduce the growth of marine biofouling on hull materials, and removed biofilm from wounded skin, and even promoted skin regrowth over the wounds.

1. INTRODUCTION

1(A) INTRODUCTION TO THE PROBLEM

The historical view of bacteria as individual cells, often free-floating or loosely attached to a substrate, has been replaced in recent years by the recognition of the importance of biofilms. In a biofilm, colonies exist within a matrix, into which other species of bacteria and fungi can co-exist, and this leads to greater resistance to anti-microbial agents. Repeated ineffective uses of anti-microbials against biofilms can promote further growth of anti-microbial resistance, as the wider environment (e.g. natural waterways, waste management infrastructure etc.) contains a vast reservoir of microbial species in which resistance can develop if diluted, sub-therapeutic doses of the agent pass from the water infrastructure into the wider environment.

This paper presents two inventions that use mechanical forces, as opposed to chemical or anti-microbial drivers, to remove biofilms. In each case, the mechanical force is developed when an appropriate acoustic field encounters a bubble, and as such that combination does not extend into the wider environment, and hence does not present opportunities to promote anti-microbial resistance.

The first device is an invention to clean marine biofouling from ship hulls. Whereas a previous design[1] used non-inertial cavitation (thereby avoiding damage to the rubber anechoic on which the fouling grew) to avoid the establishment of mature biofilms on the hull into which macroscopic biofouling can grow, this paper

uses the device to clean established macroscopic biofouling from steel hull material using non-inertial cavitation. The cleaning footprint of the device is around 10 cm by 10 cm, in a design that is easily scalable to larger footprints through the tessellation of units.

In the second invention, the substrate is delicate (human wound tissue) and requires a smaller footprint to accommodate the wound topography, and inertial cavitation is avoided. The removal of the biofilm occurs because of small-scale (of order of a few bubble radii) liquid currents and shear that can be generated on the substrate by microscopic air bubbles.[2] The bubbles generate shear and liquid currents when they are excited by an appropriate acoustic wave in the liquid: the acoustic waves stimulate ripples on the wall of the bubble,[3],[4] and these ripples in turn stimulate liquid currents and shear close to the bubble. Furthermore, the sound field generates acoustic radiation forces that drive the bubbles (and their cleaning action) into crevices that are difficult to clean using traditional brushes and wipes.[5]-[6]-[7]-[8] Suitable technology can pass both bubbles and sound down the liquid stream onto the substrate to be cleaned.[9]

1(B) THE SURFACES TO BE CLEANED

The two inventions are aimed at two types of surface substrates: ship hulls (which are substantially flat over the 10 cm scale, but will contain varying topography on the microscopic scale) and wounds (which are have undulating and varying topography on both the macroscopic and microscopic scales). The total area to be cleaned is greater with hulls, and the stand-off distance for wounds must be greater, and so the architecture of the two devices differ, even though both exploit the same acoustical phenomenon.

(I) SHIP HULLS

Biofilm formation occurs within hours of an object being placed in seawater, and as the biofilm matures, it provides the foundation and nutrients for the attachment and growth of

macroscopic marine fauna and flora. The use of copper and lead on marine vessels, centuries ago, to deter such fouling was an early, if unrecognised at the time, method of combatting biofilms.[10]-[11]-[12]

Marine biofouling reduces the efficiency of shipping by up to 50% due to increased mass and drag, with associated fuel penalties and implications for the carbon footprint of the vessel.[13]-[14]-[15] Additionally, the increased turbulence and attenuation reduces the performance of any sensors fitted to the hull (in particular sonars, but also optical sensors used for measurements of water properties and chemical sensors that rely on sample collection).[16] Turbulent flow over a vessels hull will also increase the radiated broadband noise, an effect of critical importance to warships[16] (Figure 1).

(II) CHRONIC WOUNDS

Chronic wounds differ from hull surfaces in a number of ways. Whereas the hull is substantially hard and flat (on the cm scale), wounds are generally more soft (giving less acoustic reflection), have a complicated topographical profile with multiple pockets and crevices, the patient might move during treatment, and the substrate of value is living and needs to be stimulated to optimise its self-healing properties. A device with a smaller footprint accommodates this change in substrate profile and requires a greater stand-off distance (necessitating a longer water stream).

The very existence and prevalence of chronic, non-healing wounds indicates that state-of-the-art treatments are insufficient. In the UK alone, non-healing wounds, particularly of the lower limb, affect more than 2 million patients per annum and cost the NHS an estimated £5 billion each year.[17]

Chronic wounds fail to progress through the normal stages of healing in a timely manner. The largest remediable cause of chronicity is infection in the form of a multispecies biofilm that is present in most chronic wounds. In addition, the biofilm phenotype of bacterial infection is implicated in many types of chronic, difficult to treat infections including cystic fibrosis, implanted device infections and periodontitis.[18] The biofilm

Figure 1. Biofoulant on the hull of the USS Pittsburgh (SSN 720) in Bremeton, Washington, as she awaits inactivation in dry dock at Puget Sound Naval Shipyard and Intermediate Maintenance Facility. Photograph by *Wendy Hallmark*. *This US Navy photograph is considered public domain and has been cleared for release via the Department of Defense*.

phenotype, apart from impacting wound healing, protects the microorganisms against host defences, increases adhesion and provides a relative immunity to antibiotics. Removing the biofilm without damaging the underlying tissue should improve healing.

2. METHODS

2(A) HULL PLATE CLEANING METHOD

(I) DESIGN OF THE MARINE DEVICE

Figure 2(a) shows a schematic of the ship hull cleaner. The device[1] works by non-inertial cavitation to avoid damaging anechoic linings. The study was designed to examine how non-inertial cavitation hinders the establishment of the biofilm on the hull into which macroscopic marine biofouling takes hold following the initial development of a bacterial biofilm on the hull. The device inhibits the maturation of the biofilm, so reducing the subsequent establishment of macroscopic marine biofouling. It was tested on aluminium, steel and rubber substrates.[1]

Commercial systems are available that attempt to use ultrasound to prevent antifouling, although their performance is mixed, and these methods radiate strong ultrasound into the

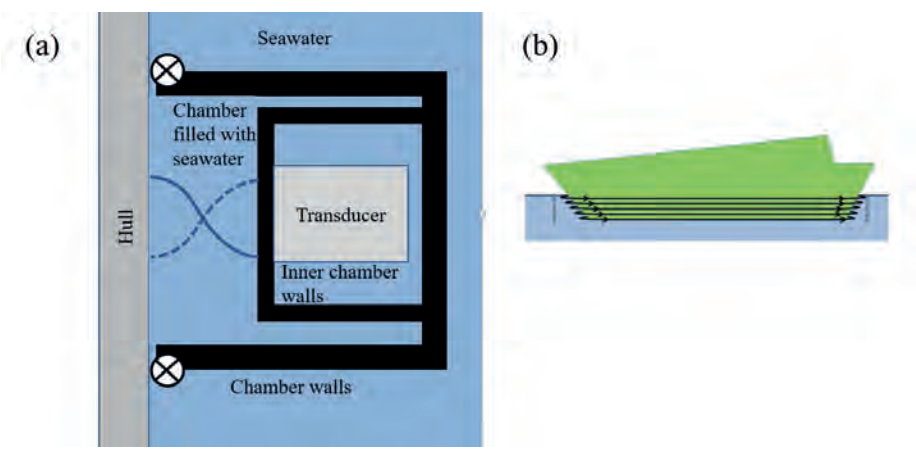

Figure 2. (a) Schematic of the hull cleaning device. A half-wavelength (λ/2) spacing is indicated as a simple illustration of the creation of an acoustic pressure antinode on the hull by making use of the acoustically rigid walls of the chamber, but in fact it is often convenient to tune the device to generate alternative modal patterns on the hull. (b) The method for covering a ship hull. The typical footprint of a single cell is around 0.1 m by 0.1 m although they can be made larger with multiple transducers. Cells like this can also tesselate to cover a larger overall footprint.

surrounding sea. Acoustic pressure as high as 214 dB re: 1 μPa have been measured close to the source, causing inertial cavitation, at 23 kHz)[19]. The leakage of sound away from devices is also an increasing concern with conventional hull treatment technologies, as lower amplitudes radiated to distance might still adversely affect behaviour (foraging, social interactions, breeding etc).[20],[21] The device design presented here reduces the likelihood for adverse effects on marine life (fish, [22] cetaceans[23] and benthic species[24]). It operates at 70 kHz (higher ultrasonic frequencies in general being less likely to produce adverse subjective response in fauna). Moreover, the design of the device uses features to contain the region of intense ultrasound to within the device, minimising the escape of acoustical radiation into the surrounding seawater. For example, the chamber walls reduce the leakage of sound into the environment. The device provides a water-filled cavity to the surface and within it creates a modal sound field that ensures an acoustic pressure antinode is present over the surface to be cleaned (the 'target').

(II) TEST DESIGN

A previous study[1] examined the ability of the device to prevent the formation of the biofilm substrate on which macroscopic biofoulant could grow, and so reduced the establishment and growth of macroscopic biofouling. In this current study, mature biofouling was allowed to grow, and was then removed using the hull-cleaning invention. This was compared to the cleaning achieved by a mechanical rotating brush system.

Samples of steel, aluminium, and rubber plates (50 samples of each material) of surface area 10 cm by 10 cm were submerged in a seawater dock for periods of 36, 41 and 50 days respectively. During these periods, mature biofouling was established on the surfaces of the plates.

The samples were then removed from the seawater and the thickness of the biofouling was measured in 10 regions on each plate, with an average thickness calculated.

The plates were then treated to remove the mature biofouling for a treatment period of 1 minute using the apparatus of Figu-

re 2(a). A single chamber was used for the reported testing, powered by a single transducer. The transducer was driven in continuous wave mode at 70 kHz, with a power amplifier supplying 100 W to the single transducer. The target surface area that was covered by the cleaning chamber at any given time was 36 cm^2, whilst the area of the sample plates was 100 cm^2 (the plates measured 10 cm by 10 cm). That means that, to cover the entire plate, the device was continuously moved over the plate containing established mature biofoulant placed for 1 minute, during which time any section might be covered for 25% of the time.

The rms acoustic pressure amplitude that could be generated over the treated surface was measured prior to testing, using a plate of the material through which a hydrophone just protruded into the water, such that its active element was aligned with the surface to be cleaned. The rms acoustic pressure over steel was 16.8 kPa, over aluminium was 17.3 kPa, but over rubber was much less, at 11.2 kPa.

These values confirm that the cleaning process here occurred by non-inertial cavitation (since inertial cavitation would have required an rms acoustic pressure in excess of 100 kPa). The rubber significantly reduced the rms pressure that could be generated across it, as expected because it is more absorbent than the metals (both in terms of not reflecting the sound back into the water to the same extent that the metals do, and absorbing a portion of the sound that enters it by converting it to heat). Nevertheless, good cleaning was still possible because the rigid walls of the chamber assisted in the formation of 11.2 kPa rms acoustic pressure on the surface of the rubber.

By design, the device is capable of cleaning samples while submerged. For this study, however, a risk assessment required that samples be removed from the sea water to be cleaned as the amplifier and high-voltage power supply did not have a sufficiently high water-proofing rating.

The thickness of the remaining biofouling after the treatment was measured in 10 places on each plate, and an average thickness calculated. The difference between the initial and final thickness measurements was calculated and expressed as a percentage value for the biofoulant that was removed from the plate surfaces.

A subset of plates were subjected to a conventional cleaning treatment using an electrically powered rotary brush for a period of 1 minute rather than acoustic energy in accordance with the present invention. The % thickness reduction was again calculated, and the results shown in Table 1.

(III) MEASUREMENT METHODS FOR THE MARINE SAMPLES

The thickness of mature marine biofouling before and after treatment was measured at multiple sites on each tested plate using an Episcopic Differential Interference Contrast (EDIC) microscope. This microscope works by having the light source and DIC prisims above the sample, meaning it is possible to measure growth on solid surfaces. The depth of field on an EDIC microscope is very narrow and as a result it is possible to focus on the top of the biofouling, the sample or anywhere in between. What this allows is for a technique whereby focussing the microscope on the base of the sample and setting an origin, it is then possible to move the sample down until the top of the sample is in focus. The difference between the 2 points, which is measured by the microscope stage, is the thickness of the foulant at this point. As the biofouling spread is heterogenous over the surface of the sample it was necessary to measure the thickness at several points. Doing this for 10 points on every plate was sufficient to quantify statistically significant results.

2(B) WOUND TREATMENT METHOD

Both devices described in this paper transmit sound and microbubbles through water to the target. However, whereas the water for the marine biofoulant invention takes the form of a cushion, giving a few millimetres stand-off of the solid cleaner from the target, the second device increases the stand-off to several centimetres by using a water stream. This LAS (Liquid Acoustic Stream) device uses a gentle stream of saline,[25] flowing to the surface at around 2 litres/minute, with a stand-off distance of around 1 cm (Figure 3). This is so that the device can efficiently treat the varying topography of a wound bed, whilst

avoiding contact with the wound. By doing this, as opposed to immersing the wound in saline, the device can treat the wound *in situ*.

Until regulatory approvals are obtained to use the device on patients, the studies in this paper are performed on a recognised model for human skin used for *in vitro* wound studies. In this study, two types of wound model were used, pig trotters and human full thickness EpiDerm tissues, to demonstrate cleaning. Pig trotter wounds infected with *Pseudomonas aeruginosa* pMF230 were cleaned with LAS and compared to untreated control samples.

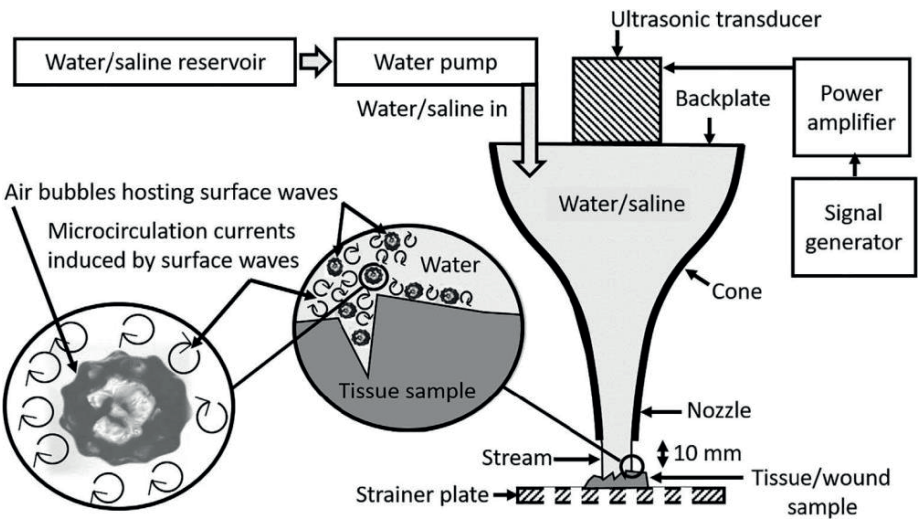

Figure 3. Schematic of liquid acoustic wound stream (LAS) system. Schematic diagram of the experimental set up for the LAS system cleaning a tissue or wound sample. The two inserts demonstrate the ultrasonically induced activity of the air bubbles that is associated with the cleaning effects of the LAS. The diagram is adapted from Malakoutikhah et al. 2020,[8] Chong et al. 2021[32] and Secker et al. 2022.[25]

It is well-recognised in clinical practice that if a wound is cleaned by removal of a biofilm, healing becomes more likely. However, one question of key importance is whether additional healing mechanisms can be stimulated during treatment, effectively enhancing the skin's own healing mechanisms that have stalled during the inflammatory stage within a chronic wound. To do this, the cleaning element must be removed from the LAS test,

since the aim was to observe whether there is any healing over and above that aided by the cleaning. To demonstrate healing, pig trotters are unsuitable, as they are dead and will no longer heal. Hence for the healing tests, pre-wounded reconstituted human epithelial tissues (EpiDerm Full Thickness, MatTek Corp., Ashland, Massachusetts) were wounded and kept in sterile conditions for 7 days. One set were untreated as a control, another set of alternative controls were treated with 0.9% saline only flowing through LAS (without the acoustics), and one set were subjected to LAS treatment. The cost of the EpiDerm Full Thickness samples meant that only triplicate repeats were affordable in this experiment.

After treatment, the EpiDerm Full Thickness samples were histologically processed and examined microscopically following Haematoxylin and Eosin (H&E) staining.

The main set-up for the LAS device, as used in the *in vitro* tests of this paper, is detailed in Figure 3, with full details of the experiment given in an earlier paper.[25] Confirmation that this device does not produce inertial cavitation on the target, was obtained through observation that it produced no sonoluminescence, no foil pitting, and no release of free iodine from KI solution.

Such stream technology had been used on a range of substrates prior to testing on this model of human skin. Previously, its 132 kHz ultrasound efficacy to remove contaminants from hard inert surfaces was shown for a range of applications, including cleaning baby equipment,[9] railway components[26]-[27]-[28], surgical instruments[29],[30] and tools,[26] bone prior to transplant[30] and pipework/packaging associated with food and beverages.[9,5,26,][31] Food itself has been cleaned without damage (including salad[32] and hay[33]), as have other soft targets including hands.[26]

Both hard (e.g. particulate[26-27-28]) and softer contaminants have been removed. Softer ones include glues,[26] greases[27] and lubricants[8], amyloid prion in brain tissue,[29,30] and biofilms (including those associated with dental[30,][34], marine[35] and gastronomic[32,33] surfaces). The effective tackling of biofilms using only sound, air and water meant that, unlike the use of conventional antimicrobial treatments (antibiotics, antivirals, antifungals etc.), the use of such technology should not so readily pro-

mote the rise of AntiMicrobial Resistance (AMR), which is projected to be killing more people than cancer by 2050, and have cost the world economy more than the current size of the global economy.[31,][36],[37]

3. RESULTS

3(A) HULL PLATE CLEANING RESULTS

Table 1 shows that, for each of the three materials tested (steel, aluminium and rubber), the treatment time of only 1 minute achieved a high percentage removal of the mature macroscopic biofouling.

Furthermore, Table 1 shows that for the steel and rubber plates the use of acoustic energy provided improved cleaning as compared to brushing. For aluminium, the biofouling thickness reductions were similar for ultrasonic and brush cleaning, except that the aluminium surface was significantly damaged, demonstrating scratches caused by the bristles of the brush (Figure 4). The brush was also mechanically damaged and required replacement. The rubber plate was also damaged by the bristles of the brush (Figure 5(a)), and the brush similarly damaged by the rubber (Figure 5(b)).

Table 1. Comparison of the effectiveness of removing macroscopic marine biofouling, from three hull materials. The results for the ultrasonic invention are compared with those from an electrically powered mechanically rotating brush.

	Percentage thickness reduction of mature biofoulant:	
	…as a result of ultrasonic treatment (+/- 1 standard deviation)	**…as a result of using a mechanically rotating brush device (+/- 1 standard deviation)**
Steel	91 (+/- 4)	40 (+/- 12)
Aluminium	94 (+/- 3)	97 (+/- 1)
Rubber	80 (+/- 1)	64 (+/- 1)

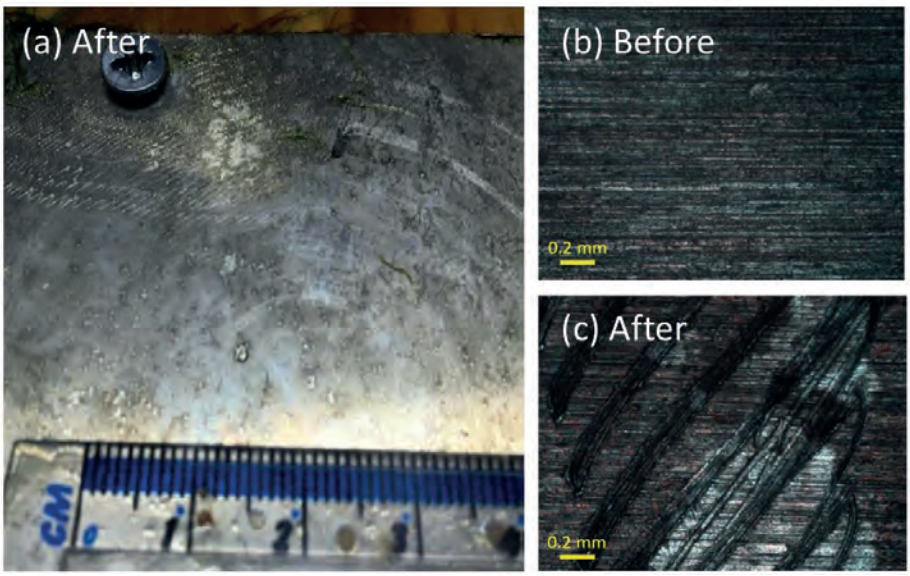

Figure 4. Photographs of surface damage to the aluminium caused by rotary brushing. Panels (a) and (c) show the condition of the aluminium surface after cleaning, at low and high magnification respectively. For comparison, panel (b) shows the aluminium surface before cleaning, at high magnification.

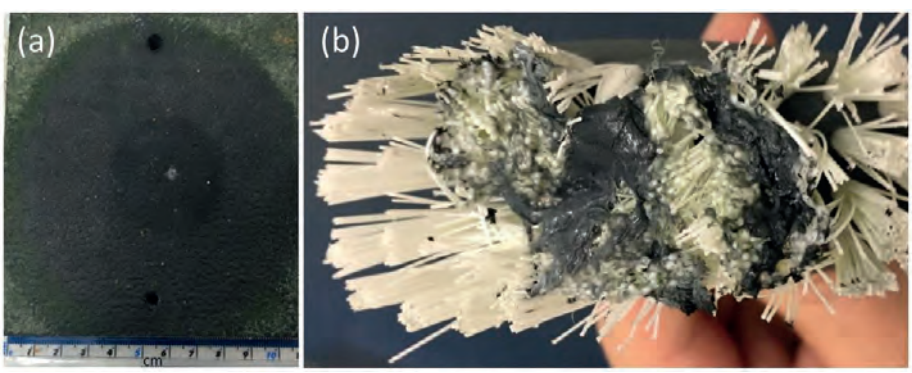

Figure 5. Photographs of (a) surface damage to the rubber caused by rotary brushing, and (b) the damage done to the brush by the cleaning undertaken in (a).

3(B) WOUND TREATMENT RESULTS

Figure 6 shows the results of cleaning biofilm of *Pseudomonas aeruginosa pMF230* from wounded pig trotters, after it had been cultured on the wound bed for 5 hours. Compared with the unwashed control wound beds, washing with saline alone had

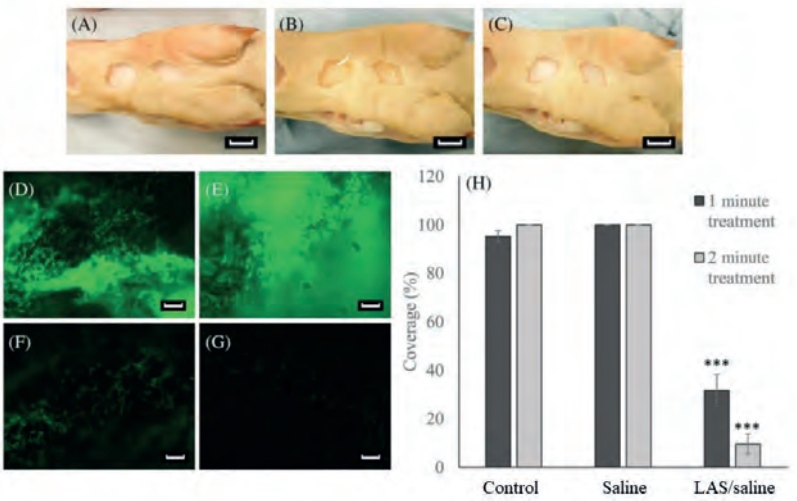

Figure 6. Pig trotter wound model. Example images of (A) _2 cm diameter wounds produced within frozen/thawed pig trotters before inoculation, (B) post inoculation of Pseudomonas aeruginosa pMF230 incubated at 37 Celsius for 5 hours, and (C) post 2 min liquid acoustic wound stream (LAS) treatment. Scale bars represent 2 cm. Representative episcopic differential interference contrast/EpiFluorescence (EDIC/EF) micrographs of green fluorescent protein (GFP)-tagged P. aeruginosa biofilms in (D) the control (untreated wounds), (E) after a 1 minute saline wash at a flow rate of 2 L/min, (F) after a 1 minute LAS treatment at a flow rate of 2 L/min, and (G) after a 2 minutes LAS treatment at a flow rate of 2 L/min. Scale bars represent 10 μm. Image analysis (H) of the EDIC/EF micrographs demonstrating the residual percentage coverage of GFP tagged P. aeruginosa pMF230 within the pig trotter wounds after 5 hour incubation at 37 Celsius: control (untreated wounds), after a 1 or 2 minutes saline wash at a flow rate of 2 L/min (saline) and after a 1 or 2 minutes LAS treatment at a flow rate of 2 L/min (LAS/saline). Error bars represent the SEM (n = 3), One-Way analysis of variance/Tukey post-hoc test demonstrated ***P ≤ .001 when compared with the untreated controls. Reproduced from Secker et al. 2022.[25]

no significant effect on the residual coverage of GFP tagged bacteria in the model. Washing with LAS for 1 minute reduced the coverage by 73% and washing for 2 minutes resulted in a 90% reduction.

Figure 7 shows the results of examination of the H&E-stained sections of uninfected wound models, which allowed measurement of the length of the tongue of reepithelialisation. The EpiDerm FT wound model is known to heal with the addition of hu-

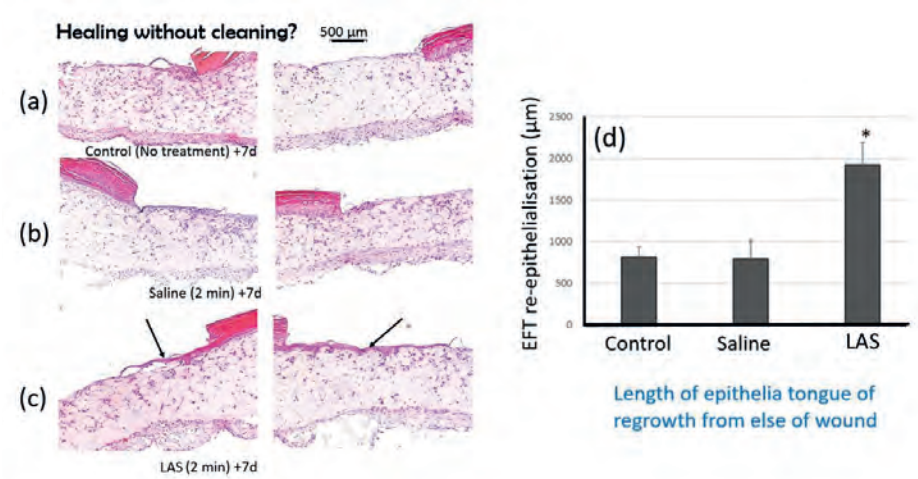

Figure 7. Epiderm full thickness (EFT) wound models that have been wounded (note there is only partial coverage of each sample by the upper (outer) layer), and presented here as Haematoxylin and Eosin (H&E) stained sections from the EFT wound models. The sections are 4 µm thick. The wounds were kept clean after wounding and imaged here after 7 days. The upper row (a) shows two control samples having no treatment. The middle row (b) shows two samples that were treated for 2 minutes after wounding by a saline stream run at 2 L/minute through the device, but without the sound activated. The lower row (c) is treated exactly the same as for row (b), but this time with the sound activated. The black arrows in the micrographs in row (c) highlight the re-epithelialisation tongue observed in these sections. Panel (d) shows data from image analysis measurements (E) of the extent of reepithelialisation 7 days post treatment are shown. Error bars represent the SEM (n = 3), One-Way analysis of variance/Tukey post hoc test demonstrated *P ≤ .05 when compared with the non-treated controls. Reproduced from Secker et al. 2022.25

man growth serum, and measurement of the length of the tongue is a method of quantifying healing within this model. There was no significant difference in tongue length between the control (no wash) and saline washed samples but the difference between the LAS treated models and the controls was significant (P ≤ .05). No acoustically-derived damage to the EpiDerm FT was seen in microscopic examination of the histological sections.

4. CONCLUSIONS

This paper introduced two inventions. The first is a marine hull cleaner to remove macroscopic biofouling. Having previously[1] tested the ability of the device to prevent the build-up of mature marine biofouling, the current study tested its ability to remove mature biofouling.

The data in Table 1 demonstrates that the method and apparatus of the present invention is highly effective at removal of mature biofouling. The removal by the ultrasonic device was significantly greater than removal observed by the rotating brush for the same treatment time, except for aluminium, where statically there was no difference in their cleaning performance.

After use, the brush was so badly damaged that it could no longer be used. Furthermore, the samples that were brushed showed scratches and damage to all three materials, particularly the rubber. No damage could be detected, either through visual or microscopic examination, of the samples that were cleaned using the ultrasonic device, and no damage was sustained to the ultrasonic device during these tests.

The second device was a wound cleaner, with a smaller contact footprint and a stand-off distance of 1 cm, to cope with the varying topography of a wound and the safety requirements of the patient and usability for the healthcare worker. It operates using only non-inertial cavitation to avoid damage to the wound bed. In addition to cleaning wounds, there was preliminary evidence that the device could stimulate wound healing over and above the beneficial treatment caused by cleaning.

ACKNOWLEDGMENTS

The authors are grateful to C. Harling, D. Voegeli and C. W. Keevil for their contributions to obtaining the wound healing data, and consequently were full authors on the paper[25] that this manuscript quotes. A. Westley undertook hull cleaning work as part of a MSc project at the University of Southampton.

REFERENCES

[1] T. G. Leighton, M. Zhu, C. N. Dolder, T. Secker and A. Westley, "Three linked inventions to mitigate marine biofouling, hospital decontamination, and currently incurable wounds using air, sound and water without chemicals" Proc. Meetings of Acoustics, 47, 032001 (10 pages) (2022).

[2] T. G. Leighton, "The Acoustic Bubble," Academic Press, 640 pages (1994).

[3] A. O. Maksimov and T. G. Leighton, "Transient processes near the threshold of acoustically driven bubble shape oscillations," Acta Acustica, 87(3), 322-332 (2001).

[4] A. O. Maksimov and T. G. Leighton, "Pattern formation on the surface of a bubble driven by an acoustic field," Proceedings of the Royal Society A, 468, 57-75 (2012).

[5] T. G. Leighton, A. J. Walton and M. J. W Pickworth (1990) Primary Bjerknes forces, *European Journal of Physics*, **11**, 47-50.

[6] A. O. Maksimov and T. G. Leighton (2018) Acoustic radiation force on a parametrically distorted bubble. *J. Acoust. Soc. Am.*, **143**, 296-305.

[7] T. G. Leighton, "Cold water cleaning in the preparation of food and beverages: The power of shimmering bubbles," Baking Europe (Summer issue) 24-28 (2018).

[8] M. Malakoutikhah, C. N. Dolder, T. J. Secker, M. Zhu, C. C. Harling, C. W. Keevil and T. G. Leighton, "Industrial lubricant removal using an ultrasonically activated water stream, with potential application for Coronavirus decontamination and infection prevention for SARS-CoV-2," Transactions of the Institute of Metal Finishing 98(5), 258-270 (2020).

[9] T. G. Leighton, "Bubble Acoustics: From whales to other worlds," Proc. Institute of Acoustics 36(3), 58-86 (2014).

[10] R. Knight, 'The Introduction of Copper Sheathing into the Royal Navy, 1779-1786', *Mariner's Mirror*, 59, 299-309 (1973).

[11] F. B. Laidlaw, 'The history of the prevention of marine biofouling', in *Marine fouling and its prevention; prepared for Bureau of Ships, Navy Dept.*, Ketchum, B.H. and Redfield A.C., Eds, George Banta Publishing Co., Mensha, WI, 1952, 211 -223.

[12] J. P. Vischer, 'Nature and extent of fouling of ships' bottoms', *Bulletin of the United States Bureau of Fisheries*, 43(1), 193-252 (1927).

[13] R. L. Townsin, "The ship hull fouling penalty," Biofouling, 19(Suppl) pp. 9-15 (2013).

[14] M. P. Schultz, J. A. Bendick, E. R. Holm and W. M. Hertel, “Economic impact of marine biofouling on a naval surface ship,” Marine biofouling, 27(1), 87-98 (2011).
[15] P. Balcombe, J. Brierley, C. Lewis, L. Skatvedt, J. Speirs, A. Hawkes and I. Staffell, "How to decarbonise international shipping: Options for fuels, technologies and policies" Energy Conversion and Management, 182, 72-88 (2019).
[16] F. B. Laidlaw, A. C. Redfield and L. W. Hutchins, ‘The Effects of Fouling’, in *Marine fouling and its prevention;* prepared for Bureau of Ships, Navy Dept., Ketchum, B.H. and Redfield A.C., Eds, George Banta Publishing Co., Mensha, WI, 3-19 (1952).
[17] J. F. Guest, N. Ayoub, T. McIlwraith, I. Uchegbu, A. Gerrish, D. Weidlich D, *et al.* “Health economic burden that wounds impose on the National Health Service in the UK,” BMJ Open. 7;5(12): e009283–9 (2015).
[18] T. Bjarnsholt, “The role of bacterial biofilms in chronic infections,” APMIS Suppl. 4 ed. 121(136):1–51 (2013).
[19] J.-S. Park and J.-H. Leeb, "Sea-trial verification of ultrasonic antifouling control" Biofouling, 34(1), 98–110 (2018).
[20] B. Martin, A. MacGillivray, J. Wood et al., "Sound emissions from ultrasonic anti-fouling equipment" The Effects of Noise on Aquatic Life (Berlin, Germany, 10-15 July 2022) (Book of Abstracts, page 99) (2022).
[21] J. S. Trickey, G. Cardenas-Hinojosa, L, Rojas-Bracho et al., "Ultrasonic antifouling systems: A novel but increasingly pervasive noise pollutant" The Effects of Noise on Aquatic Life (Berlin, Germany, 10-15 July 2022) (Book of Abstracts, page 165) (2022).
[22] A. N. Popper and T. J. Carlson, "Application of Sound and other Stimuli to Control Fish Behavior" Transactions of the American Fisheries Society, 127(5), 673-707, (1998).
[23] L. S. Weilgart, "The impacts of anthropogenic ocean noise on cetaceans and implications for management" Canadian Journal of Zoology 85(11), 1091-1116(2007)
[24] M. Solan, C. Hauton, J. Godbold, et al., "Anthropogenic sources of underwater sound can modify how sediment-dwelling invertebrates mediate ecosystems properties" Scientific Reports (Nature Publishing Group), 6: 20540 (doi: 10.1038/srep20540) (2016).
[25] T. J. Secker, C. C. Harling, C. Hand, D. Voegeli, C. W. Keevil and T. G. Leighton, “A proof-of-concept study of the removal of early and late phase biofilm from skin wound models using a liquid acoustic stream,” International Wound Journal, 1-22, doi=10.1111/iwj. 13818 (2022).
[26] T. G. Leighton, "The acoustic bubble: Oceanic bubble acoustics and ultrasonic cleaning" Proceedings of Meetings on Acoustics

(POMA), Acoustical Society of America, 24 (070006) doi: 10.1121/2.0000121 (2015).

[27] T. G. Leighton, "The acoustic bubble: Ocean, cetacean and extra-terrestrial acoustics, and cold water cleaning", Journal of Physics: Conference Series 797, 23 pages, ISBN: 1742-6596, doi: 10.1088/1742-6596/797/1/012001 (2017).

[28] L. R. Goodes, T. J. Harvey, N. Symonds, and T. G. Leighton, "A comparison of ultrasonically activated water stream and ultrasonic bath immersion cleaning of railhead leaf-film contaminant," Surface Topography: Metrology and Properties, 4, 6 pages, doi: 10.1088/2051-672X/4/3/034003 (2016).

[29] T. J. Secker, T. G. Leighton, D. G. Offin, P. R. Birkin, R. C. Herve and C. W. Keevil, "A cold water, ultrasonic activated stream efficiently removes proteins and prion-associated amyloid from surgical stainless steel," Journal of Hospital Infection, 106(4), 649-456 (2020).

[30] P. R. Birkin, D. G. Offin, C. J. B. Vian, R. P. Howlin, J. I. Dawson, T. J. Secker, R. C. Herve, P. Stoodley, R. O. C. Oreffo, C. W. Keevil, and T. G. Leighton, "Cold water cleaning of brain proteins, biofilm and bone–harnessing an ultrasonically activated stream," Physical Chemistry Chemical Physics 17, 20574-20579 pages, doi: 10.1039/C5CP02406D (2015).

[31] T. G. Leighton, "Climate change, dolphins, spaceships and antimicrobial resistance: the impact of bubble acoustics," Proceedings of the 24th International Congress on Sound and Vibration ICSV24, London, United Kingdom, 23-27 July 2017, Editor: B. Gibbs, 6 pages, ISBN: 978-1-906913-27-4 (2017).

[32] W. Y. Chong, T. J. Secker, C. N. Dolder, C. W. Keevil and T. G. Leighton, "The possibilities of using Ultrasonically Activated Streams to reduce the risk of foodborne infection from salad," Ultrasound in Medicine and Biology, 46(6), 1616-1630 (doi: 10.1016/j.ultrasmedbio.2021.01.026) (2021).

[33] W. Y. Chong, C. Cox, T. J. Secker, C. W. Keevil and T. G. Leighton, "Improving livestock feed safety and infection prevention: Removal of bacterial contaminants from hay using cold water, bubbles and ultrasound," Ultrasonics Sonochemistry, 71, article 105372 (6 pages) (doi: 10.1016/j.ultsonch.2020.105372) (2021).

[34] R. P. Howlin, S. Fabbri, D. G. Offin, N. Symonds, K. S. Kiang, R. J. Knee, D. C. Yoganantham, J. S. Webb, P. R. Birkin, T. G. Leighton, and P. Stoodley, "Removal of dental biofilms with an ultrasonically activated water stream," Journal of dental research 94, 1303-1309 pages, doi: 10.1177/0022034515589284 (2015).

[35] M. Salta, L. R. Goodes, B. J. Maas, S. P. Dennington, T. J. Secker, and T. G. Leighton, "Bubbles versus biofilms: a novel method for

the removal of marine biofilms attached on antifouling coatings using an ultrasonically activated water stream," Surface Topography: Metrology and Properties, 4, 10 pages, doi: 10.1088/2051-672X/4/3/034009 (2016).

[36] T. G. Leighton, "Can we end the threat of anti-microbial resistance once and for all?," Science in Parliament, 74, 29-32 (2018).

[37] T. G. Leighton, "To stop AMR once and for all: stop killing the bugs!," November 2017, Available: https://epsrc.ukri.org/blog/stopamr/ (2017) (last accessed 22 July 2022).

CZESŁAW DYRCZ
Polish Naval Academy

SOUND PROPAGATION IN WATER — OVERVIEW OF RELEVANCE FOR THE SEARCH FOR SUBMARINES

ABSTRACT

Sound propagation in water is an important factor affecting submarine search operations in dive position. Knowing the distribution of sound propagation in seawater is essential for both submarines and surface ships in anti-submarine warfare (ASW) operations. The article is a review and presents examples of sound wave propagation emitted from surface and submarine ships during sea search operations. The aim of the article is to illustrate the propagation of sound waves in sea water depending on the location of the source of sound emitted by surface ships or submarines. Of course, the presented examples are general in nature, typical for ideal images of sound propagation and do not take into account their variability that occurs in real situations.

KEYWORDS: sound propagation in sea water, refraction of sound waves, underwater sound channel

1. INTRODUCTION

The characteristics of the sound propagation in sea water is a feature of significant importance for navies. The sund propagation in water in the conditions of navies is associated with ASW, which is an activity related with the use of surface warships,

aircraft, submarines (Figure 1), or other platforms – nowadays and in nearest future unmanned autonomous vehicles (UAVs), to find, track, deter, damage, and/or destroy other submarines. The sound propagation in the area of operation it is important for both submarines and surface ships.

Figure 1. The Polish KILO class submarine ORP *Orzeł*
(Source: Photo – C. Dyrcz)

Sound propagation in water is a function of its velocity. And velocity is a function of water density and compressibility. As such, sound velocity is dependent upon temperature, salinity, and pressure and is normally derived expressing these three variables. The speed of sound in water changes by 3–5 metres per second per °C, by approximately 1.3 metres per second per PSU (Practical Salinity Unit) salinity change, and by about 1.7 metres per second per 100 m change in depth (compression). The speed of sound in seawater increases with increasing pressure, temperature, and salinity (and vice versa) [1].

Sample curves of temperature, salinity and density compared with depth are shown in Figure 2.

$$\frac{\sin\varphi}{\sin\psi} = \frac{c_1}{c_2} \tag{1}$$

where:
φ – an angle of incidence,
ψ – an angle of refraction,
c_1 and c_2 – speed of sound waves propagation in adjacent layers of water with different values of temperature, salinity, and pressure [4].

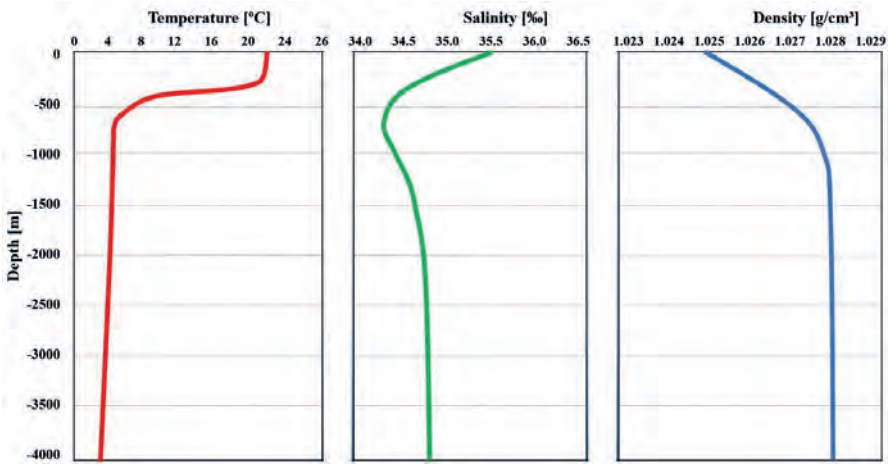

Figure 2. Sample curves of temperature (red), salinity (green) and density (purple) with depth

It follows from equation (1) that if the sound velocity in the second layer is lower than in the first, the ray direction will decrease and the sound ray will deflect towards the seabed. On the other hand, if the speed of sound in the second layer is greater than in the first, the direction of the ray will increase and the ray of sound will deviate away from the seabed. Depending on the speed of sound in the water, the direction of the sound ray propagating in the individual layers of water changes as it moves from layer to layer. In hydroacoustic, this phenomenon is called refraction of sound waves. The dependence of refraction on the speed of sound in water is shown in Figure 3.

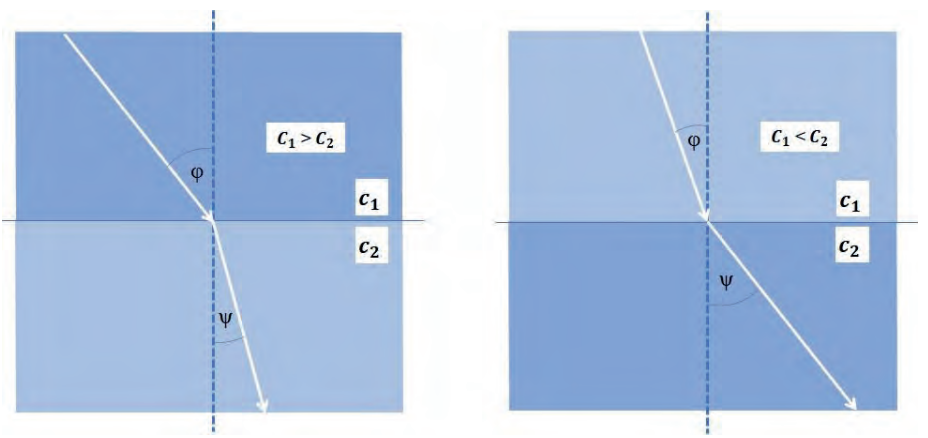

Figure 3. Refraction of sound waves in layers of water [4]

In shallow waters, the nature of refraction depends mainly on the temperature distribution, and in some cases also on salinity. In deep water, regardless of temperature and salinity distributions, hydrostatic pressure has a large influence on the nature of refraction. An example of the sound speed distribution made in shallow water (Baltic Sea) in the summer on July 22, 2022 is shown in Figure 4.

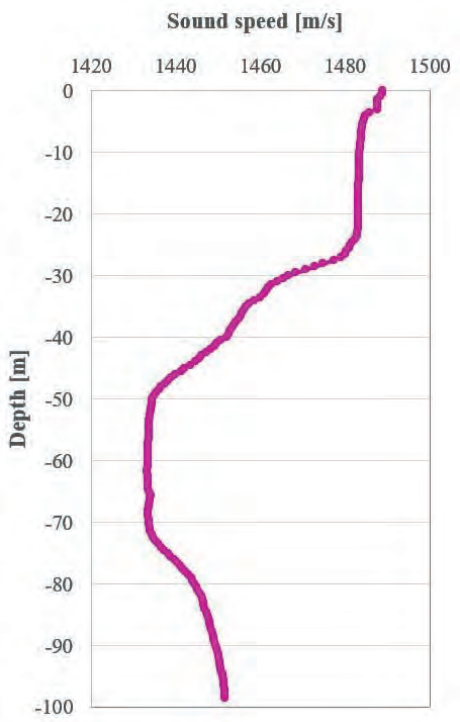

Figure 4. An example of the sound speed distribution made in shallow water (Baltic Sea) on July 22, 2022

Typical deep-sea sound profiles (Atlantic Ocean) are illustrated in Figure 5.

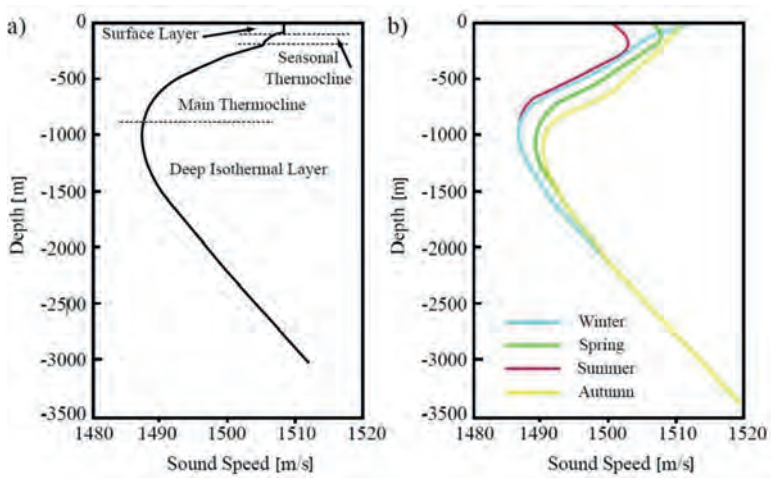

Figure 5. Typical deep-sea sound speed profiles. (a) Profile showing layer structure of the sound speed in the water due to temperature variations (b) Average sound speed profiles in different seasons in an area halfway between Newfoundland and Great Britain [5]

2. THE TYPE OF SOUND PROPAGATION IN SEA WATER AND ITS IMPORTANCE FOR SUBMARINES

Depending on the hydrological conditions, the following types of sound propagation in water occur:

- Linear propagation,
- Negative refraction,
- Positive refraction,
- Underwater Sound Channel (USC).

In the article, the figures below present the ideal distributions of sound propagation in water, which is a simplification used to clearly illustrate the individual types of propagation. In real conditions, the variation in the speed of sound in water is significant [2, 3].

Linear propagation – is a characteristic phenomenon for shallow water areas, especially in the autumn and winter season. As a result of the mixing process, the temperature of the water in the layer equalizes from the surface to the bottom. Such conditions may also arise in summer with an intensive mixing process during storms. During these hydrological conditions, when the speed of sound is constant, the phenomenon of refraction does not occur, and the sound rays propagate linearly. Linear propa-

gation of sound from the position of the submarine and the surface ship is illustrated in the Figures 6 and 7 below. These are good detection conditions in both cases. However, it does happen in shallow waters.

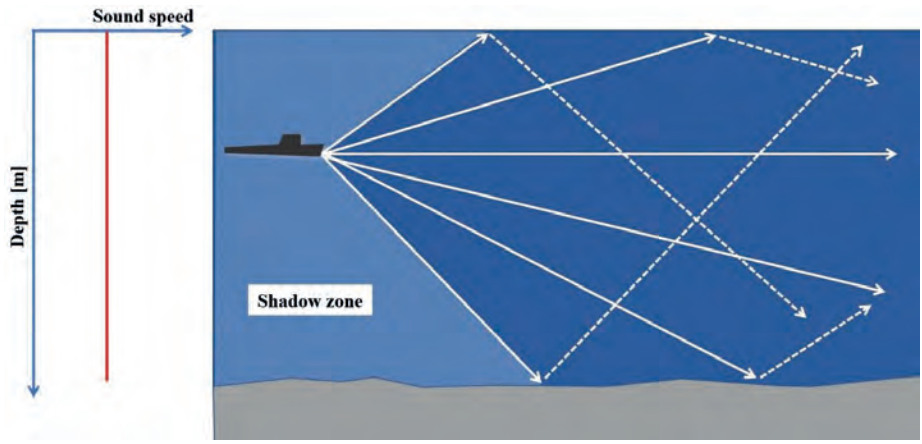

Figure 6. Linear propagation of sound waves from a submarine [3]

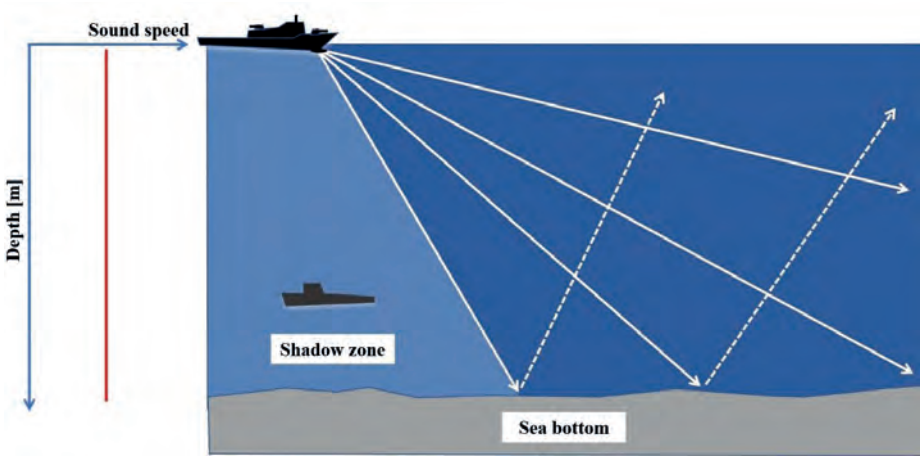

Figure 7. Linear propagation of sound waves from a surface ship [3]

Positive refraction – it is characteristic for deep-water areas, where surface waters cool down during autumn and winter and the influence of hydrostatic pressure on the speed of sound is large. The speed of the sound increases with the depth. Sound waves coming from the sound source deflect towards the surface of the sea, are then reflected and then return through the water

depth to the surface. With this refraction, there are favorable conditions for the propagation of sound in the water. Positive refraction is beneficial for conducting ASW operations. The phenomenon of damping and absorbing sound energy by water is the result of shortening the sound range. The positive refraction of sound waves in the water from the position of the submarine and the surface of the sea is illustrated in Figures 8 and 9 below.

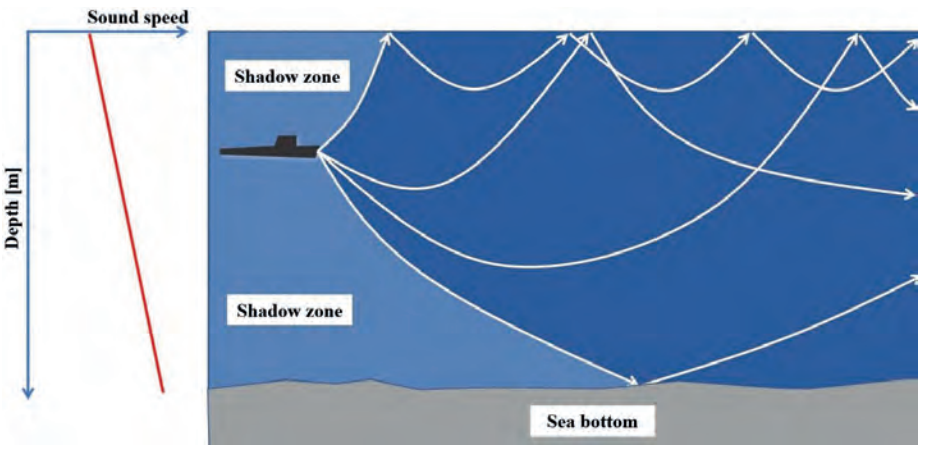

Figure 8. Positive refraction of sound waves from a submarine [3]

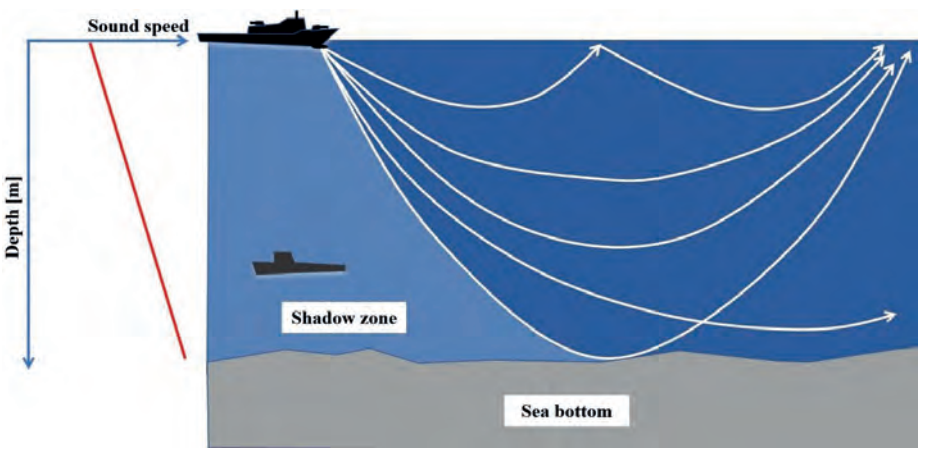

Figure 9. Positive refraction of sound waves from a surface ship [3]

Negative refraction – occurs when a decrease in the speed of sound in the water causes the sound rays to deflect towards the seabed (towards lower velocity values). It occurs in shallow

waters during spring and summer, when the surface layer of water is strongly heated and the speed of sound reaches the highest value on the surface, and the depth dimension decreases. Sound rays come out of the sound source, deflect towards the seafloor, reflect off it and deflect again. In the case of negative refraction, the range of sound in water is the smallest and there are shadow zones that cannot be reached by sound rays. Negative refraction is an unfavourable phenomenon in ASW. The negative refraction of sound waves in the water from the position of the submarine and the surface of the sea is illustrated in Figures 10 and 11 below.

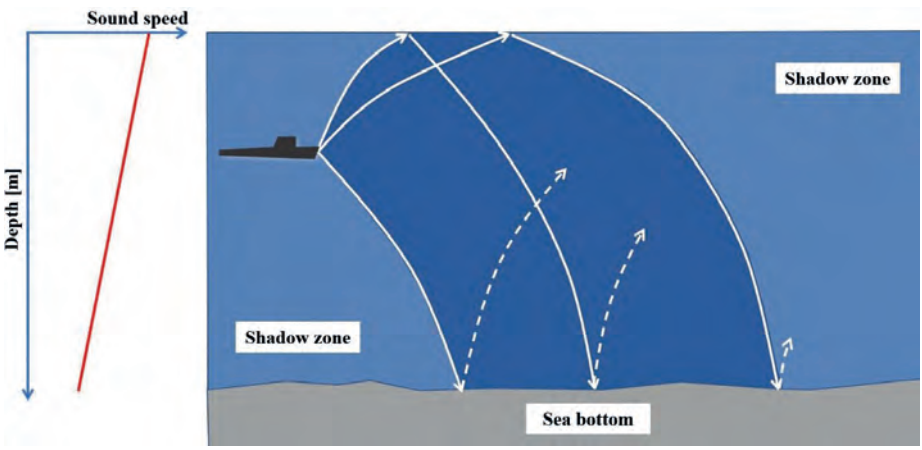

Figure 10. Negative refraction of sound waves from a submarine [3]

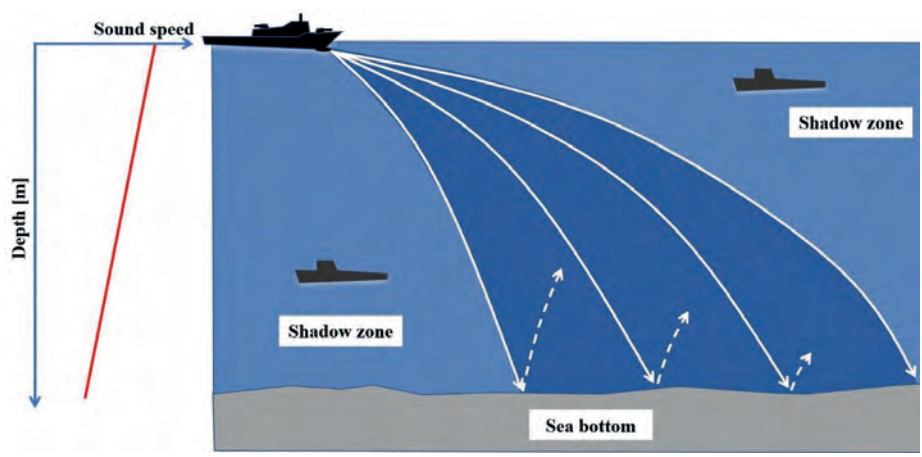

Figure 11. Negative refraction of sound waves from a surface ship [3]

Underwater Sound Channel (USC) – occurs in conditions where in the upper layer of sea water the sound velocity distribution is determined by negative refraction, and in the lower layer – by positive refraction. A characteristic feature of the underwater sound channel is the existence of a layer at a certain depth with a minimum value of the speed of sound. This layer is called the axis of the underwater sound channel. Due to changes in the refractive nature, sound rays experience multiple full internal reflection on both sides of the channel axis. If the sound source is placed close to the channel axis, the hearing range is extremely large. The range of sound in the underwater sound channel areas is up to several thousand nautical miles. Underwater sound channel from the position of the submarine and the surface of the sea is illustrated in Figures 12 and 13 below.

An underwater sound channel is formed in the oceans and open sea areas, when there is a constant or seasonal warm water layer, the speed of sound slows down and then increases. Underwater sound channels exist at depths of up to several hundred meters, however, subsurface sound channels are observed at depths of 10 to 60 m. This is the case, for example, in the Baltic Sea.

The phenomenon of super-long ranges related to the propagation of sound in the underwater sound channel was used to build a distance determination system based on measuring the differ-

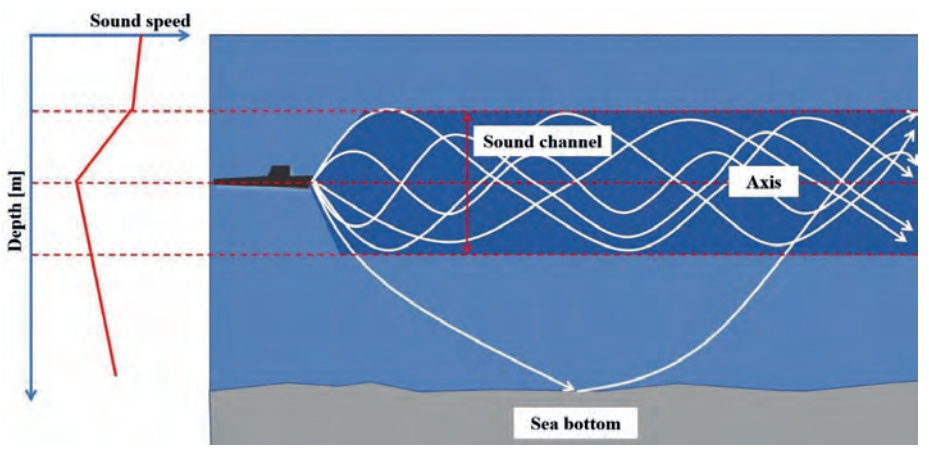

Figure 12. Underwater sound channel from a submarine [3]

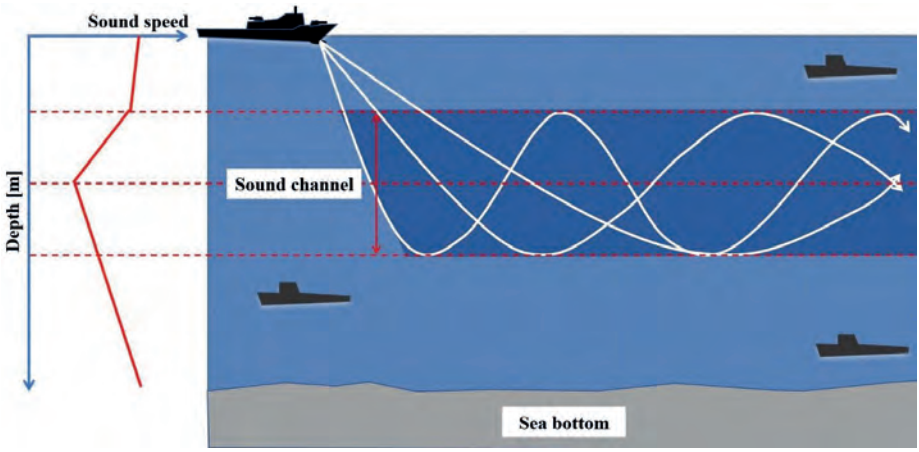

Figure 13. Underwater sound channel from a surface ship [3]

ences in the arrival time of a sound pulse called the Sound Fixing and Ranging (SOFAR). The system was developed during World War II and was used by the US Navy. Currently, the system is being developed not only in military applications, mainly for ASW, but also for the identification of earthquakes and other events.

Positive refraction in the upper layer and negative in the lower layer – this is the opposite of the underwater sound channel formation conditions and at a certain depth there is a maximum value of the speed of sound. Above we have positive refraction and below negative refraction. In the layer with positive refraction, there are conditions for distant sound propagation. This situation is referred to as the **near-surface sound channel**. Positive refraction in the upper layer and negative in the lower layer from the position of the submarine and the surface of the sea is illustrated in Figures 14 and 15 below.

The examples of refraction presented above have been simplified, because in fact, due to the complicated shapes of the sound velocity profiles, the images of sound rays are more complicated. The energy of sound waves propagating in the sea water environment is weakened by the process of absorbing and dispersing sound in the water [3].

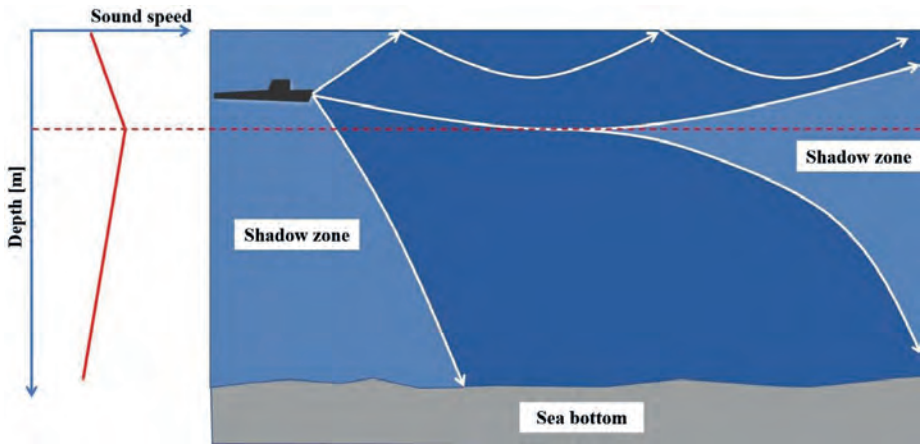

Figure 14. Positive refraction in the upper layer and negative in the lower layer from a submarine [3]

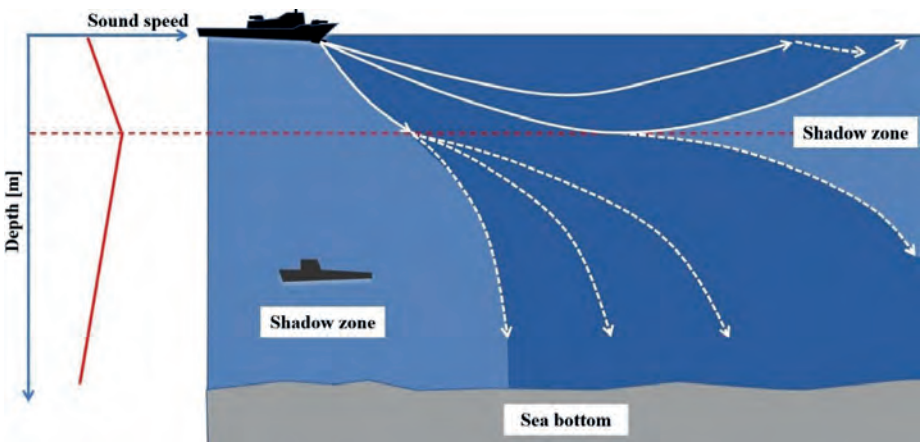

Figure 15. Positive refraction in the upper layer and negative in the lower layer from a surface ship [3]

3. CONCLUSION

Knowing the speed of sound in seawater at a particular location is essential for naval search for submarines. The above-presented examples of refraction dependent on the sound velocity distribution include the idea of tactical use of this phenomenon in the conducted operations. It emphasizes the importance of this phenomenon for both surface forces and submarines. The considered phenomenon is necessarily taken into account during

hydrographic works. When performing hydrographic measurements with the use of sonars, the sound speed distributions should be measured each time before and after the measurements, because refraction, especially at a large penetration angle, can cause large errors in determining the position of objects. For the above-described operations, the measurement of sound speed before commencement of operations is of particular importance.

REFERENCES

1. Christ R. D. and Wernli R. Sr., *The ROV Manual. A User Guide for Remotely Operated Vehicles*, Second Edition, Butterworth-Heinemann 2014.
2. Duxbury A. C., Duxbury A. B., Sverdrup K. A., Oceany świata, Wydawnictwo Naukowe PWN, Warszawa 2002 [available in Polish].
3. Dyrcz C., Oceanography for students of the Polish Naval Academy, Polish Naval Academy, Gdynia 2022.
4. Holec M., Wiśniewski B., *Zarys oceanografii Cz. 1. Statyka morza,* WSMW, Gdynia 1983 [available in Polish].
5. Simao N., Seismicity of the Mid-Atlantic Ridge in the MoMAR area at a regional scale, observed by autonomous hydrophone arrays, Geophysics, Universite de Bretagne occidentale – Brest 2009.

LECH ROWINSKI
Gdansk University of Technology
rowinski@pg.edu.pl

HIGH RESOLUTION IMAGING OF SEA-BOTTOM, WHAT THE EYE DOESN'T SEE, THE HEART DOESN'T GRIEVE OVER

Objective of this article is to emphasise importance of work of inventors and scientists that work on development of tools (sonars) that allows for imaging features of water space that is invisible for human senses. The article indicate extent of damage of sea-bottom environment resulting from fishing activity. This activity performed for centuries results in substantial reduction of valuable biological productivity of Batlic Sea waters. The reason was lack of means that allows for easy look into the depths. One of the tool that can be used to evaluate this activity in real time, is hydroacoustic imaging using scanning sonars and multibeam echosounders. Acoustic imaging methods were already utilized to indicate the extent of damage to bottom habitats. Particular areas of the bottom are archeological sites (wrecks) that "document" damage done by fishing and mooring activity and to study influence of this activity on sea bottom environment. Results of these studies give impressive information regarding scale of possible influence of fishing activity on sea bottom and its biological conditions as well as real reason for the "overfishing". They also indicate importance of bottom related environmental issues during current and planned extensive offshore activities such as deep sea nodule mining.

INTRODUCTION

While looking from a beach perspective, marine environment seem to be endless and sustainable. It is due to optical phenomena at the water surface like ray reflection, As result, we are not able penetrate the depth with our senses. Momentary appearance of water body depends on weather but finally waved or calm water surface seems always the same and self-healing. This is the reason while people consider the ocean as unlimited source of wealth and unlimited sink for all anthropogenic wastes.

The direct reason for this paper was appearance of the photograph of nesting grounds of Jonah's icefish (*Neopagetopsis ionah*) discovered recently under sea cover of Weddell Sea. This colony of icefish is the largest found to date, stretching across more than 150 miles (240km) of the seabed. The sheer size of the colony 60-million-nests suggests the whole Weddell Sea ecosystem is influenced by these nests. The images show active fish parents that bild nest and take care for their roe. At the same time the author was investigating means of detailed imaging of sea-bottom features. Studies of old wrecks are examples of such activity. Example images of such sites (fig. 4) are really horrifying while put aside to images of Jonah's icefish nesting grounds. Without explanation it is difficult to guess what we see on the fig. 2. I fact it is side scan image of the wreck site. Parallel lines on the image illustrate extent of local fishing activity and magnitude of physical influence to sea bottom caused by this activity. Simply say-

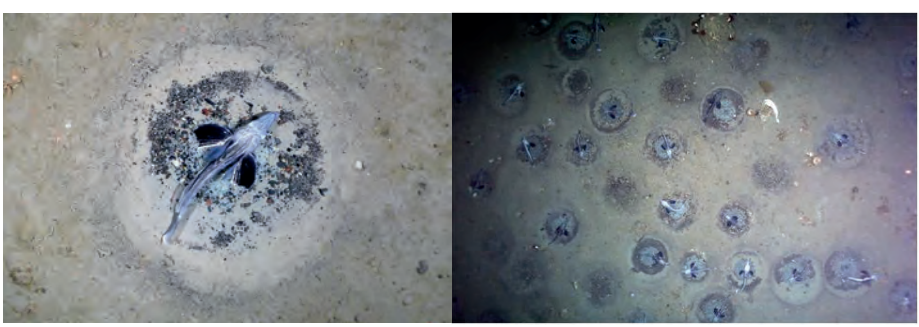

Fig. 1. Photograph of nesting grounds of Jonah's icefish (*Neopagetopsis ionah*) discovered under sea cover of Weddell Sea Alfred Wegener Institute January 14, 2022. (https://scitechdaily.com/spectacular-discovery-in-antarctica-massive-icefish-breeding-colony-with-60-million-nests/)

Fig. 2. Left: A species of cnidarian in the genus Relicanthus with 8-foot long tentacles attached to a dead sponge stalk on a nodule in the eastern Clarion-Clipperton Zone. These are closely related to anemones [1],
Right: Sea bottom covered by manganese modules and invisible layers of bacteria appears as life-less gravel Location: At the Godzilla Mullion in the Parece Vela Basin May 16, 2009
[https://www.jamstec.go.jp/gallery/e/geology/resource/003.html] .

ing, the bottom was deeply ploughed. One can guess the image of nesting grounds of Jonah's icefish if they would not be protected by thick ice. While archeological sites are not usually protected by thick ice cover, they are exposed to damage by fishing activity. In fact majority of sites are badly damaged. Substantial part of human heritage was destroyed this way already. However after being discovered, wreckage remaining are usually studied for many years ad offer quantitative information regarding processes of destruction of both archeological artifacts and surrounding environment.

WHAT IS TECHNOLOGY OF INDUSTRIAL FISHING

Till quite recently the author awareness of industrial fishing technology can be imagined by a trawling net suspended in water space that catches schools of fish possibly detected by trawler's sonar. It is true in some cases, but reality is much more complicated. The list of "fishing" technologies and tools is very long and includes several real strange devices. It starts with bottom trawls illustrated on fig 4 but includes scallop drags that can be seen on fig. 6, left. The dredges consist of a triangular frame, about 750mm wide, with a toothed bar at the front to flip the scallops

out of the seabed and into a collecting bag behind it. This bag is made of chain links forming a chain mesh on the bottom and usually netting on the top. **Several** of these dredges are towed behind a heavy spreading bar, usually one from each side of the vessel. The length of bar and number of dredges is dictated by the power of the vessel and its length of side deck to work the dredges over. The number can vary from 3 or 4 on a small 10m boat up to 18-20 on a 30m vessel with 1500hp engine. It is apparent that fish nesting grounds after fishing for scallops look as can be seen on fig. 6, right. Simply nothing is left intact.

Use of heavy beams to facilitate fishing activity in European waters was confirmed for at least nine century. Environmental awareness of the potentially destructive power of fishing technologies on the marine environment is a centuries-old dilemma. As early as 1376 a

Commons Petition to King Edward III of England complained about a newly introduced fishing gear, the 'wondyrechoun', a "three fathoms long and ten of men's feet wide" state-of-the-art device[3].

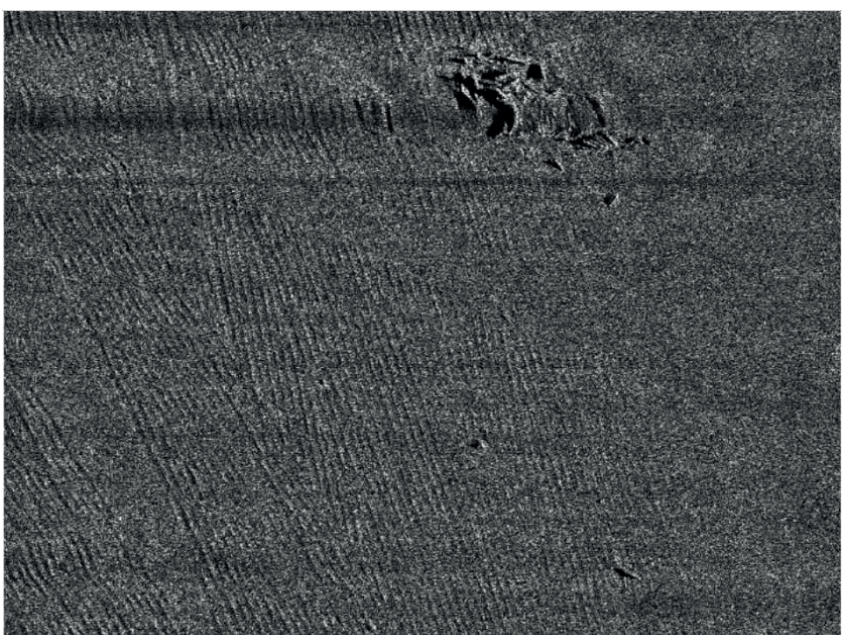

Fig. 3. A side-scan sonar image in the Western Approaches to the English Channel showing furrow lines cut by a scallop dredge boat through a rare shipwreck of c. 1670-90 (Odyssey site 35F). At a depth of 110m,[2]

Fig. 4. A ceramic cargo fallen on one side on a mid to late 19th-centurywooden shipwreck (Site 2T11w24b-1; Target 581). The top edges of the plates have been 'shaved' by a trawler/dredge. Atlas shipwreck survey zone, depth 124.0m.[3]

Fig. 5. Bottom beam trawling by sailing trawler around year 1850[4]. Till year 1980 weight of the trawling gear increased to 30 tons[5] .

Fig. 6. Left: A scallop dredge [6], Right: Result of application of a scallop dredge to bottom environment [7],

"made in the manner of an oyster dredge... upon which instrument is attached a net so close meshed that no fish be it ever so small which enters therein can escape... the great and long iron of the wondyrechoun runs so heavily and hardly over the ground when fishing that it destroys the flowers of the land below water there... the fishermen take such quantity of small fish that they do not know what to do with them; and that they feed and fat their pigs with them, to the great damage of the commons of the realm and the destruction of the fisheries, and they pray for a remedy" (Alward, 1932: xx).

Since development of effective fishing gears and steam powered vessels in nineteen century we face so called "overfishing". It "industrial" fishing developed slowly from 100 000 tons and finally ended at 80 mln tons annual catch. Significant collapse of robbery was inevitable. It is sometimes assumed that introduction local catch quotas is enough to re-build productivity of the fishing ground. While considered extent of damage caused by tens of years of ploughing the bottom there is probably no return to virgin conditions. At least not in short period of time. It is possibly the case of Baltic Sea where this is not really helping. This is because the bottom habitat may not be renovated this way. Knowing extent and longevity of fishing operations on European waters we can easy assume that no one really knows original nestling behaviour of various fish species, that used to live on undisturbed bottom. Unknown mechanically damaged (levelled) bottom features and appreciated by different local species need to be recreated and re-populated by sea-creatures already ceased to exist.

SEA BOTTOM MINING FOR METALS

New potential area of marine large scale industrial activity and appropriately large scale damage to environment, is sea bottom mining or minerals. There are various minerals of interest like metal reach crusts and phosphates. However the most representative to the problem and most abundant are manganese nodules. They cover vast areas of ocean bottom with density of up to 20 kg per square metre. Since sixties of last century they are considered to be "readily available and unlimited" source of more

or less strategic metals. Area of the Clarion-Clipperton Zone, currently under jurisdiction of International Seabed Authority, is mostly considered and prepared for exploitation. It is deep-water plain wider than the continental United States. Should commercial deep-sea mining take place, the controversy over its environmental impacts may be just the beginning. While the ISA's principle of common heritage has legal force, the practical realities of sharing the financial proceeds and environmental issues are not clear. When the Mining Code is approved, more than a dozen contractors could begin commercial extraction there. And there is no legal means to stop this activity.

What would be the ecological consequences of future mining for polymetallic nodules in the deep sea in not really known. Phenomena such as sediment mixing, removal of nodules and sediment plumes that extend influence of activity several kilometre are considered to be of most importance. Some studies are under way in the framework of the European project "Ecological Aspects of Deep-Sea Mining". Scientists from Germany and other European countries have revisited a disturbance experiment conducted 26 years ago in more than 4,000 meter water depth in the eastern equatorial Pacific. They report "that even bacterial activity is still low in the plough tracks"[8].

Despite the great potential for the global metals market, polymetallic nodules remain a great promise. However, the situation may change quickly if the supply of raw materials from land deposits is not able to meet the growing demand. In order to be able to join the international division of labor in this field, it is necessary to constantly analyze the state of the art, define and prepare proposals for solutions. In fact, some 30 years ago, Gdansk University of Technology developed a concept of the mining system for industrial recovery of 5 mln tons of, so called, "wet nodules" annually [9]. The mining complex concept was prepared for the Interoceanmetal organization. It differs from the most frequently considered technologies that use pumping for vertical transport (recovery from depth) of nodules. Large, autonomous, vehicles were intended for collection and vertical transport of nodules. It also adopted a somewhat controversial concept of release of solid ballast to balance the weight of nodules and to propel the vehicle.

he system (while build) would yield 100 000 tons of strategic metals annually at cost of annual destruction of 500 km^2 of sea-bottom and destruction of 10 000 km^2 during 20 years of planned operation. Specific positive aspect of proposal presented by Gdansk University of Technology was idea to replace nodules with solid state ballast (rocks) that would replace nodules as supports for living creatures that require such bases to fix and grow.

Fig. 7. Proposals of manganese nodule mining systems that will cause sea bottom damage and images of this damage similar to that of resulting from bottom fishing with use of contact gears.

HIGH RESOLUTION IMAGING AS A TOOL FOR LARGE SCALE DOCUMENTATION OF CHANGES OF SEA BOTTOM STRUCTURE

It is opportunity to pay tribute to the persons that developed the technology of hydroacoustic and made it available to investigators of environment before bottom habitat is damaged beyond ability of recovery. To make society aware of consequence of industrial activity, is compulsory to illustrate processes and their results, providing citizens with pictures that are easy to understand. Photographic technology was used and can be used for this purpose. This is excellent tool to visualize local phenomena like damages shown on fig. 3 and fig. 5. However, but it is difficult to use photography to document processes that take place on vast areas such as “fishing grounds”. Laser scanners can im-

prove imaging processes in specific circumstances (for example in shallow waters), but hydroacoustic imaging gives best results since many years both in achieved resolution and productivity (area imagined in unit of time). Hydroacoustic imaging of water space started with use echosounder like transducer mounted on side of a ship. First side scanning sonars were transmitting conical beams and were able to show silhouette of a submarine. First side scan imaging sonar on towed body was developed in year 1950 as military equipment. Its commercial version was fielded in year1960. Up until the mid-1980s, commercial side scan images were produced on paper records. The present day these systems, military and commercial, have been augmented by developments in swath bathymetry, multi-beam echo sounders, and synthetic aperture sonars (SAS) 1970 and various advances in signal processing.

Best tool to be used to document subtle features on wide areas seems to be high frequency side scanning sonars (SSS) and more advanced version of this technology, synthetic aperture sonars (SAS) with adequate gap fillers. Both types SSS and SAA sonars offer resolution of 30 x 30 mm. However, synthetic aperture systems offer up to 5 time higher imaging rate at similarly higher equipment cost. Due to much lower operational cost (short time required to scan the same area) the SAS solution is very favourable imaging of for large areas. For shallow, low turbid waters it wise to consider laser scanners (LIDARs) that provide centimetre resolution up to 25 water depth.

LITERATURE

[1] D. Amon and C. Smith, "Abundant, Diverse EcosystemFound in Area Targeted for Deep-Sea Mining," *Eco Mag.*, 2016, [Online]. Available: https://www.ecomagazine.com/news/deep-sea/abundant-diverse-ecosystem-found-in-area-targeted-for-deep-sea-mining

[2] S. A. Kingsley, "Out of Sight, Out of Mind? Fishing & Shipwreked Heritage, Wreck WatchInt., London, UK,2012," *Herit. Wreck Watch Int.*, 2012.

[3] S. A. Kingsley, "Deep-sea fishing impacts on the shipwrecks of the english channel & western approaches," 2010.

[4] L. G. Thompson, “Bottom trawling,” *Wikipedia*. 1893. [Online]. Available: https://en.wikipedia.org/wiki/Bottom_trawling
[5] J. W. Collins, “Grampus, Trawl-Heads.” 1887. [Online]. Available: https://commons.wikimedia.org/wiki/File:FMIB_34023_Grampus.jpeg
[6] Anonymous, “Scallop dredge,” *wikipedia*. 2012. [Online]. Available: https://en.m.wikipedia.org/wiki/File:Scallop_dredge_2.jpg
[7] Anonymous, “Anger-over-reports-illegal-scallop-dredging,” *Scotsman*, 2018. [Online]. Available: https://www.scotsman.com/news/environment/anger-over-reports-illegal-scallop-dredging-193884
[8] D. S. W. de Jonge *et al.*, “Abyssal food-web model indicates faunal carbon flow recovery and impaired microbial loop 26 years after a sediment disturbance experiment,” *Prog. Oceanogr.*, vol. 189, 2020, doi: 10.1016/j.pocean.2020.102446.
[9] R. Lech, “Autonomus submersible vehicle system for manganese nodule mining,” 1990.
[10] A. Fuhrboter and M. Mittelstadt, “System for gathering solids from ocean floor and bringing them to the surface,” 1977 [Online]. Available: https://patft.uspto.gov/netacgi/nph-Parser?Sect2=PTO1&Sect2=HITOFF&p=1&u=%2Fnetahtml%2FPTO%2Fsearch-bool.html&r=1&f=G&l=50&d=PALL&RefSrch=yes&Query=PN%2F4052800

DARIUSZ BISMOR[1], MICHAŁ KACZMARCZYK[2]

[1]*Department of Measurements and Control Sciences, Silesian University of Technology, ul. Akademicka 16, 44-100 Gliwice, Poland; Dariusz.Bismor@polsl.pl*

[2]*Student, Faculty of Automatic Control, Electronics and Computer Science, Silesian University of Technology, ul. Akademicka 16, 44-100 Gliwice, Poland*

PORTABLE SYSTEM WITH HIGH SAMPLING-FREQUENCY MEMS ACCELEROMETER

ABSTRACT

Vibration monitoring is a well-known and widely-used technique for technical diagnosis of devices. Using this technique, it is possible to foresee an incoming problem with a technical device, and avoid excessive environmental noise pollution. Vibration monitoring mainly uses piezoelectric accelerometers, which are high-precision and wide bandwidth devices, with price being the only serious disadvantage. Modern MEMS sensors, on the other hand are cheap, but usually with highly limited frequency bandwidth. The latter does not apply to the ADXL100x series of accelerometers by Analog Devices, which have a linear frequency response from DC to 11 kHz and the resonant frequency of 21 kHz. Such devices allow for application technical diagnosis using cheap hardware solutions. The goal of this paper is to present an example of a portable device built using two ADXL1001 accelerometers and a popular BeagleBone Black development board. The system allows for a maximum of 96 kHz sampling rate, which is more than required for the goal application. The system was tested using a calibration setup with a reference accelerometer.

MEMS accelerometers, vibration signal processing, BeagleBone, mobile system.

1. INTRODUCTION

Sounds and vibrations are inherently correlated: sounds are produced by vibrations of objects, which in turn cause movement in the surrounding medium molecules. The connection works also the other way: sound can induce vibration of an object–a useful phenomenon which is a principle of microphone operation. Sounds can be pleasant and wanted, or unpleasant and unwanted, in which case we call them 'noise'. However, noise can also be useful, even if it is unpleasant for humans. This unwanted sound can contain a lot of information about its source vibrations, and therefore be used to observe and diagnose the source. If the source is a technical object, one can use the sound and vibrations it produces for detection of possible faults and malfunctions.

Early detection of machinery faults and failures is nowadays an important issue in industry and other applications, due to the fact that it allows to reduce maintenance costs and downtime. It is a branch of more general technique that is known under the 'condition monitoring' term. Condition monitoring usually uses microphones and accelerometers as a measurement sensors, with the latter being more frequently used [1].

There are several types of accelerometers, e.g. piezoelectric, piezoresistive, capacitive, and others. Piezoelectric accelerometers are the most popular in industrial applications due to their very good properties, like wide frequency and dynamic ranges, good linearity, etc. Their only drawback is the price, which is not very low. Therefore, capacitive accelerometers, manufactured as microelectromechanical systems (MEMS), gained considerable attention in recent years [2]. This type of accelerometers is nowadays very popular and present in many different types of portable devices, e.g. cell phones, automobiles, remote controls, game controllers. The main drawback of MEMS accelerometers is a relatively narrow frequency range, which can be as low as from zero to a couple of hundreds Hz. Fortunately, this drawback is slowly eliminated, since there are already accelerometers with the frequency range exceeding 10 kHz. One of such accelerometers, namely ADXL1001 by Analog Devices [3], is the central component of the mobile system presented in this paper.

2. HARDWARE DESIGN

The design of hardware presented in this publication was based on the following functional requirements.

- The designed system should be portable, capable of operation with its own power supply.
- The system should be able to acquire at least two channels, with the sampling frequency at least 16 kHz.
- The data should be stored in persistent memory and available for later retrieval.
- The system should be compact and shock-resistant.
- The design should be cost-effective.

The above requirements resulted in selection of the BeagleBone Black (BBB) embedded system as a core of the developed solution. The BeagleBone Black is one of commercially available, low-cost development platforms, produced by Texas Instruments, featuring a powerful OMAP3530 System-On-Chip with ARM Cortex-A8 core. It is also open-source and community-supported, requiring no licenses or other charges. It allowed to speed up the development by omitting a very time-consuming phase of hardware design and prototyping. The main specifications of the BBB are presented in Table 1. The board price varies from $100 to $150.

Table 1. The BeagleBone Black main specifications [4].

Processor	Sitara AM3358BZCZ100, 1 GHz, 2000 MIPS
Memory	SDRAM 512 MB, Flash 4 GB
General purpose IO ports	69
Power source	miniUSB or DC Jack
Power consumption	210-460 mA
Other connectors	Ethernet, USB, microSD, HDMI
Dimensions and weight	86x53 mm, 40 grams

The main goal of the BBB platform was to acquire and process data from the ADXL1001 accelerometer, which was available in a form of the ADXL1001Z evaluation module. The ADXL1001 is a single in plane axis MEMS accelerometer, with ultra low noise

density, analog output and linear frequency response from DC to 11 kHz. The main specifications of the ADXL1001 are presented in Table 2.

Table 2. The ADXL1001 main specifications [3].

Measurement range	±100 g
Linear frequency range (3 dB)	0-11 kHz
Resonant frequency	21 kHz
Noise density	30 μg/√Hz
Power supply	3.3-5.25 V
Sensitivity	20 mV/g
Temperature range	-40-125 °C

To connect the BBB and the accelerometer boards, add power supply (with basic protection) and a minimalistic user interface, a simple electronic circuit was designed, as presented in a form of a block diagram in Figure 1. The circuit comprises a power supply board, which was designed with the aim of providing a basic protection (over-voltage and reverse polarization) and automatic switching from internal to external power supply. The power supply uses the LM7805 stabilizer to provide a stable 5 V output to the BBB board for a wide range of the input voltage (9–14 V). The circuit also includes an LED diode and a switch, which allow the user to used to select one of the two operating modes and provides a visual output.

Another important function of the designed electronic circuit is anti-aliasing filtration. Although the ADXL1001Z board contains a basic anti-aliasing filter, the filter order is too low (1st order Butterworth filter), the filter cutoff frequency is too high (around 23 kHz) and the filter is located near the sensor, allowing the spurious signals induced in the connection wires to enter the analog-to-digital converters (ADCs). Therefore, an additional 3rd order Butterworth filter was designed, with the cutoff frequency equal to 8 kHz. The filter also serves as a voltage divider, as the ADCs input range is 0-1.8 V. Unfortunately, even such filter provides only around 10 dB of attenuation at the accelerator resonant frequency (21 kHz), which is not enough to effectively filter aliasing signals. For this reason, an oversampling and digital filtration was also implemented, as discussed in the next section.

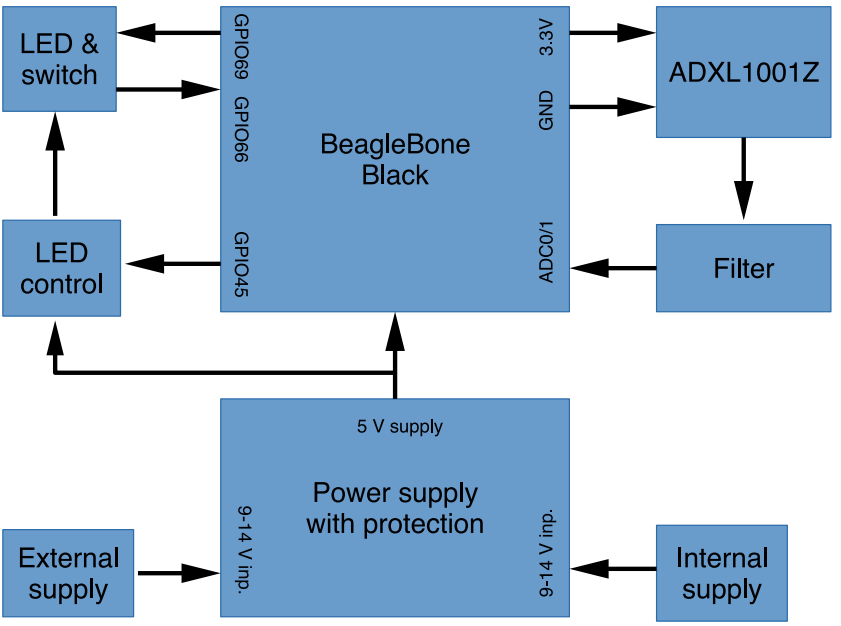

Figure 1. Hardware design block diagram.

3. SOFTWARE DESIGN

By default, the BBB board ships and operates under the Linux Debian operating system, although other OS are also available [5]. Therefore, once powered, the board starts the Linux kernel and accompanying processes first. The general purpose input-output (GPIO) ports and the ADCs are managed by the part of the kernel called the *device tree*, which is a data structure and language for describing hardware and its configuration. By simple means of editing selected text files, the device tree kernel subsystem allows to configure the hardware. In case of this work, the device tree was used to set the ADCs sampling frequency to 96 kHz. Such high sampling frequency was selected to oversample the input signal and allow for effective anti-aliasing filtration.

The next step was to write a software that will be responsible for final configuration, data acquisition, filtration and storing the acquired data on an SD card. The program was created in the C language, in a modular form, containing the following five modules:

- **configurator** – the module responsible for final configuration of GPIO ports and internal data structures,
- **acquisitor** – the module responsible for data acquisition from the ADCs,
- **gpioManager** – the module which allows to read and write the GPIO ports,
- **fileManager** – the module responsible for SD card mounting, file creation, data storage, etc.,
- **filter** – the module designed to perform the final data filtration and decimation.

The last of the above modules was designed to downsample the acquired accelerometer data from the original sampling frequency 96 kHz to the desired 16 kHz. To avoid aliasing, the procedure must be preceded with effective digital filtration [6], and the whole process is called *decimation*. On the other hand, the filtration must be fast, as it will be implemented in the real time. Therefore, a cascaded integrator-comb (CIC) filter was selected, which in fact is an optimized finite impulse response (FIR) filter combined with the downsampling.

The CIC filter transfer function is given by [7]:

$$H(z) = \frac{\left(1 - z^{-RM}\right)^N}{\left(1 - z^{-1}\right)^N} \tag{1}$$

where R is the decimation ratio, M is the number of samples per stage (usually 1), and N is the number of stages. In the discussed case, the decimation ratio is equal to 96/16 = 6, while the number of stages was selected as N = 5. Figure 2 presents the frequency response of the selected CIC filter. It can be observed that the filter exhibits a deep null around the frequency 16 kHz, i.e. the Nyquist frequency after decimation, and the largest side lobe has magnitude -60 dB, which is quite enough for the discussed application.

Figure 3 presets the estimated power spectral density (using the Welch method) of the unfiltered and filtered accelerometer exemplary data before downsampling. One can notice that the frequency components above 8 kHz (the new sampling frequency) are effectively attenuated after the filtration. Therefore, no aliasing will occur during the downsampling of such signal.

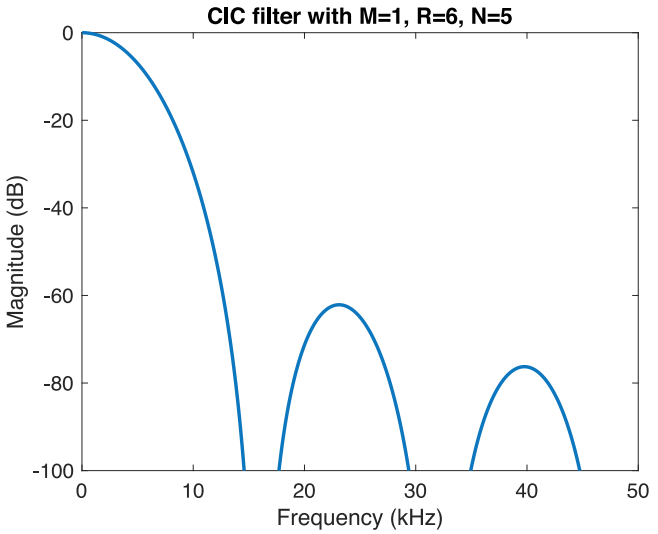

Figure 2. Frequency response of the CIC filter with M=1, R=6 and N=5.

4. CALIBRATION AND TESTS

The device was tested using a dedicated laboratory setup, consisting of the Brüel&Kjær Type 4809 vibration generator, equipped with the reference accelerometer and the Type 2525 Measuring amplifier. The accelerometers were excited using a single sine signal, with frequencies 160 Hz and 500 Hz, and with different amplitudes of vibrations. The acquired data were then analyzed to determine the amplification factor necessary to scale the data properly. This was necessary due to the fact that the accelerator sensitivity was only given for the supply voltage of 5 V, while in the developed solution the accelerators were supplied with 3.3 V. Moreover, the electronic circuit introduced a voltage divider, with a division factor imprecise due to imprecise resistor values.

An exemplary signal recorded during this calibration is presented in Figure 4. The accelerometer was excited with the frequency of 160 Hz, and with an amplitude of acceleration of 13.86 m/s^2. From the figure it can be observed that the amplitude of the recorded signal (that is half of the peak-to-peak value) is around 0.02 V. Therefore, the scaling factor should be around 700.

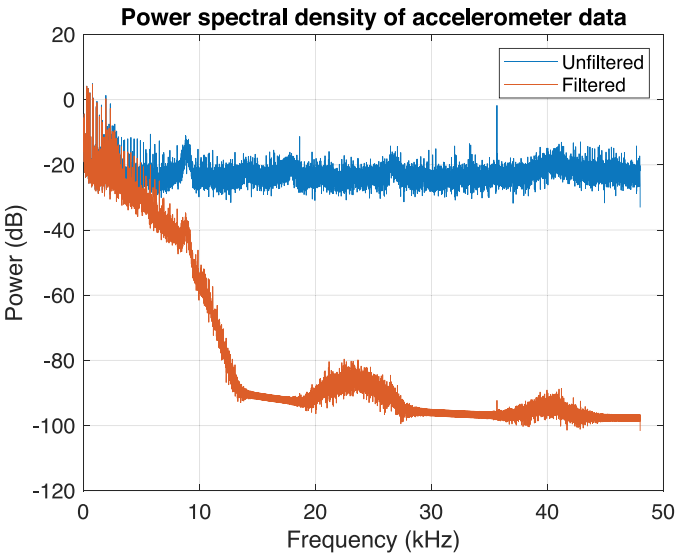

Figure 3. Exemplary power spectral density of the accelerometer data.

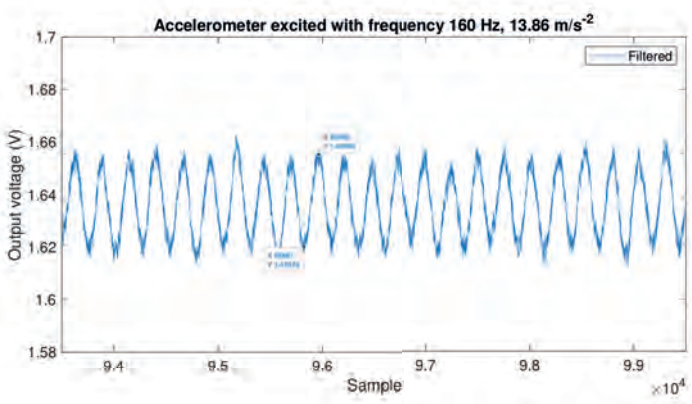

Figure 4. Data recorded during the device calibration.

5. CONCLUSIONS

A portable device for vibration measurement and recording using MEMS accelerometers were designed and constructed. The device is based on the BeagleBone Black development board, which provides a processing power necessary for fast sampling at a price of reasonable power consumption. The device uses the ADXL1001 MEMS accelerometers, offering a wide frequency

range, exceeding 10 kHz, therefore, the sampling frequency of 96 kHz was seleted. However, due to potential application of the device [8], the frequency band was narrowed down to 8 kHz using digital signal filtration and decimation. The device was calibrated using a vibration exciter and a reference accelerometer.

REFERENCES

1. S. Kan, A. C. C. Tan, and J. Mathew, “A review on prognostic techniques for non-stationary and non-linear rotating systems”, Mechanical Systems and Signal Processing, 62–63 (2015), pp. 1–20.
2. Mohammed, Z., Elfadel, I.M. & Rasras, M., "Monolithic multi degree of freedom (MDoF) capacitive MEMS accelerometers", Micromachines, vol. 9, no. 11 (2018).
3. Analog Devices, Low Noise, High Frequency MEMS Accelerometers Data Sheet, https://www.analog.com/media/en/technical-documentation/data-sheets/ADXL1001-1002.pdf (accessed 16.08.2022).
4. Gerald Coley, “Beaglebone black system reference manual”, https://github.com/beagleboard/beaglebone-black/wiki/System-Reference-Manual#beaglebone-black-system-reference-manual (accessed 16.08.2022).
5. BeagleBone Black: Wiki page, https://elinux.org/Beagleboard:BeagleBoneBlack#Software_Resources (accessed 16.08.2022).
6. Sanjit K. Mitra, “Digital Signal Processing. A Computer-Based Approach”, McGraw-Hill, Boston, 2001.
7. E. Hogenauer, "An economical class of digital filters for decimation and interpolation" IEEE Transactions on Acoustics, Speech, and Signal Processing, vol. 29, no. 2, pp. 155-162, April 1981, doi: 10.1109/TASSP.1981.1163535.
8. M. Ashan, D. Bismor, “Early-Stage Fault Diagnosis for Rotating Element Bearing Using Improved Harmony Search Algorithm With Different Fitness Functions”, IEEE Transactions on Instrumentation and Measurement, Vol. 71, 2022, doi: 10.1109/TIM.2022.3192254.

ALEKSANDRA KLIMEK[A], MARCIN DUDAŁA[B], ANDRZEJ DOBRUCKI[A]

[a] Department of Acoustics, Multimedia and Signal Processing, Wroclaw University of Science and Technology, 27 Wybrzeże Wyspiańskiego St. 50-370 Wrocław, Poland

[b] MESCO Sp. z o.o., Aleja Legionów 4, 41-902 Bytom, Poland

Corresponding author at: Department of Acoustics, Multimedia and Signal Processing, Wroclaw University of Science and Technology, 27 Wybrzeże Wyspiańskiego St. 50-370 Wrocław, Poland

Email address: Aleksandra.Klimek@pwr.edu.pl (Aleksandra Klimek)

MODELLING OF PLATE-TYPE ACOUSTIC METAMATERIALS USING ANSYS

ABSTRACT

The acoustic metamaterials are frequently designed using FEA techniques. This paper presents the detailed method of employing the periodic boundary condition and Floquet periodic boundary condition in the FEA software – ANSYS 2022 R1. The procedure operates on APDL (Ansys Parametric Design Language) code inserted into analysis in Mechanical Application. An example of plate-type metamaterial with antisymmetric periodicity is used for verification of the procedure.

KEYWORDS: FEM, acoustic metamaterials, periodicity, periodic boundary condition, Floquet periodicity

1. INTRODUCTION

Acoustic metamaterials (AMMs) are artificial periodic structures, which enable control of the acoustic field to a level not reachable by conventional methods. The 2D structures, such

as plate-type AMMs, received growing attention over the last decades, especially in noise control. Locally resonances forming in the given grid lead to band gaps development and hence, break the law mass for acoustic insulation. This advantage is attainable only for a finite frequency range. Therefore, acoustic metamaterials may be employed to control tonal and narrow-banded noise or in applications with weight and space limitations.

The design process of AMMs frequently operates on Finite Element Analysis (FEA). FEA joins the usage simplicity with the ability to compute the solutions for complex geometrical objects. The possible analysis types which could estimate the AMMs features are Linear Dynamic Analysis (e.g., Modal and Harmonic Response) or Acoustic Analyses (e.g., Harmonic Acoustics). All mentioned types are the issue of this paper.

The single metamaterial design consists of a dense grid of periodically distributed cells. Each cell may contain thousands of mesh elements thus only practical method to solve the results is to use the periodic boundary condition or Floquet periodic boundary condition on a single cell.

2. MATERIALS

The model sample employed to present the following analysis will be low-band plate-type metamaterial as in Fig. 1. The resonant structures are beams fixed rigidly in the middle with a holder to the flat panel. The whole plate is periodic in the XY plane and excited by an incident plane wave along the Z axis. The periodicity in the given material is odd (marked in Fig 1 with dashed lines), which means that along the axis X, the cell is inverted through the axis Y and vice versa. The four adjacent cells (marked with blue in Fig 1) assemble a larger partition with regular periodicity.

Table 1. presents all material parameters and dimensions implemented in the model. The materials utilised in simulations are orthotropic (cardboard for beams and holders and paper honeycomb for the base panel).

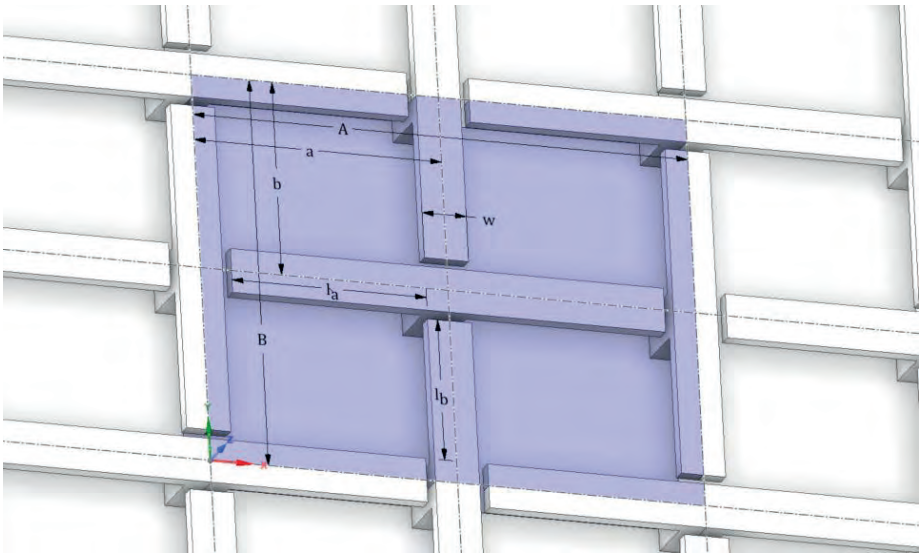

Fig. 1 The simulated plate-type metamaterial scheme. The single cell is marked with colour blue. With antiperiodic cells are marked with dashed lines.

Table 1 Material parameters and structure dimensions used in simulation

	Material parameters			**Structure dimensions**		
	Parameter	**Direction**	**Value**	**Dimension**	**Direction**	**Value**
Beams and holders	Young Modulus	y & z	1,02 GPa	Regular lattice constants A	x (A)	112 mm
		x	2,05 GPa		y ()	88 mm
	Poisson's ratio	xy, xz & yz	0,3	Antiperiodic lattice constants	x ()	56 mm
					y ()	44 mm
	Material dependent damping ratio	x, y & z	0,0344	Beam length	x ()	44 mm
					y ()	32 mm
	Density	–	667 kg/ m^3	Beam thickness	x, y	3 mm
				Beam width	x, y	10 mm
				Holder dimensions	x, y	10 x 10 x 3 mm
Base panel	Young Modulus	x, y & z	0,11 GPa	Panel thickness	–	10 mm

3. METHODS

The basic analyses needed to simulate the plate-type acoustic metamaterials are:

- Linear Dynamic Analysis - to calculate the results only concerning AMMs body, e.g., Modal Analysis to obtain modes and dispersion curve or Harmonic Response Analysis to obtain the vibration response to known excitation,
- Acoustic Analyses, to calculate the AMM behaviour coupled with the surrounding acoustic field (*Acoustic Region*) e.g., Harmonic Acoustics to calculate the Transmission Loss.

To limit the size of the periodic model, the periodic Boundary Condition should be applied. In Ansys Mechanical Application there is a tool enabling such condition – the Linear Periodic Symmetry Region. This tool specifies the constraint equations linking the degrees of freedom (DOFs) of the cells' low to the high boundary (Fig. 2). Unfortunately, its application is restricted to structural and thermal or thermal-electric analyses. Furthermore, the symmetry is viable only in a single direction, preventing its implementation in 2D AMM. [1]

The concept will be recreated in terms of APDL Commands and executed within every performed analysis.

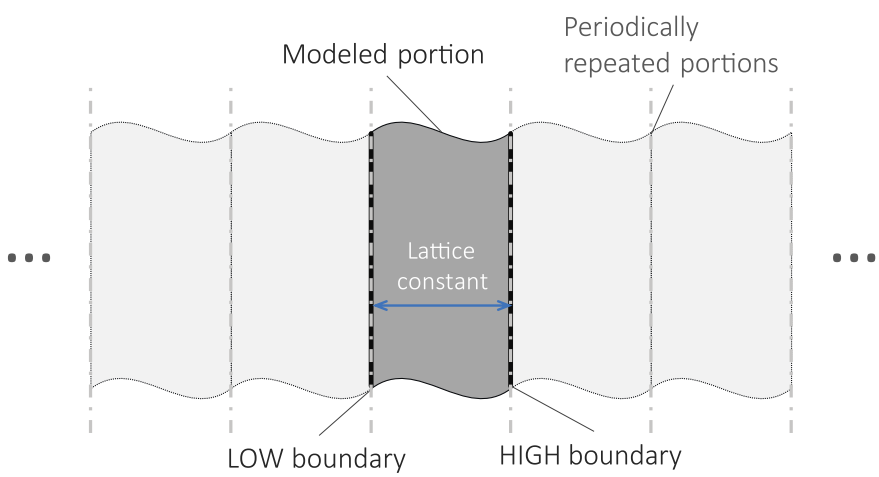

Fig. 2 Linear Periodic Symmetry in one direction

3.1. PERIODIC BOUNDARY CONDITION

Let us consider the model illustrated in Fig 3. Every marginal surface belongs to one of the low or high boundaries in both directions:

- Low X/Y – name selection for low X/Y boundary,
- High X/Y – name selection for high X/Y boundary.

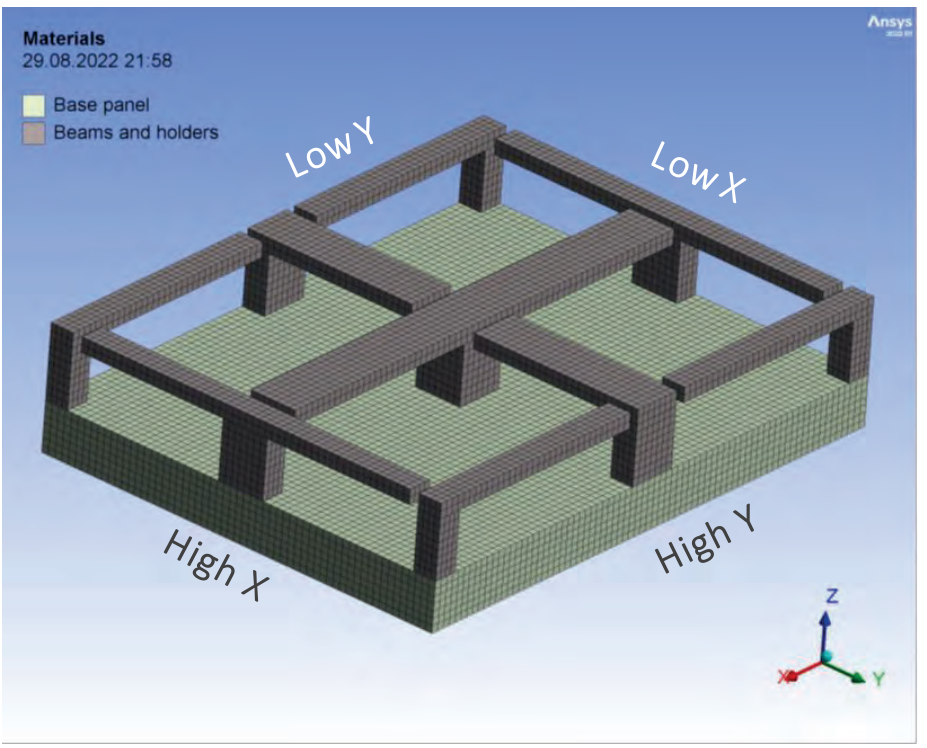

Fig. 3 Exemplary model with generated mesh for regular lattice

The mesh on each pair of boundary surfaces must be identical. The bottom surface of the base panel is fixed and every connection between the bodies is set to "bonded".

The prepared model and mesh enable to execute the APDL Commands.

The valid constrain equation requires the definition of pilot nodes for both directions (`Pilot_X/Y`). Each pilot node is located in the invariable point. Pilots should be assigned to mass-type elements with the weight of zero and DOFs specified exclusively

to displacements (KEOPT(3) of MASS21 element set to 2). Correspondingly, pilots must have separate materials and real constants. This condition could be defined by the means of APDL.

The easiest method to constrain the nodes is to define corresponding matrices for both low and high boundaries. This is accomplished by defining the matrix with every node index number and location for the low boundary followed by building the complementary matrix for the high boundary. The second may be implemented by searching each node by its location respectively to the opposite one. The commands for X direction are:

```
nsel,s,LOC,X,(Low_X(ii,2)-tol_X)+shift_X,(Low_X(ii,2)+tol_X)
+shift_X
nsel,r,LOC,Y,Low_X(ii,3)-tol_X,Low_X(ii,3)+tol_X
nsel,r,LOC,Z,Low_X(ii,4)-tol_X,Low_X(ii,4)+tol_X
*get,High_X(ii,1),node,,num,max
```

where:

Low/High_X – the matrix of low/high boundary, the row number refers to node index and column number to data type: 1 – node index, 2, 3, 4 – locations in X, Y and Z directions respectively;
tol_X/Y – toleration of node location – with the value of approximately 1/10 of the minimal element size;
shift_X/Y – lattice constants: *A* or *B*.

For the Y direction, commands are congruent.

For antisymmetric geometry (Fig 4), as in the examined example, the Y-component position for X direction periodicity and X-component position for Y direction periodicity should be reversed, hence the code lines should be replaced with:

```
nsel,r,LOC,Y,shift_Y-Low_X(ii,3)-tol_X,shift_Y-Low_X(ii,3)
+tol_X
nsel,r,LOC,Y,shift_X-Low_Y(ii,2)-tol_Y,shift_Y-Low_Y(ii,2)
+tol_Y
```

Finally, the symmetric nodes are in relation according to equation linking their DOFs. For Linear Dynamic Analysis the only DOFs linked are displacements:

$$\mathbf{u_H} = \mathbf{u_L} + \mathbf{u_P} \tag{1}$$

where $\mathbf{u_H}$, $\mathbf{u_L}$, $\mathbf{u_P}$ are nodes displacement vectors.

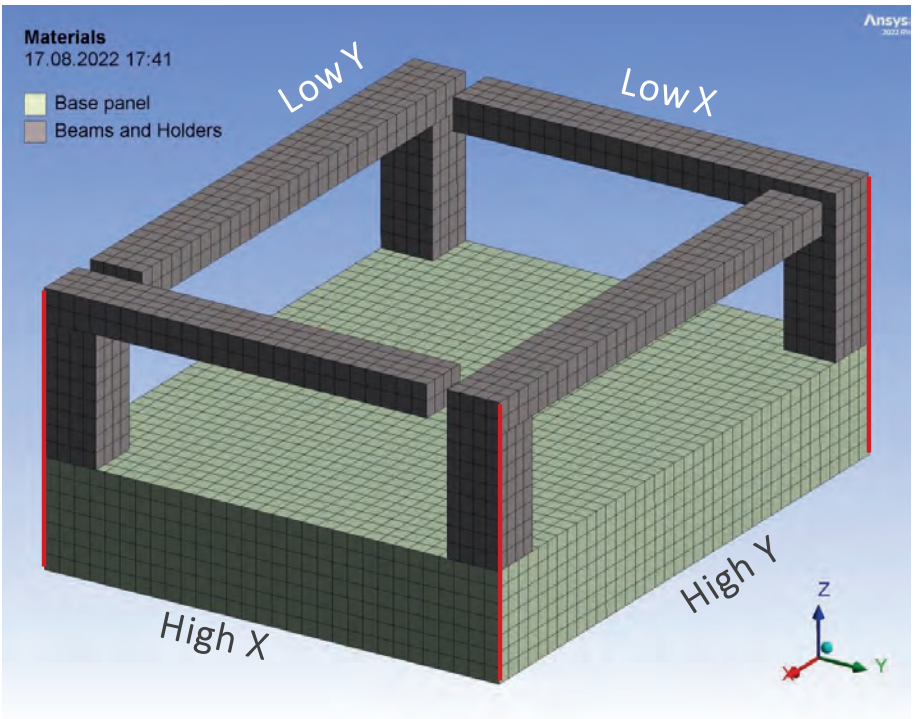

Fig. 4 Exemplary model with generated mesh for antiperiodic lattice

The APDL implementation (in example of X direction) for regular periodic lattice is as follows:

```
CE,NEXT,,Low_X(ii,1),UX,-1,High_X(ii,1),UX,1,Pilot_X,UX,1
CE,NEXT,,Low_X(ii,1),UY,-1,High_X(ii,1),UY,1,Pilot_X,UY,1
CE,NEXT,,Low_X(ii,1),UZ,-1,High_X(ii,1),UZ,1,Pilot_X,UZ,1
```

For the Y direction, commands are congruent.

For antiperiodic lattice, the Y-component displacements for X direction of periodicity and the X-component displacements for Y direction of periodicity are reversed, which replaces the respective lines with:

```
CE,NEXT,,Low_X(ii,1),UY,-1,High_X(ii,1),UY,-1,Pilot_X,UY,1
CE,NEXT,,Low_Y(ii,1),UX,-1,High_Y(ii,1),UX,-1,Pilot_Y,UX,1
```

In the case of Acoustic Analyses, the additional equation links the acoustic pressure for surrounding medium (*Acoustic Region*):

$$p_H = p_L \tag{2}$$

where p_H, p_L, p_P are nodes acoustic pressures.

The APDL command (in example of X direction) is given only for single constraint equation. Since the quantity is scalar, there is no need to diversify the relation for antisymmetry:

```
CE,NEXT,,Low_X(ii,1),PRES,-1,High_X(ii,1),PRES,1
```

The above procedure for antiperiodic lattice is *not* precise. Reversing the axes of location and displacement twice for x and y directions leads to significant error. The X and Y displacement components on the marginal edges (marked with red lines in Fig. 4) are falsely fixed. The explanation is, that the diagonal nodes of low and high edges have linked displacements in simultaneously +X, +Y and -X, -Y directions. The consequence of the error is explained in paragraph 4.

3.2. FLOQUET PERIODIC BOUNDARY CONDITION

The dispersion curve relates the frequency of a wave propagating through the medium to its wave number. The homogeneous body dispersion curve is linear for any given wave frequency, whereas in metamaterials the band gaps could form. The width and height of a band gap may be crucial conditions in the metamaterial project process. The dispersion relation is the solution of the Bloch-Floquet theorem [2], [3]:

$$\mathbf{u}(\mathbf{x}) = \mathbf{u}(\mathbf{x}_0)e^{i\mathbf{k}(\mathbf{x}-\mathbf{x}_0)} \tag{3}$$

where: $\mathbf{u}(\mathbf{x}),\ \mathbf{u}(\mathbf{x}_0).$ are the displacement vectors in the respective locations, and $\mathbf{k}$ is the wave vector (Floquet wavenumber).

The relation in examined model will adopt the form of:

$$\mathbf{u_H} = \mathbf{u_L}e^{i\mathbf{k}r} \tag{4}$$

where r stands for lattice constant (A or a for X direction and B or b for Y direction).

Such relation is the eigenvalue problem with defined values of $\mathbf{k}$, with the results obtainable in Ansys through the Modal Analysis. Prior to the analysis, the $\mathbf{k}$ vector must be specified. The $\mathbf{k}$ vector should cover the whole indivisible Brillouin Zone. In a given 2D model with perpendicular lattice, the Brillouin Zone

with every possible **k** vector is as in Fig 5. This means that for each **k** value in directions *x* and *y,* starting from point Γ through X, M to Γ, an individual Modal Analysis is conducted. k equal to 0 simplifies the equation (4) to the eq. (1), which makes this a simple Modal Analysis as in paragraph 3.1.

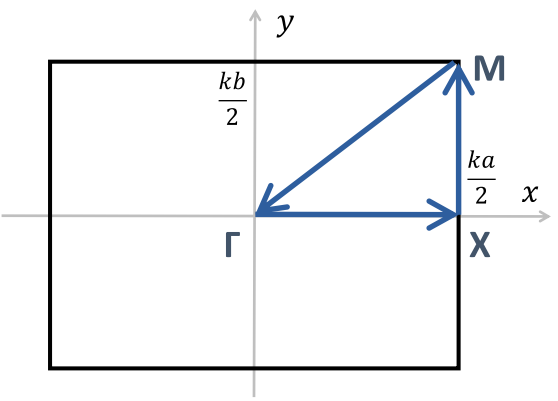

Fig. 5 Brillouin zone for perpendicular lattice

After expanding equation (4), the complex relation emerges:

$$\begin{bmatrix} \mathbf{u}_H^R \\ \mathbf{u}_H^I \end{bmatrix} = \begin{bmatrix} \cos ka & -\sin ka \\ \sin ka & \cos ka \end{bmatrix} \begin{bmatrix} \mathbf{u}_L^R \\ \mathbf{u}_L^I \end{bmatrix} \tag{5}$$

The imaginary displacement field $\mathbf{u}^I$ requires duplicating the mesh as in the Fig. 6. [2].

The APDL implementation of constraint equations based on eq. (4) are as follows.

For real high boundary, the periodicity in X direction for each node is represented by:

```
CE,NEXT,,Low_RX(ii,1),U,-COS(K_X*shift_X),High_RX(ii,1),U,-1,…
 … Low_IX(ii,1),U,SIN(K_X*shift_X)
CE,HIGH,,Pilot_X,U,1
```

Where `U` stands for `UX`, `UY` and `UZ` displacements and `K_X` is wave number in X direction.

The lines for Y direction are corresponding:

```
CE,NEXT,,Low_RY(ii,1),U,-COS(K_Y*shift_Y),High_RY(ii,1),U,1,…
 … Low_IY(ii,1),U,SIN(K_Y*shift_Y)
CE,HIGH,,Pilot_Y,U,1
```

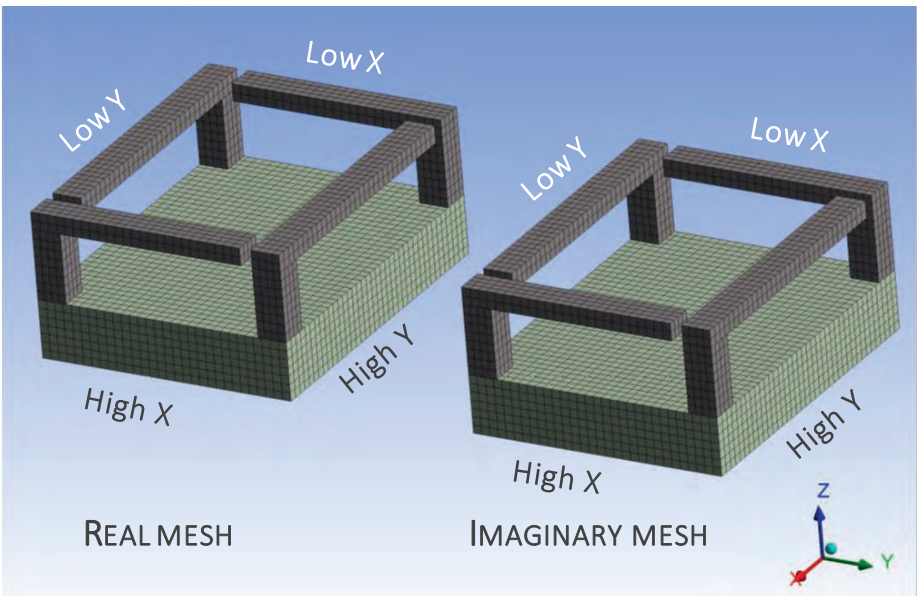

Fig. 6 Real and imaginary mesh – the antiperiodic lattice example

For the imaginary high boundary, the lines are:

```
CE,NEXT,,Low_RX(ii,1),U,-SIN(K_X*shift_X),High_IX(ii,1),U,-1,…
 … Low_IX(ii,1),U,-COS(K_X*shift_X)
CE,HIGH,,Pilot_X,UZ,1
CE,NEXT,,Low_RY(ii,1),U,-SIN(K_Y*shift_Y),High_IY(ii,1),U,1,…
 … Low_IY(ii,1),U,-COS(K_Y*shift_Y)
CE,HIGH,,Pilot_Y,U,1
```

4. RESULTS AND DISCUSSION

The procedure was assessed by the Modal and Mode-Superposition Harmonic Response Analyses. The Modal Analysis was prepared as described in paragraph 3, while Harmonic Response Analysis had an acceleration load of 1 mm/s^2 applied to the fixed surface. The response spectra of vibration velocity level were averaged from displacements in the Z direction for nodes located near the free end of the beam.

The verification of the Linear Dynamic Analyses results confirms that the procedure links the low boundary surfaces to high boundary surfaces properly. The mode shape for both directions

is compatible with its representations on the opposite boundary (Fig 7). Unfortunately, the falsely fixed edges remove from the results modes with non-zero displacements. Table 2 represents the frequencies of identically shaped modes for both lattices – modes 1 and 3 are not perceptible in the antiperiodic lattice. Nevertheless, in specific circumstances, the procedure gives a partial solution with valuable information. When the flat structure operates on an acoustic wave perpendicular to itself (which is often the case in plate-type AMMs), it is excited in the Z direction. If the local resonators are symmetrical to the mentioned supports and the supports are located on the cell edges, the max-

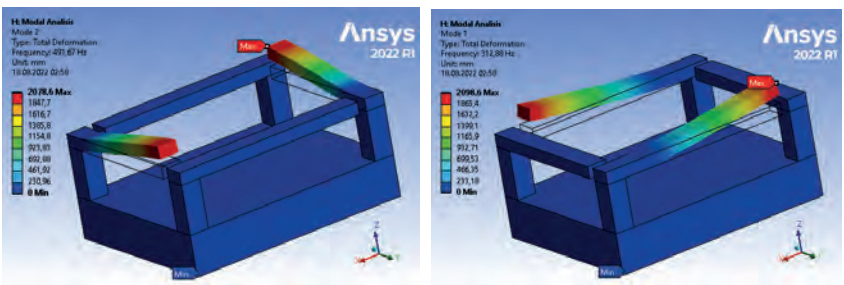

Fig. 7 Total deformation of primary modes in Z direction for antiperiodic lattice

Table 2 Modes for antiperiodic and regular lattice

Mode number	**Antiperiodic lattice mode [Hz]** *partial solution*	**Regular lattice modes [Hz] (with quadruple antiperiodic cell)** *full solution*
1	-	244,18
		245,45
2	245,87	248,21
		249,89
3	-	286,67
		287,19
4	**312,88**	**312,15**
		312,88
5	336,06	341,26
		343,74
6	**491,67**	**491,12**
		491,14

imal Z-component displacements in the whole structure arise when these supports move entirely in this direction. This leads to the conclusion that the crucial information about AMM's nature of motion could be read only from selective modes.

The vibration velocity response spectra indicate the resonance corresponding to the first Z-directional mode for every beam (Fig. 8). The results for both procedures are almost identical.

That proves the partial results could deliver the approximate solution i.e., in the first design stage or in the optimization process. A smaller model can lower the computation time by four

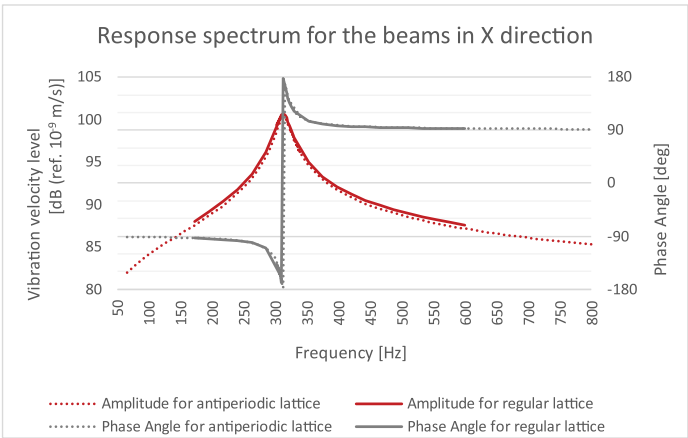

Fig. 8 Response spectra of Z-component vibration velocity level of free end of the beams – a beam turned in the x direction

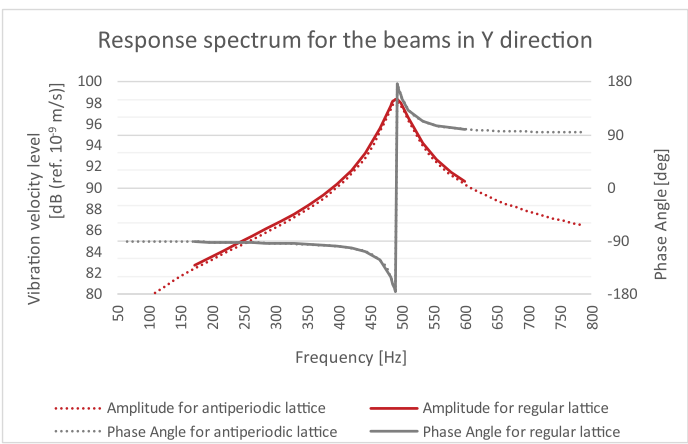

Fig. 9 Response spectra of Z-component vibration velocity level of free end of the beams – a beam turned in the y direction

times or more. Regardless, the antiperiodic lattice procedure could only be used for certain requirements and should not replace the full solution.

5. CONCLUSIONS

The exemplary acoustic plate-type metamaterial demonstrates the method of simulating the periodicity using ANSYS. The procedure allows conducting the periodic or Floquet periodic boundary conditions in both directions simultaneously. The paper offers the antiperiodic lattice approach, which is an alternative to the direct periodic lattice. The presented approach omits the modes requiring the perpendicular deflection of the marginal edges from the result and consequently gives only the partial solution. Nevertheless, when carefully applied, this method yields results almost identical to the full solution, with more than four times less computational time.

LITERATURE

[1] I. ANSYS, "Mechanical User ' s Guide," *Ansys*, vol. 15317, no. July, p. 1028, 2021.

[2] A. Melnikov, M. Hankec, and S. Marburg, "Dispersion Curves of Elastic Metamaterials and Sonic Crystals with ANSYS Pianissimo-Development of Noise Optimized Stage Elevator View project," in *36. CADFEM ANSYS Simulation Conference*, 2018, no. October, [Online]. Available: https://www.researchgate.net/publication/327792206.

[3] C. Hakoda, J. Rose, P. Shokouhi, and C. Lissenden, "Using Floquet periodicity to easily calculate dispersion curves and wave structures of homogeneous waveguides," *AIP Conf. Proc.*, vol. 1949, no. April, 2018, doi: 10.1063/1.5031513.

KAROLINA DEJA[1], MICHAŁ WITEK[1], AGATA TOBOŁA, DR HAB ANNA ZALESKA-ŻMIJEWSKA[1],
DR HAB. INŻ. GRZEGORZ KLEKOT, PROF. UCZELNI[2],
PROF. DR HAB. PIOTR SKOPIŃSKI[1]

[1] Department of Ophthalmology of the Faculty of Medicine of the Medical University of Warsaw The Independent Public Clinical Ophthalmology Hospital in Warsaw

[2] Faculty of Automotive and Construction Machinery Warsaw University of Technology

HISTORY OF SONOGRAPHY IN OPHTHALMOLOGY

ABSTRACT

Since first reports in 1949, the application of sonography have been expanded in medicine and ophthalmology.Starting from A-mode ultrasound used for differential diagnosis of retinal detachment and choroidal melanoma, to advanced corneal epithelial thickness measurement using Very High Frequency enabling more accurate outcome for refractive surgery. In our paper we describe a historical development of ultrasound technique as a diagnostic tool in ophthalmology. We conducted database research, using Pubmed and Google Scholar. As a result we present historical beginnings and current interests in ophthalmic ultrasound.

KEYWORDS: ultrasound, ultrasound biomicroscopy, very high frequency ultrasound, clinical applications, ophthalmology

Ultrasounds are defined as acoustic oscillations distributed in a medium with frequency higher than 20 KHz, that are inaudible for humans [1]. First reports considering use of ultrasound in medicine are from 1949 and consider use of reflectoscope, an apparatus generating frequencies between 1-2.5 MHz for assessment of the quality of industrial metal . George Ludwig employed the reflectoscope for measurement the acoustic impedance of gallstones, by comparing them to human muscle tissue and beef tissue. He defined impedance as a product of density and velocity of sound in the substance. The differences between different tissue impedances allowed for differentiation between gallstone and muscle tissue. Additionally the author concluded that wavelength should not exceed the diameter of a visualized object [2]. In 1951, John Wild and John Reid built the first B-mode scanner [3]. In 1956 Henry Mundt described the first application of ultrasound in distinguishing between retinal detachment and choroidal melanoma in humans. Studies performed before on calves' eyes using different parameters of ultrasound machines resulted in secondary cataracts after 20 minutes exposure [4]. Before performing exams on patients, authors examined pigs eyes in order to determine output signal and complications. Using reflectoscope authors were able to differentiate between retinal detachment and choroidal melanoma, the two diagnoses that appear similar in clinical examination, however differ significantly in treatment and prognosis [5]. Higher frequency transducers provide finer resolution of more superficial structures, whereas lower frequency transducers provide greater depth of penetration with less resolution. Nowadays ophthalmic ultrasound is particularly useful when the visual pathway is unclear, due to corneal opacities, cataracts or vitreous hemorrhage (image 1). It provides a cheaper, faster and complications-free alternative to other imaging methods such as CT or MRI. Current indications for ophthalmic ultrasound have been summarized in table 1[6].

In our paper we present historical and modern aspects of application ultrasound in ophthalmology. As per methodology, we searched Pubmed and Google Scholar using keywords: ophthalmic ultrasound, ultrasound ophthalmology, b presentation ultrasound ophthalmology, a presentation ophthalmology. We cite newest articles as well as historically significant papers.

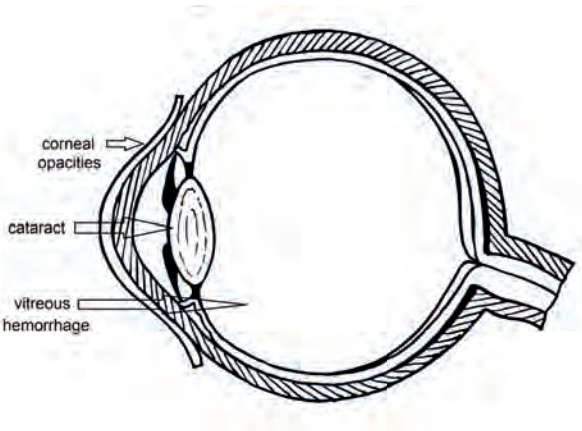

Image 1. Causes of unclear visual pathway

An A-mode (amplitude) is a two-dimensional method of presenting the acquired signal in time. Ultrasound probe generates acoustic waves that are reflected back to the probe, then the signal is plotted on screen as a function of depth. The first applications of ultrasound in ophthalmology in 1956 used that mode for diagnosing choroidal melanoma. The output was a linear chart with waves that correspond to the distribution of acoustic waves passing through consecutive parts of the eyeball (image 2). Authors also made an observation that the length of the record depends on the length of the eyeball and is significantly shorter

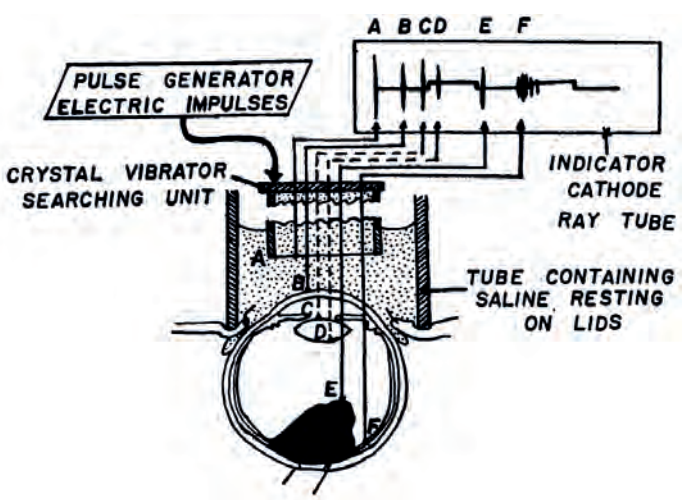

Image 2. Interpretation of a-mode ultrasound in relation to the eye

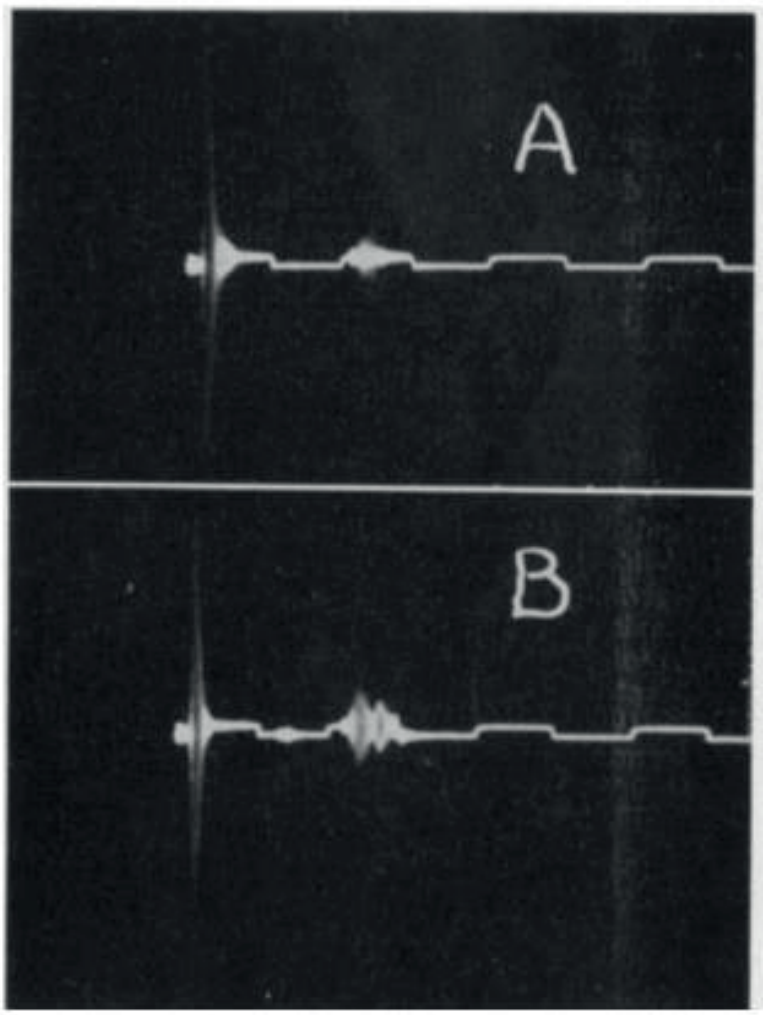

Image 3. A-mode scan of healthy eye (A), a-mode scan of eye with retinal detachment, scans are similar

in children with microphthalmos (congenital small eyeball), also the posterior pole tumor creates bigger reflection in the A-mode scan when the probe is directly above the tumor. They proved that A-mode ultrasound is a suitable method for qualitative differential diagnosis of retinal detachment and choroidal melanoma. (image 4). Limitations of that method were uncomfortable patients' position - an eye had to be immersed in saline solution, long exposure time and inability to demonstrate differences between tumor and subretinal hemorrhage [5]. The ultrasound

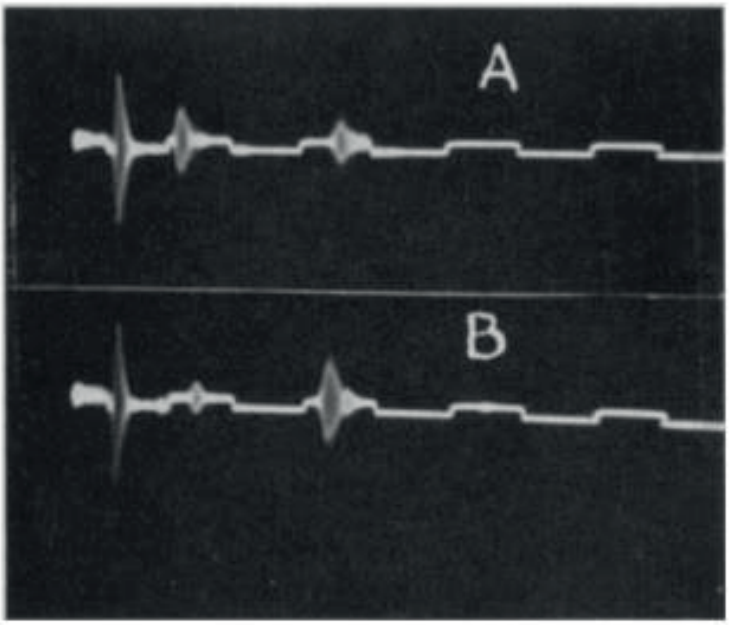

Image 4. A-mode scan of a healthy eye (A), a-mode scan of an eye with melanoma, posterior reflection is stronger (B)

projection A machine was presented in Boston in 1972 and it used a 10 MHz head. The camera was handheld and could be held directly to the eye. The device allowed to obtain images with a resolution of 0.3 mm. [7]

The A-mode ultrasound was also used in quantitative measurement of axial length, lens thickness and vitreous chamber depth. The velocity of ultrasound in temperature of 37 degrees Celsius was found to be 1536 m/s in artificial aqueous humor and 1532 m/s in the vitreous [8, 9]. Knowing the distance between two waves in ultrasound transcript (image 5) – one from the cornea and other from the lens – the depth of the anterior chamber can be calculated. For practical reasons, the velocity in the anterior chamber and vitreous have been approximated to 1532 m/s. The ratio of the distance traveled by ultrasound in one medium (a1) to that in another medium (a2) is the same as the ratio of the velocity in the first medium (V1)to that in the other medium (V2) when the passing time is the same in both. The formula is:

$$\mathrm{a1}/\mathrm{a2} = \mathrm{v1}/\mathrm{v2}$$

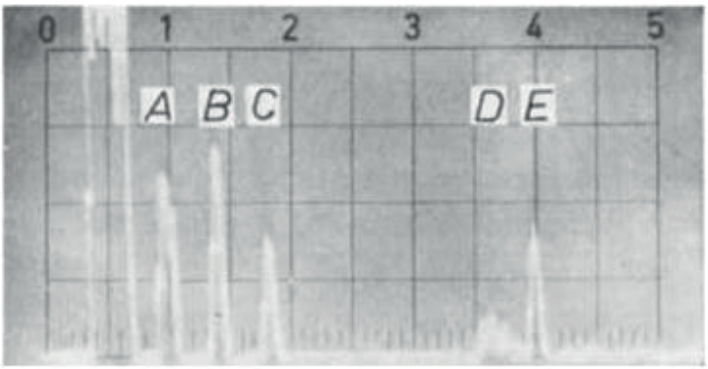

Image 5. A-mode scan A - anterior corneal surface, B - anterior lens surface, C- posterior lens surface, D - posterior wall, E- interferometer

The passing time between cornea and anterior lens surface is the same as the passing in the distance of water (d1) between echo A and B in the ultrasound transcript. The velocity of ultrasound in water in temperature = t is 1557 - 0.0245 (74 - t)^2, so the formula for the depth of the anterior chamber (d2) is

anterior chamber depth = $1532 * \mathrm{d1}/1557 - 0.0245(74 - \mathrm{t})^2$

When that formula was created, the anterior chamber depth could be alternatively assessed with an optical apparatus manufactured by AB Visus, Gothenburg, Sweden using Stenstrom's method [10], authors of the study obtained similar results from both methods. In order to determine lens thickness one needs to determine the velocity of ultrasound in healthy lenses, it was tested to be 1641 m/s [8,9]. The formula for the lens thickness is

lens thickness = $1641 * \mathrm{d2}/1557 - 0.0245(74 - \mathrm{t})^2$

where d2 is the distance of water between the interference position of echo B and echo C. Similarly, the velocity of ultrasound in vitreous chamber was determined 1532 m/s in temperature +37 degrees Celsius [7,8] and the apparent position of vitreous was defined as the distance between echo C and D (d3)

length of the vitreous = $1532 * \mathrm{d3}/1557 - 0.0245(74 - \mathrm{t})^2$

The average anterior chamber depth in the age group 40-49 years old was 3,58 mm for men and 3,45 mm for women and the number decreased with age. Results were similar to those ac-

quired by optical device. The lens thickness in the age group 40-49 years old was 4,189 mm for men and 4,098 mm for women and the number increased with age. The vitreous chamber length in the age group 40-49 years old was 15,79 mm for men and 15,38 for women and the number decreased with age. The axial length was calculated as the sum of the values above and corneal thickness as well and totalled 24,00 mm for men and 23,13 mm for women [11]. Similar results were reported by Stenstrom in 1946, he determined using roentgen rays that axial length was 24,04 mm for men and 23,89 mm for women. Additionally in the study the correlation between axial length and refraction was found: subjects with longer eyeballs were myopic and those with shorter eyeballs were hypermetropic [12]. Similar finding was reported by Franken in 1961 using the ultrasound (image 6) [11, 13]. Knowledge of the length of those structures allows for calculating the power of the intraocular lens implanted into the eye during cataract surgery. Nowadays A-mode ultrasound in applanation technique has been declared safe and is still used

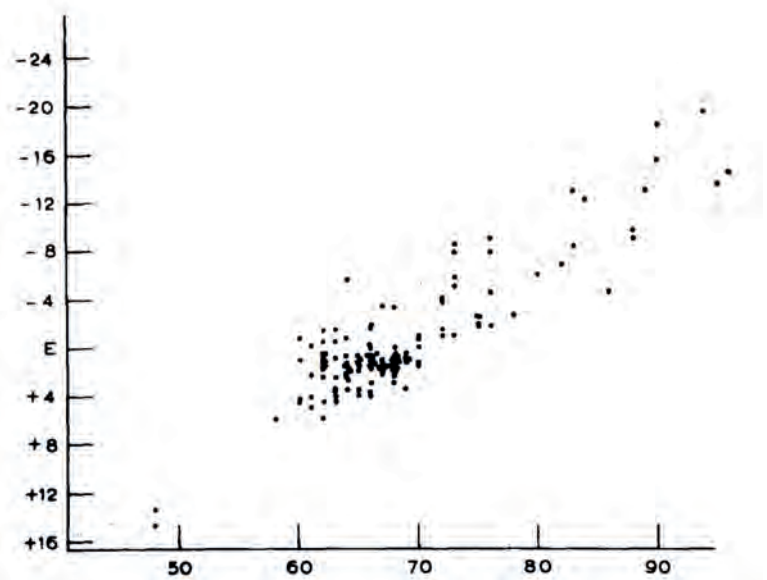

Image 6. Correlation between length of optic axis and refraction; x-axis: length of optic axis expressed in scale divisions; 50 = 16.7 mm, 60 = 20.0 mm, 70 = 23.3 mm, 80 = 26.7 mm, 90 = 30.0 mm; y-axis the refraction

before cataract surgery, however new techniques have been introduced [14]. Partial coherence interferometry (PCI) is an optical method of axial length measurement used in IOL Master 700 (Carl Zeiss, Jena, Germany). PCI uses a projection of 6 light spots of an infrared laser (780 nm) illuminating the cornea (projected radius of 2.3–2.5 mm) [15]. The light source separates into two beams then both of them are reflected from separated ocular interfaces at different times. If the delay of these two light beam equals an intraocular distance within the coherence length of the light source, an interference signal (called partial coherence interferometry signal) is detected, similar to that of ultrasound A- scan, but with a very high resolution (approximately 12 um) and precision (0.3 to 10 um) (image 7). In biometry, PCI based measurements resulted in fever refractive errors compared to ultrasound (applanation) biometry, however it cannot be used in patients with dense cataracts, or with motor disabilities such as tremor [16]. Optical low coherence reflectometry (OLCR) is another optical technique used in apparatus LENSTAR LS900 (Haag-Streit, Bern, Switzerland). It uses a superluminescent diode (wavelength: 845 nm, coherence length: ~30 μm) to mea-

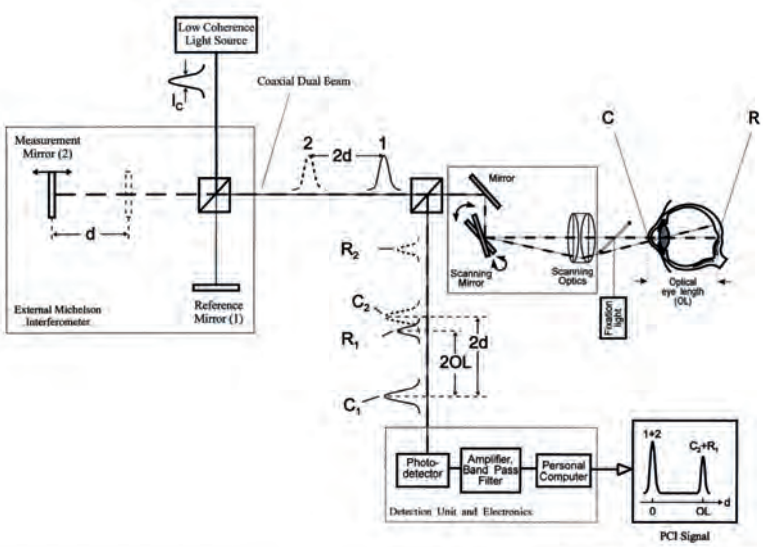

Image 7. Sketch of the partial coherence interferometer. The eye is illuminated by the interferometer, then reflected signals, for example C1, C2, R1, and R2, are superimposed on and detected by a photodetector.

sure coherence of the light source [17]. In comparison to applanation biometry OLCR is similar to PCI and it produces more accurate results, however it has the same limitations as PCI – when the cataract is dense the beam of light cannot penetrate through the tissue, hence there is no result. When comparing listed methods of measurement the axial length, the smallest magnitude of mean and SD of difference in AL (0. 01 mm±0.03 mm) was in the IOLMaster-LENSTAR comparison, followed by the LENSTAR-applanation comparison (0.18 mm±0.23 mm; −0.52 D±0.93 D). It means that PCI and OLCR offer the resolution 10 times better that A-mode ultrasound biometry (10 micron vs 100 micron), nevertheless due to the limitations of optical methods there are still some indications for A-mode biometry, such as dense cataract, lack of cooperation with the patient or general diseases such as parkinson disease or tremor in general.

Presentation B enables two-dimensional imaging of the posterior segment of the eye, and therefore allows the detection of bleeding into the vitreous chamber, retinal detachment, and intraocular tumors. Since ophthalmic examination is based on visual structural assessment in direct examination,during a vitreous hemorrhage visual inspection of the fundus is not possible. Ultrasound allows to differentiate between fresh haemorrhages and old lesions, also to assess the degree of blood absorption.

In B-view ultrasound, the presence of tears, detachments, or clinically insignificant retinal dissections can be detected. The detachment itself can only be diagnosed by an experienced ultrasound specialist in the A projection – however, it is not used in clinical practice. Ultrasound examination in a patient with a retinal detachment allows to plan the scope of the operation and the location of possible scleral support, which is a surgical technique used in retinal detachment. It allows to assess the safety of vitrectomy – vitreous removal. [18] The diagnosis of subretinal bleeding is largely based on ultrasound. It enables to assess the coexistence of a retinal tear at an early stage, requiring lasering. The ultrasound determines further treatment. [19] Nowadays, ultrasound examination in B presentation allows for the diagnosis of vitreous haemorrhage [20] and retinal detachment with high sensitivity and specificity. [21]

Projection B combined with the measurements made in the A projection and subjected to their evaluation based on a predefined algorithm allows for the improvement of the efficiency of the diagnosis of eye cancerous tumors. [22] In some cases, ultrasound is more useful than other imaging methods, such as MRI, in diagnosing tumor infiltration of surrounding tissue. [23] Projection B is not free from limitations. The higher the resolution (frequency), the shallower the signal penetration [21]. In a general sense, a useful ultrasound machine is one allowing to image structures as large as 1 mm to a depth of about 150 mm. Ultrasound travels through the tissues at a speed of about 1500 m/s. [24] Wavelength is one of the factors that determine the final resolution of the image generated by an ultrasound scanner. The depth of the imaging depends on the signal frequency used. Signals with a frequency of 10 MHz can penetrate to a depth of 50 mm, and signals with a frequency of 60 MHz to about 5 mm. Unfortunately, the opposite is true with the resolution of the image obtained. Higher frequency waves give a higher resolution image, but allow for shallower structures to be imaged. [25] This is reflected in practice. Ultrabiomicroscopy uses high-frequency waves to obtain high-resolution images. In the case of an ophthalmic examination, it is used to assess the angle of infiltration, the depth of the anterior chamber or the condition of the ligamentous apparatus [26]. The ideal ultrasound transducer features a high-performance transmitter and a highly sensitive receiver. Its acoustic impedance is similar to that of the human body. Currently, the heads use synthetic ferroelectric ceramic zirconate titanate (PZT) as an ideal material for the construction of the transducer [26]. Tissues absorb ultrasound according to the 0.2-0.5 dB per cm per MHz rule. The attenuation increases with increasing frequency and distance. For some time, the sensitivity of the head is too low to effectively receive and analyze the signal – it does not penetrate the background echo [24].

An interesting issue is ultrasonic computed tomography, which uses ultrasound to obtain transverse scans and then merge them into a three-dimensional image. The expectations regarding this technology are high. The first studies, however, do not show promising results.

Due to the problem of deflection of sound waves on heterogeneous tissue, the image produced on the basis of the scans differs significantly from the real one. [27] In the case of an ophthalmological examination, the lack of hard bone structures obscuring the viewed image may give hope for the development of this technology and its use in the future in ophthalmic diagnostics.

The highest frequency of ultrasound in medicine in general is used for imaging the anterior segment of the eye. The ultrasound biomicroscopy (UBM) is a contact, non-invasive method that requires topical anesthesia and uses frequencies from 35 to 60 MHz. It was first described in 1992 by Pavlin et al [28]; authors used 50–100 MHz transducers that produced 4 x 4 mm filled within 4 mm depth with 512 images lines at scan rate 5 frames per second. The probe was immersed in a cup that was placed on the cornea and was filled with methylcellulose solution. The used value for the speed of sound in ocular media was 1540 m/s. Average anterior chamber depth was 3,128 ± 0,372 mm. Contrary to the A-mode measurement the distance was obtained from the posterior surface of the cornea to the lens surface [image 8], hence the results were more accurate. Since the study was designed to assess the capabilities of new diagnostic methods, the study group was relatively small (9 subjects), so the

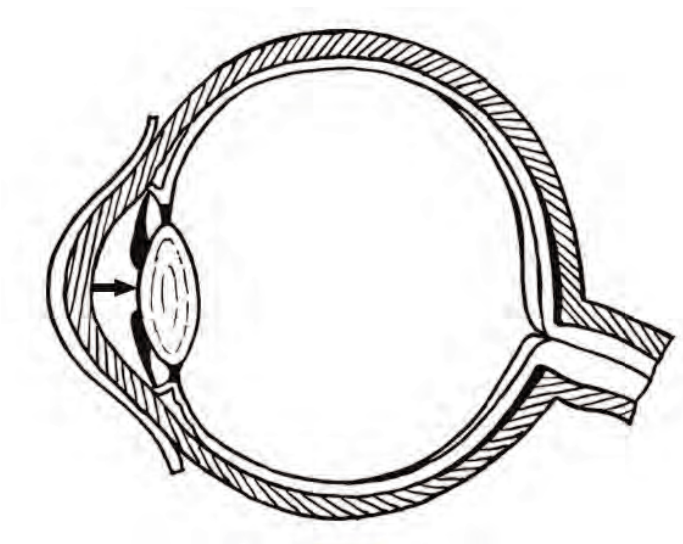

Image 8. Anterior chamber depth

authors did not observe narrowing the anterior chamber with age. UBM also for quantitative measurement of iridocorneal angle, the structure that can be visually examined via gonioscopy exam. The gonioscopy is the gold standard for iridocorneal angle examination, however it is a qualitative method that requires patient cooperation. Using ultrasound the angle (θ1) was measured with the apex in the iris recess and the arms of the angle passing through a point on the trabecular meshwork 500 um from the scleral spur and the point on the iris perpendicularly opposite [image 9]. UBM can be used in evaluation of iridocorneal angle, especially when rubeosis iridis is observed. In this condition new pathological blood vessels are formed on the surface of the iris as well as in the filtration angle, causing block and spike in intraocular pressure [image 10]. Other pathology visualized by UBM is angle recession, the implication of ocular trauma [image 11] [29]. Modern units operate at frequency of 50 MHz and obtain a resolution between 25 and 50 um, with tissue penetration 4-5 mm. Nowadays the technique is used for assessment of the iridocorneal angle, before a cataract surgery or when diagnosing nodules of the iris. When assessing the width of iridocorneal angle it is a golden standard for patients that do not cooperate during gonioscopy exam. Narrowing of the iridocorneal

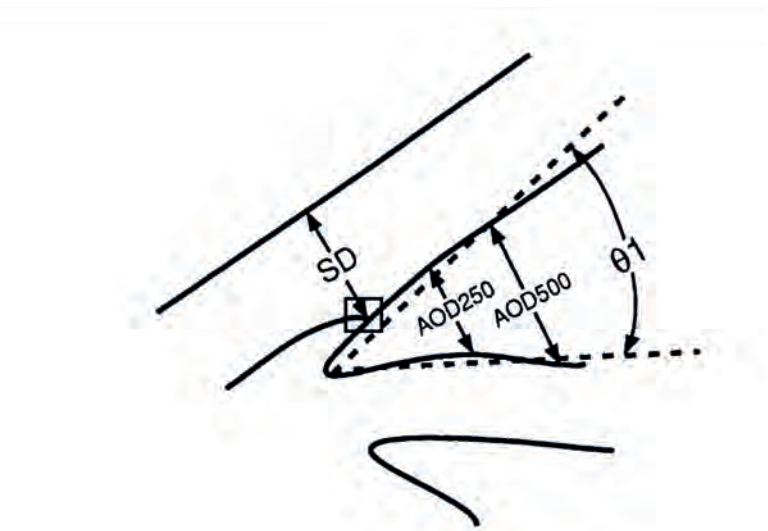

Image 9. Iridocorneal angle (θ1) measurement made from ultrabiomicroscopy imaging, ▫ - scleral spur

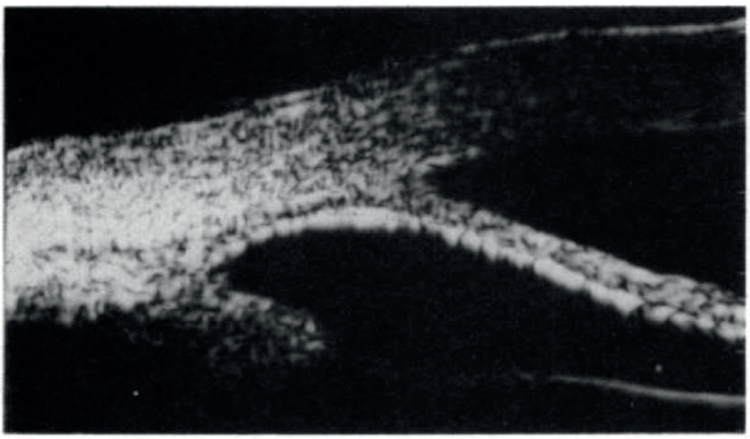

Image 10. Anterior synechiae — visual representation of blood vessels forming in iridotrabecular angle

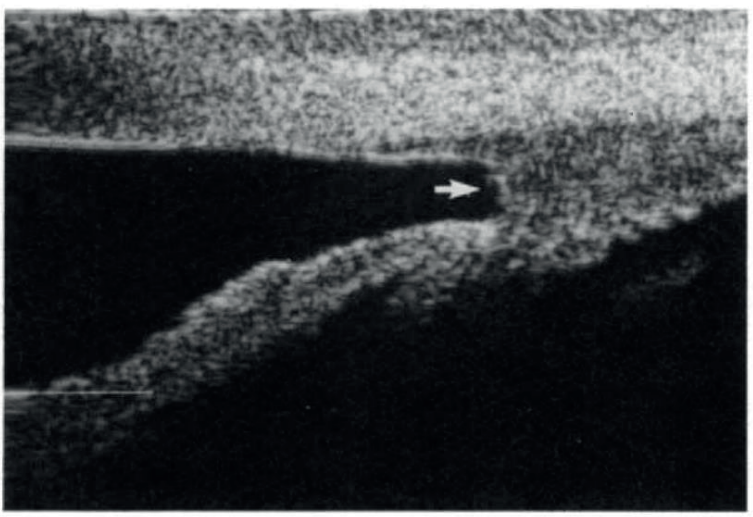

Image 11 Angle recession - loss of continuity of ciliary body post-trauma

angle can cause angle closure glaucoma [image 12] Scleral spur position is used as a marking point because it is easily distinguished from iridocorneal angle's anatomy repetitively. The evaluation of Zinn ligaments, the structures that hold the eye's lens in position, is essential before cataract surgery among patients who experienced head trauma in the past [30,31, 32]. If the ligaments are elongated or torn, there is higher risk of lens luxation

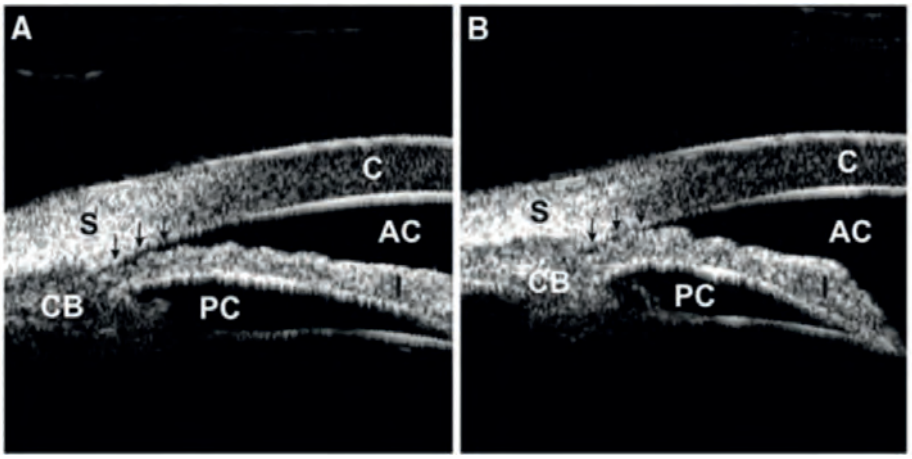

Image 12. Narrowing of the iridocorneal angle in a provocative test in the dark, s-sclera, C - cornea, CB - cillary body, AC - anterior chamber, PC - posterior chamber. Arrows mark iridocorneal angle that narrows in dim lighting

during the procedure (image 13, image 14). Patients with subluxed lens require experienced surgeon or different implantation technique. UBM is useful also in differentiating solid from cystic lesions of the iris [30]

In 1993 a very-high frequency (VHF) ultrasound was introduced in corneal layers imaging. Corneal surface poses a challenge for the ultrasound imaging due to its curvature and superficial location. Conventional A-scan imaging is made from rectified echo and as each echo contains peaks and null, the obtained image has a grained structure. In contrary, the VHF uses deconvolved analytic signal (DAS) which is a representation of echo change over time, thus it produces image resolution of 49 um, enabling it to visualize and measure the epithelial thickness (image 15) [33] Modern VHF units allow to create corneal epithelial thickness map, particularly useful in post refractive

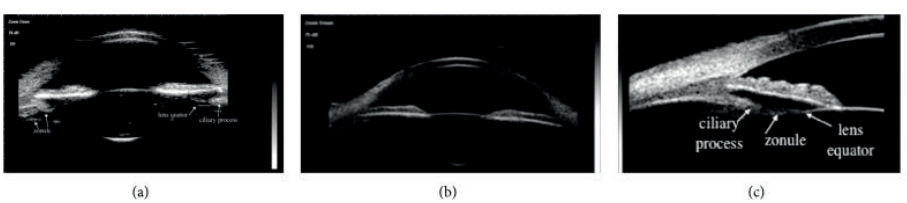

Image 13. Physiological position of the lens

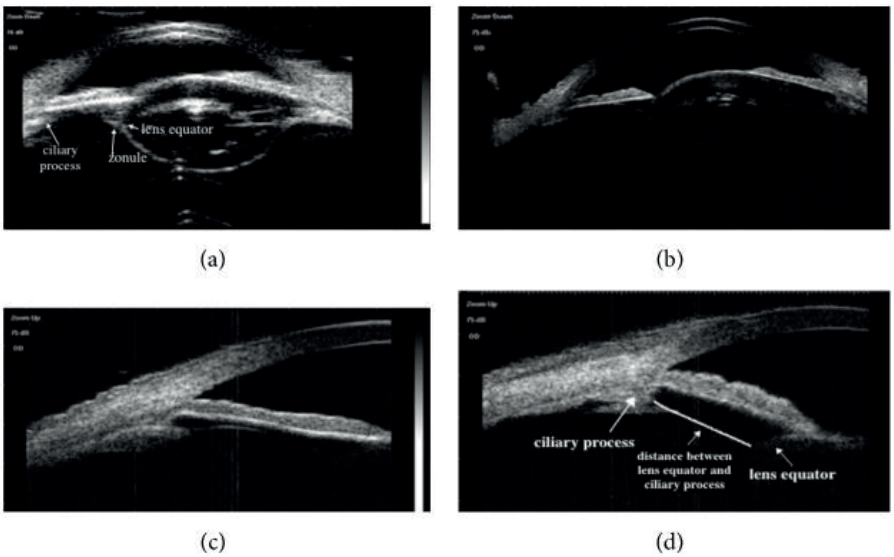

Image 14. Lens subluxation

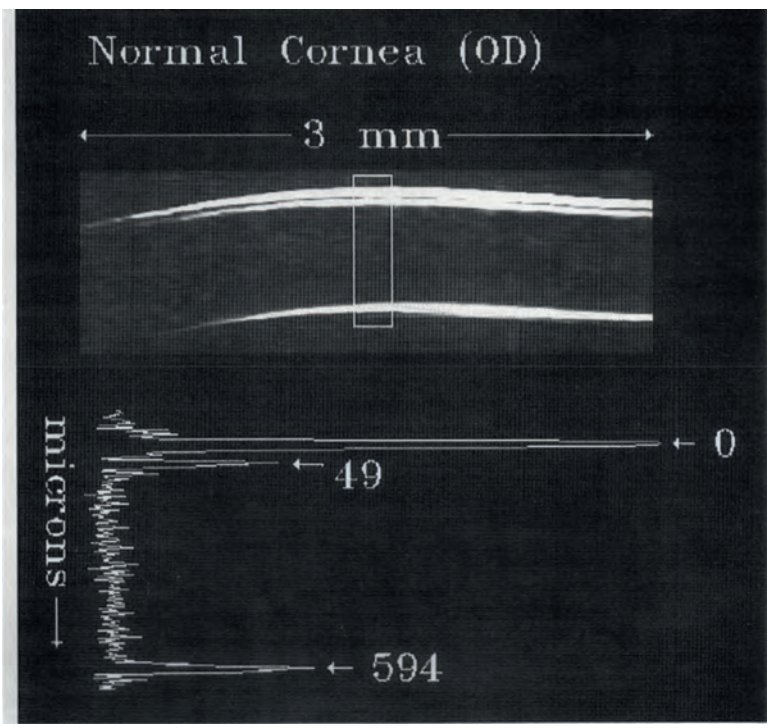

Image 15. Corneal epithelial thickness measurement using VHF

surgery observation. In superficial refractive surgery a laser beam is used in order to remodel the surface of the cornea and achieve the emmetropia, meaning the state of vision in which a faraway object at infinity is in sharp focus with the eye lens in a neutral or relaxed state (image 16) [34]. Accurate laser depth allows for stable outcomes, however abnormal thickness or distribution of epithelial thickness might interfere with the refraction, so the assessment of epithelial thickness becomes a standard procedure preoperatively. Using arc-B VHF unit for corneal epithelial mapping and pachymetry creates accurate and reproducible images [35]. When calculating ACD both UBM and VHF give similar results [36]

In summary, although sonography is a relatively dated technique and despite the introduction of new optical methods, it is still valuable in everyday diagnosis. Among the advantages are a wide imaging field, unit's mobility, real-time examination and a broad range of diagnostics that one can perform using only one unit. Despite having Optical Coherence Tomography (OCT), Computed Tomography (CT) and Magnetic Resonance Imaging (MRI) only with ultrasound the central and peripheral retina can be examined when the visual pathway is obscured. The exam can be performed at the bedside, and is relatively safe for all patients, including pregnant women. Using different transducers allows for visualizing anterior and posterior segments of the eye. In the anterior part anterior chamber depth can be measured and iridocorneal angle assessed, especially when primary angle clo-

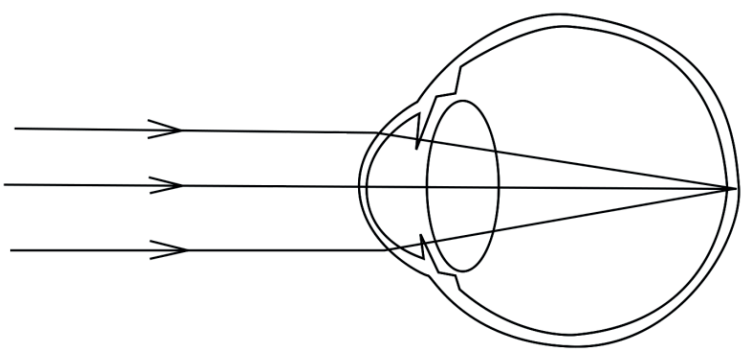

Image 16. Emmetropia, a state when light beams traveling from infinity through an eye focus on the surface of the retina

sure glaucoma is suspected. Sonogram is also used in diagnosing cancerous lesions of the iris and ciliary body. It is worth mentioning that it is the only technique allowing the examiner to visualize behind the iris. This region is unreachable for optic devices because laser beam cannot penetrate through the iris. When using a transducer for the posterior portion of the eye vitreous detachment, retinal detachment and tears and choroidal tumors such as melanoma can be detected. Among the disadvantages there is lower resolution and operator dependency, meaning that the conclusion of the exam and the description can be made only after performing it, not just by looking at obtained images.

BIBLIOGRAPHY

[1] Hans Breuer, Atlas Fizyki, Rosemarie Breuer (ilust.), Jerzy Gronkowski (tłum.), Warszawa: Prószyński i S-ka, [2007], s. 101, ISBN 83-7469-196-4, OCLC 839122450
[2] Ludwig, G., Struthers, F.,(1949) Considerations underlying the use of ultrasound to detect gallstones and foreign bodies in tissue
[3] Hagen-Ansert SL. Society of diagnostic medical sonographers—A timeline of historical events in sonography and the development of the SDMS: In the beginning.... Journal of Diagnostic Medical Sonography. 2006;22:272-278. DOI: 10.1177/8756479306291456
[4] LAVINE O, LANGENSTRASS KH, BOWYER CM, FOX FE, GRIFFING V, THALER W. EFFECTS OF ULTRASONIC WAVES ON THE REFRACTIVE MEDIA OF THE EYE. AMA Arch Ophthalmol. 1952; 47(2):204–219. doi:10.1001/archopht.1952.01700030211006
[5] A, Mundt, G. H.; Hughes, W. F. Ultrasonics in ocular diagnosis. AM J. Ophthalmol. 41:488-498; 1956.
[6] Fledelius HC. Ultrasound in ophthalmology. Ultrasound Med Biol. 1997;23(3):365-75. doi: 10.1016/s0301-5629(96)00213-x. PMID: 9160904.
[7] Schutz, J.S. and N.R. Bronson, II, Ophthalmic Contact B-Scan Ultrasonography: A Practical Clinical Tool. Archives of Ophthalmology, 1974. 92(4): p. 291-296.
[8] Jansson F, Sundmark E. Determination of velocity of ultrasound in ocular tissues at different temperatures. Acta Ophthalmol. 1961;39(5):899–910. doi: 10.1111/j.1755-3768.1961.tb07754.x.
[9] Jansson, F. & Kock, E. Determination of the velocity of ultrasound in the human lens and vitreous. Acta Ophthalmol. Kbh. 40: 420 (1962).

[10] STENSTROM S. An apparatus for the measurement of the depth of the anterior chamber, based on the principle of Lindstedt. Acta Ophthalmol (Copenh). 1953;31(3):265-70. doi: 10.1111/j.1755-3768.1953.tb03293.x. PMID: 13079732.
[11] JANSSON F. Measurement of intraocular distances by ultrasound and comparison between optical and ultrasonic determinations of the depth of the anterior chamber. Acta Ophthalmol (Copenh). 1963;41:25-61. doi: 10.1111/j.1755-3768.1963.tb02420.x. PMID: 13957439.
[12] Stenstrom, Solve. "Untersuchungen uber die Variation undKovariation der optischen E; emente des menshlichen Auges" Acta Ophthal (1946): 218-232.
[13] Franken, Simon. Metingen aan het levende menselijke oog met behulp van de echo van ultrasone trillingen: On the use of the echo of ultrasonic waves to obtain the measurements of the living human eye. Diss. 1961.
[14] Petrella, L., Fernandes, P., Santos, M., Caixinha, M., Nunes, S., Pinto, C., ... & Gomes, M. (2020).Safety Assessment of an A Scan Ultrasonic System for Ophthalmic Use. Journal of Ultrasound in Medicine, 39(11), 2143-2150
[15] Whang, WJ., Yoo, YS., Kang, MJ. et al. Predictive accuracy of partial coherence interferometry and swept-source optical coherence tomography for intraocular lens power calculation. Sci Rep 8, 13732 (2018). https://doi.org/10.1038/s41598-018-32246-z
[16] Drexler W, Findl O, Menapace R, Rainer G, Vass C, Hitzenberger CK, Fercher AF. Partial coherence interferometry: a novel approach to biometry in cataract surgery. Am J Ophthalmol. 1998 Oct;126 (4):524-34. doi: 10.1016/s0002-9394(98)00113-5. PMID: 9780097.
[17] Schmid, Gregor F., et al. "Measurement of eye length and eye shape by optical low coherence reflectometry" International ophthalmology 23.4 (2001): 317-320.
[18] Saxena, S., et al., Management of Vitreous Haemorrhage. Indian Journal of Ophthalmology, 2003 51(2): p. 189-196.
[19] Sandinha, M.T., et al., Accuracy of B-scan ultrasonography in acute fundus obscuring vitreous hemorrhage using a standardized scanning protocol and a dedicated ophthalmic ultrasonographer. Clin Ophthalmol, 2017. 11: p. 1365-1370.
[20] Rabinowitz, R., et al., Comparison between clinical and ultrasound findings in patients with vitreous hemorrhage. Eye, 2004. 18(3): p. 253-256.
[21] Lahham, S., et al., Point-of-Care Ultrasonography in the Diagnosis of Retinal Detachment, Vitreous Hemorrhage, and Vitreous Detachment in the Emergency Department. JAMA Netw Open, 2019. 2(4): p. e192162.

[22] Fonkeu, Y., et al., Diagnostic A-Scan of Choroidal Melanoma: Automated Quantification of Parameters. Ocul Oncol Pathol, 2019. 5(5): p. 350-357.
[23] Jacobsen, B.H., C. Ricks, and R.P. Harrie, Ocular ultrasound versus MRI in the detection of extrascleral extension in a patient with choroidal melanoma. BMC Ophthalmology, 2018. 18(1): p. 320.
[24] Wells, P.N. and H.D. Liang, Medical ultrasound: imaging of soft tissue strain and elasticity. J R Soc Interface, 2011. 8(64): p. 1521-49.
[25] Rosen, D.B., et al., A Brief Overview of Ophthalmic Ultrasound Imaging. Novel Diagnostic Methods in Ophthalmology, 2019.
[26] Wells, P.N.T., Ultrasound imaging. Physics in Medicine and Biology, 2006. 51(13): p. R83-R98
[27] Lasaygues, P., et al., Progress towards<i>in vitro</i> quantitative imaging of human femur using compound quantitative ultrasonic tomography. Physics in Medicine and Biology, 2005. 50(11): p. 2633-2649.
[28] Pavlin CJ, Harasiewicz K, Foster FS. Ultrasound biomicroscopy of anterior segment structures in normal and glaucomatous eyes. Am J Ophthalmol. 1992 Apr 15;113(4):381-9. doi: 10.1016/s0002-9394(14)76159-8. PMID: 1558111.
[29] Ishikawa H, Schuman JS. Anterior segment imaging: ultrasound biomicroscopy. Ophthalmol Clin North Am. 2004 Mar;17(1):7-20. doi: 10.1016/j.ohc.2003.12.001. PMID: 15102510; PMCID: PMC1978090.
[30] Liu YZ, Liu YH, Wu MX, Luo LX, Zhang XY, Cai XY, Chen XQ. [Clinical applications of ultrasound biomicroscopy in diagnosis and treatment of lens subluxation]. Zhonghua Yan Ke Za Zhi. 2004 Mar;40(3):186-9. Chinese. PMID: 15307991.
[31] Shi M, Ma L, Zhang J, Yan Q. Role of 25 MHz Ultrasound Biomicroscopy in the Detection of Subluxated Lenses. J Ophthalmol. 2018 Oct 17;2018:3760280. doi: 10.1155/2018/3760280. PMID: 30416825; PMCID: PMC6207873.
[32] Reinstein, Dan Z., Ronald H. Silverman, and D. Jackson Coleman. "High-frequency ultrasound measurement of the thickness of the corneal epithelium" Journal of Refractive Surgery 9.5 (1993): 385-387.
[33] Reinstein DZ, Silverman RH, Coleman DJ. High-frequency ultrasound measurement of the thickness of the corneal epithelium. Refract Corneal Surg 1993;9:385-387.
[34] https://en.wikipedia.org/wiki/Emmetropia
[35] Reinstein, Dan Z., et al. "Arc-scanning very high-frequency digital ultrasound for 3D pachymetric mapping of the corneal epithelium

and stroma in laser in situ keratomileusis" Journal of Refractive Surgery 16.4 (2000): 414-430.

[36] Al Farhan, H.M. Agreement between Orbscan II, VuMAX UBM and Artemis-2 very-high frequency ultrasound scanner for measurement of anterior chamber depth. BMC Ophthalmol 14, 20 (2014). https://doi.org/10.1186/1471-2415-14-20

ISBN 978-83-66847-55-2